INFORMATION TO USERS

This material was produced from a microfilm copy of the original document. While the most advanced technological means to photograph and reproduce this document have been used, the quality is heavily dependent upon the quality of the original submitted.

The following explanation of techniques is provided to help you understand markings or patterns which may appear on this reproduction.

1. The sign or "target" for pages apparently lacking from the document photographed is "Missing Page(s)". If it was possible to obtain the missing page(s) or section, they are spliced into the film along with adjacent pages. This may have necessitated cutting thru an image and duplicating adjacent pages to insure you complete continuity.

2. When an image on the film is obliterated with a large round black mark, it is an indication that the photographer suspected that the copy may have moved during exposure and thus cause a blurred image. You will find a good image of the page in the adjacent frame.

3. When a map, drawing or chart, etc., was part of the material being photographed the photographer followed a definite method in "sectioning" the material. It is customary to begin photoing at the upper left hand corner of a large sheet and to continue photoing from left to right in equal sections with a small overlap. If necessary, sectioning is continued again — beginning below the first row and continuing on until complete.

4. The majority of users indicate that the textual content is of greatest value, however, a somewhat higher quality reproduction could be made from "photographs" if essential to the understanding of the dissertation. Silver prints of "photographs" may be ordered at additional charge by writing the Order Department, giving the catalog number, title, author and specific pages you wish reproduced.

5. PLEASE NOTE: Some pages may have indistinct print. Filmed as received.

University Microfilms International
300 North Zeeb Road
Ann Arbor, Michigan 48106 USA
St. John's Road, Tyler's Green
High Wycombe, Bucks, England HP10 8HR

A RAMAN SPECTROSCOPIC INVESTIGATION OF CRYSTALLINE POLY (1,4 TRANS BUTADIENE) AND THE RELATIONSHIP BETWEEN THE THERMODYNAMIC PROPERTIES OF POLY(1,4 TRANS BUTADIENE) AND ITS CRYSTALLINE STRUCTURE

by

HILTON F. EVANS

A dissertation submitted to the Graduate Faculty in Chemistry in partial fulfillment of the requirements for the degree of Doctor of Philosophy, The City University of New York

This manuscript has been read and accepted for the Graduate Faculty in Chemistry in satisfaction of the dissertation requirement for the degree of Doctor of Philosophy.

9/20/77
DATE

Arthur E. Woodward
CHAIRMAN OF EXAMINING COMMITTEE

9/20/77
DATE

Leonard H. Schwartz
EXECUTIVE OFFICER

Stanley P. Rudtl
Raymond L. Disch

SUPERVISORY COMMITTEE

'A Raman Spectroscopic Investigation of Crystalline Poly(1,4 Trans Butadiene) and the Relationship Between the Thermodynamic Properties of Poly(1,4 Trans Butadiene) and its Crystalline Structure'

by Hilton F. Evans

Advisor: Prof. Arthur E. Woodward

ABSTRACT

Raman spectra were obtained for various preparations of crystalline poly 1,4 trans butadiene(PTBD) at temperatures ranging from 25° to 80°C. Several bands were found to disappear upon annealing at temperatures between 80° and 90°C, which suggests that they are associated with a metastable crystalline modification present in solution grown PTBD single crystals. The I_{1331}/I_{1311} ratio was not found to be a satisfactory crystallinity parameter. Nor were any amorphous/crystalline band pairs analogous to those present in the infrared spectrum found in the Raman spectrum. The spectrum above the phase transition temperature was interpreted in terms of a monoclinic lattice with conformationally mobile molecules.

Theoretical calculations of the lattice energy were carried out on the PTBD form II hexagonal lattice proposed by Stellman, Woodward and Stellman(17), and on monoclinic form I and II lattices of PTBD. The Scott-Scheraga empirical potential energy function for hydrocarbons was used, and found to yield satisfactory interchain spacings for the monoclinic form I lattice at 20°C and for the form II lattice at 75°C when thermal expansion was taken into account.

A, H, and S, which are the Helmholtz free energy, the

enthalpy and entropy changes for the transformation of form I to form II were computed as functions of temperature. Only 50% of the enthalpy of transtion was accounted for.

The method of generalized frequencies of Dobratz(47) was adapted for calculating thermodynamic functions of crystalline polymers, and was applied to computing the specific heats of several polymers at 25°C. The method was found to yield specific heats which agreed with experimental values to within 1 cal/deg-mole. The specific heat of PTBD was also computed between 75° and 139°C and was found to be in substantial agreement with the experimental value of C_p. S was also computed by the above method, and was found to agree with the value obtained experimentally by Stellman et al(17).

TABLE OF CONTENTS

INTRODUCTION TO PART I	1
STATEMENT OF THE EXPERIMENTAL PROBLEM	13
EXPERIMENTAL PROCEDURES	14
PTBD samples	14
Single Crystal Preparation	14
H23, H43 and H63 crystals	14
T23 crystals	15
Crystal Mats	15
H63A crystals(annealed crystals)	16
H63M crystals(melt recrystallized crystals)	16
H63MQ crystals(melted then quenched crystals)	16
Raman Spectroscopy	16
Experimental Set-ups	17
Room Temperature Spectra	17
High Temperature Spectra	22
RESULTS	24
Captions for Figs. 5-12	29
Captions for Fig. 14-16	47
DISCUSSION	52
CONCLUSIONS	57
INTRODUCTION TO PART II	58
The Crystal Lattice Model	58
The Calculation of the Specific Heat	60
Computational Errors	60
The Free Energy Function	60
The Relationship Between Free Energy and Crystal Structure	64
The Method of Generalized Frequencies	65

TABLE OF CONTENTS(Cont'd)

STATEMENT OF THE THEORETICAL PROBLEM 69

COMPUTATIONAL PROCEDURES 70

Description of PTBD Molecular and Lattice Geometries 70

PTBD Chain Geometry 70

Cartesian Coordinate Generation 70

PTBD Chain Generation 73

PTBD Unit Cell and Lattice Generation 73

Units I - III 74

Unit IV 75

The Monoclinic Lattice 75

The 'Hexagonal' Lattice 75

The Empirical Potential Energy Functions 75

Computer Experiments 77

Calculation of Phase Transition Thermodynamic Properties 77

Application of the Method of Generalized Frequencies 78

RESULTS 80

Crystal Lattice Constants 80

Mean Lattice Vibrational Frequencies 80

Computed Thermodynamic Quantities 88

Results from the Method of Generalized Frequencies 88

DISCUSSION 95

Crystal Structure and Phase Transition Properties 95

The Phase Transition Thermodynamic Properties 98

The Method of Generalized Frequencies 99

CONCLUSIONS 101

APPENDIX A 102

TABLE OF CONTENTS(Cont'd)

APPENDIX B 110

APPENDIX C 111

REFERENCES 113

LIST OF TABLES

NUMBER	CAPTION	PAGE
A	The Irreducible factor group representation of the PTBD unit cell.	7
I.	Raman spectral frequencies for various preparations of PTBD	26
II.	Same as above	27
III	I_{1331}/I_{1311} ratios for various preparations of PTBD	28
IV	Unit cell parameters for PTBD I	74
V	Parameters for the Scott-Scheraga function	76
VIA	Generalized frequencies for hydrocarbon bond types	79
VIB	Generalized frequencies for non-hydrocarbon bond types	79
VII	Lattice conformational energy(excluding torsion terms) as a funcion of interchain spacing for forms I and II monoclinic lattices for the Stellman et al 'Hexagonal'lattice	81
VIIIA	Calculated and experimentally derived lattice constants for various PTBD crystal lattices	85
VIIIB	PTBD lattice constants computed by Stellman et al (17)	86
IX	Calculated lattice vibrational frequencies for various forms of PTBD	87
X	Thermodynamic propertations as functions of temperature-for the transformation(=4.67A, ϕ=109°) (=4.92A, ϕ=80°)	89

LIST OF TABLES(CONT'D)

NUMBER	CAPTION	PAGE
XI	Thermodynamic properties of several preparations of crystalline PTBD	90
XII	Phase transition thermodynamic properties of several preparations of crystalline PTBD	91
XIII	Heat capacities of various polymers computed with eq(24)	93

LIST OF FIGURES

FIGURE	CAPTION	PAGE
1(a)	Set up for annealing and melt recrystallizing a single crystal mat	18
1(b)	Set up for melt quenching a crystal mat	18
1(c)	Exploded view of sample holder for high temperature treatment	18
2.	Opaque sample holder for Raman spectrometer	19
3.	Opaque sample holder for high temperature Raman spectrometry	20
4.	Resistance vs. log(temperature) curve for the thermistor probe(see text)	21
.	Raman spectra for various preparations of crystalline PTBD	
5.	H23 crystals	30-31
6.	H43 crystals	32-33
7.	H63 crystals	34-35
8.	H63P-H63 crystals pressed under 25000psi pressure	36-37
9.	H63A-H63 crystals	38-39
10.	H63MQ-H63 crystals melted then quenched in liquid nitrogen	40-41
11.	H63MR-melt recrystallized H63 crystals	42-43
12.	H63 crystals at 77°C	44-45
13.	490-570 cm^{-1} Raman spectral region of several preparation of PTBD crystals	46
14.	Raman spectral scans between 50 and 300 cm^{-1} at temperatures between 25°and 78°C	48

LIST OF FIGURES(CONT'D)

FIGURE	CAPTION	PAGE
15(a)	Raman scans of the 1300-1350 cm^{-1} region for different PTBD preparations at room temperature	50
15(b)	Raman scans of 1300-1350 cm^{-1} region for H63 crystals at 45°, 65°, 71° and 75°C	50
16.	Raman scans of the 2800-3050 cm^{-1} region for H63 crystals at 45°, 65°, 71°and 75°C	51
17.	The definition of a Ø dihedral angle	62
18.	no caption	70
19.	no caption	71
20.	no caption	73
21.	U-E_{tor} vs. interchain spacing for the PTBD 'hexagonal'lattice	82
22.	U-E_{tor} vs. interchain spacing for the Form I PTBD lattice	83
23.	Energy vs. interchain spacing for the form II PTBD lattice	84
24.	Computed and experimentally derived PTBD specific heats	92

INTRODUCTION TO PART I

The existence of dilute solution grown polymer single crystals has been known for twenty years(1). Since the initial discovery of polyethylene single crystals, single crystals of a variety of polymers have been grown and studied in order that their morphology, internal structure and physicochemical properties could be determined(2). Generally, polymer single crystals grown from dilute solution are platelets of about 50 to 200 A thick and several hundred microns wide. X-ray and electron diffractometry have shown that polymer chains tend to orient themselves perpendicular to the broad plane of the crystallite surface.

The techniques applied to the study of single crystals have included dynamic mechanical techniques, dilatometry, calorimetry, x-ray diffractometry, infrared spectroscopy, Raman spectroscopy and NMR spectroscopy; all of the above are physical in nature. Single crystals have also been subjected to chemical treatments which have includednitric acid etching, epoxidation and bromination.

Dynamic mechanical methods measure the variation of a material's viscoelastic properties with temperature. One such technique measures the rate of decay of the amplitude of a vibrating system containing the subject material. The technique is sensitive to changes in inter- and intramolecular interactions of the component molecules, and can therefore be used to detect the various phase transitions which occur in the material.

Dilatometry uses the principle that a small change in a large volume of liquid contained in a flask is detectable

as a large change in the volume of the liquid contained in an attached capillary(3). This method is used to detect changes in the volumes of materials undergoing chemical reactions or phase transformations.

DSC or differential scanning calorimetry has been applied to the study of polymer single crystals. This well known technique measures the energy needed to maintain the sample at the same temperature as a reference material while both are heated at the same constant rate. From this data phase transformations can be detected and associated thermodynamic properties such as T_{tr}, ΔS, ΔH, and C_p are computed.

Two types of x-ray diffractometry have been applied to single crystals. These are wide angle and low angle x-ray diffractometry. The low angle technique detects long range periodicity; crystal thicknesses and molecular chain orientation can be determined. The name low angle x-ray diffractometry derives from the fact that the angle of incidence of the x-ray beam is usually less than about 10^{o}.

Wide angle x-ray diffractometry gives diffraction patterns which are characteristic of short range order. From these data the spatial distribution of the atoms in the lattice can be determined.

The most widely used vibrational spectroscopic methods are infrared and Raman spectroscopy. Although both methods are used to 'look' at molecular vibrations, they arise from different mechanisms. If the molecules of the crystals being examined possess any symmetry, these differing mechanisms can give rise to differences between the optically active bands

in the IR and Raman spectra. The energies of molecular vibrations usually fall in the 200 to 3200 cm^{-1} range.

The derivation of IR and Raman selection rules can be accomplished via group theoretical methods. Discussions of these methods suitable for chemists can be found in works by Wilson, Decius and Cross(4) and Cotton(5) for fluids and by Turrell(6) and Fately, Dollish, McDevitt and Bentley(7) for solids. A good discussion fo Raman and IR spectroscopy of solids can be found in reference (6). The IR and Raman selection rules for solids differ from those of gases in that the symmetry of the crystal unit cell, upon which the spectrum depends, may be different from the symmetries of the molecules composing it. Solids also tend to be optically anisotropic so that the spectrum of the solid can depend on the direction of the incident radiation, and in the case of Raman spectroscopy on the direction from which the scattered radiation is detected.

An additional difference between solid and gas phase vibrational spectra arises from the conversion of translations and rotations of gas phase molecules into translatory and rotatory lattice vibrations in the solid phase. The selection rules of these vibrations are also derivable from group theory, as outlined in Fately(7).

The laws governing IR and Raman spectra of polymer crystals are the same as those for other solids; however the spectra differ from those of other types of solids because strong covalent bonds link monomer units in adjacent unit cells(unlike the weaker dipole-dipole and Coulombic forces

which occur in molecular and ionic solids, respectively).

The dynamics of molecular vibration have been formulated by Wilson(4,8,9). This well known 'FG matrix method' was extended to helical polymers by Higgs(10). Miyazawa(11) used these methods to demonstrate that certain skeletal vibration frequencies vary with molecular conformation. It will be seen later that conformation dependent bands can be used to measure the quantity of amorphous material in polymer crystals.

The application of broad line NMR spectroscopy to the investigation of crystalline polymers was first made by Wilson and Pake(12). In that study the traces of polyethylene and polytetrafluoroethylene absorption signals were decomposed into narrow and broad line components which were associated with mobile and static regions respectively. Since the signal intensity is directly proportional to the number of absorbing nuclei, the broad and narrow line components provide a method of determing the composition of non-mobile and mobile regions in the polymer crystal. The value of NMR and other physical techniques as they apply to the study of crystalline poly 1,4 trans butadiene, will be discussed below.

Among the polymers whose single crystals can be precipitated from a variety of solvents is high trans content poly 1,4 butadiene, hereafter referred to as PTBD. Crystalline PTBD has been the subject of a number of investigations which have exploited the aforementioned physical techniques (13-31).

These investigations have also included chemical assay techniques applied to the crystallites' surfaces(22,31,32). These will be described later.

X-ray diffraction studies have shown that PTBD can exist in two crystalline modifications at atmospheric pressure. Form I, which is stable at room temperature has been assigned by Iwayanagi and coworkers(14) to a $P2_1/a$ crystallographic space group with a monoclinic lattice. Each unit cell contains four PTBD monomer units. Form II is stable between 71° and 139°C, the melting temperature. X-ray diffraction studies by K. Suehiro et al(16) have revealed the molecular packing in form II to be pseudohexagonal; however no space group could be assigned. Crystalline PTBD undergoes a first order solid-solid phase transition at temperatures ranging from 55° to 75°C depending upon the method of sample preparation and its thermal history(15,17,27,30, 31,33,34,35). Entropies of transition derived from DSC measurements by Ng, Stellman and Woodward(25), and by Bermudez and Fatou(35) for melt recrystallized and bulk crystallized samples are in a 2:1 ratio to the entropies of melting of the samples. The relative magnitude of ΔS_{tr} to ΔS_m suggests that a considerable increase in conformational freedom occurs in the change from form I to form II. The diffuseness of the X-ray diffractograms of form II(16) tends to support this suggestion. Further evidence for high conformational freedom in form II is given by infrared spectra secured for crystalline and amorphous samples of PTBD

by N. Neto et al(18) and D. Morero et al(19). The IR spectrum of form II is almost identical to that of molten PTBD.

The space group of PTBD(viz. $P2_1/a$) contains the inversion operation. Molecules with inversion centers fall into a special group whose IR and Raman active frequencies form nonoverlapping sets. Therefore in order to have the total optically active vibrational spectrum of PTBD a Raman spectrum is necessary. The factor group representation of PTBD appears in Table A.

Prior to the completion of the present work, the only published Raman spectra of poly 1,4 butadienes were those of Cornell and Koenig(36).for amorphous samples. A single chain normal coordinate calculation due to N. Neto and C. di Lauro (18) was used to make group frequency assignments. The force field used in this calculation was derived from low molecular weight analogs. Concurrent with the work of this author (21), Raman spectra of solution grown crystals of PTBD were obtained by Hsu, Moore and Krimm(20). In that study a normal vibration calculation for the entire unit cell which took into account inter- as well as intramolecular force constants was used to make the most complete group frequency assignments for form I to date. Hsu et al and this author have reported Raman spectra for PTBD in its high temperature phase (21,37). The results of these investigations will be reported in the results and discussion sections of this dissertation.

Much effort has gone into determining the distribution

Table A

The irreducible factor group representation of the PTBD unit cell

Factor group = $P2_1/a(C_{2h})$

Number of atoms = 40, Number of molecules = 4

Representation of total genuine vibrations

$$\Gamma_{total} = 30A_g + 30B_g + 29A_u + 28B_u$$

Representation of libratory lattice vibrations

$$\Gamma_{rot,lat} = 3A_g + 3B_g + 3A_u + 3B_u$$

Representation of translatory lattice vibrations

$$\Gamma_{trans} = 3A_g + 3B_g + 2A_u + B_u$$

Totals: 60 Raman active and 57 IR active vibrations

and quantity of amorphous material in single crystals of PTBD. An early investigation by Tatsumi and coworkers(29), which involved dynamic mechanical measurements concluded that the amorphous component of the PTBD single crystals manifests itself in the form of loose chain folds and cilia projecting from the surfaces of the crystals. Woodward and coworkers have applied a number of different techniques to the problem; including IR spectroscopy(23), NMR spectrosopy(15,25) and DSC. Stellman and Woodward have assayed the number of surface double bonds by reacting them with chloroperbenzoic acid(22). The fraction of the total number of bonds present which reacted was used as a measure of the surface amorphous content. Ng and Woodward used broad line NMR spectroscopy to measure what fraction of a single crystal could be wetted by carbon disulfide(15,25). It has been shown that low molecular weight solvents such as CS_2 are capable of enhancing the motion in amorphous associated mobile regions(38); therefore the amorphous-crystalline composition can be computed. Hendrix, Whiting and Woodward(23) have applied infrared spectroscopy to the problem of determining the amorphous crystalline composition. Earlier the 1050, 1220 and 1335 cm^{-1} bands were found to disappear above the crystal transition temperature(18) while the 1075 and 1350 cm^{-1} bands were enhanced in intensity. The results are interpreted as meaning that 1050, 1220 and 1335 cm^{-1} are associated with crystalline material while 1075 and 1350 cm^{-1} are associated with 'amorphous conformations.' In the investigation by Hendrix et al(23) the ratio of the 1350 cm^{-1} intensity to that of the 1335

cm^{-1} band was used as a measure of the amorphous/crystalline mole fraction ratio. Calorimetric measurements(DSC) were carried out by Stellman et al on different preparations of PTBD single crystals(15,17,22). The enthalpy of transition was assumed to be proportional to the crystallinity(the crystalline mole fraction) and was used as a parameter to fix the values of the crystallinities of PTBD samples relative to that of heptane grown singles crystals of PTBD.

Two important conclusionscould be drawn from the aforementioned investigations. First the crystalline content was highest for crystals grown nearest to the crystal-crystal phase transition temperature. The chains are considered to be freer to take on different conformations at these temperatures so that they can 'search for the most stable conformation which is that of the crystal. Second, for certain preparations IR, NMR and DSC results gave higher amorphous mole fractions than did the results of epoxidation. These results suggest that in those preparations amorphous material exists both in the crystal interior as well as on the surface.

In a more recent study, A. Marchetti and E. Martuscelli (30,31) subjected both PTBD crystals whose surfaces had been treated with bromine and untreated crystals to DSC, IR and X-ray diffraction measurements. In that investigation two crystal phase transitions were observed in untreated crystals which suggests the existence of two different crystalline forms below $75^{o}C$ with different thermodynamic stabilities. Heating above $76^{o}C$ resulted in the disappearance of the ex-

tra DSC peak. In the case of crystals whose surfaces had been brominated, a 40 to 60% reduction in the enthalpy of transition was observed along with a reduced ability of the polymer chains to reorganize themselves during annealing which suggests that the bromine groups, which readily add to the surface double bonds, impede the ability of the chains to 'diffuse' through the crystal.

The presence of crystalline and amorphous bands in the PTBD infrared spectrum suggests that such bands might exist in the Raman spectrum. In the infrared study(23) it was assumed that the 1335 and 1350 cm^{-1} bands had similar molar extinction coefficients so that the ratio of I_{1350}/I_{1335} represented the ratio of amorphous to crystalline mole fractions.

Classical electromagnetic theory tells us that the intensity of scattered radiation is given by (39)

eq(1) $$I = \frac{2\ddot{P}^2}{3c^2}$$

where $P = \alpha E$, E is the electric field of the incident radiation. α is the polarizability of the medium and c is the speed of light. P is known as the polarization. If Raman scattering is present, P can be resolved into (40) the sum of a Rayleigh component, a Stokes component and an anti-Stokes component as follows:

eq(2) $$P = E_0\alpha_0\cos\omega t + \tfrac{1}{2}E_0\sum_n [\alpha_n(\cos(\omega+\omega_n)t + \cos(\omega-\omega_n)t]$$

In the above equation α_0 is the static polarizability, α_n is the polarizability associated with the nth normal mode of vibration, ω and ω_n are the circular frequencies of the exciting radiation and the nth normal mode of vibration res-

pectively. $\omega + \omega_n$ and $\omega - \omega_n$ represent Stokes and anti-Stokes scattering respectively The intensity of an anti-Stokes band, I_n (these are usually used in Raman spectroscopy) is given by substituting the anti-Stokes component of P for that line into eq(1).

eq(3) $$I_n = \frac{2\alpha_n^2 E_o^2 (\omega-\omega_n)^4 \cos^2(\omega-\omega_n)t}{12c^2}$$

If α_n^2 is the total polarizability then I_n can be written in terms on the average square polarizability per molecule $\overline{\alpha_n^2}$ as

eq(4) $$I_n = \frac{2\overline{\alpha_n^2} N E_o^2 (\omega-\omega_n)^4 \cos^2(\omega-\omega_n)t}{12c^2}$$

where N is the number of molecules.

Let I_c and I_a be the intensities of hypothetical crystalline and amorphous bands respectively. The ratio of these two intensities is

eq(5) $$\frac{I_a}{I_c} = \frac{N_a}{N_c} \frac{\overline{\alpha_a^2}}{\overline{\alpha_c^2}} \left(\frac{\omega-\omega_a}{\omega-\omega_c}\right)^4 \frac{\cos^2(\omega-\omega_a)t}{\cos^2(\omega-\omega_c)t}$$

If I_c and I_a are born of bands with similar frequencies and normal modes of vibration then $\omega - \omega_c \simeq \omega - \omega_a$, and $\overline{\alpha_a^2} \simeq \overline{\alpha_c^2}$ so that

eq(6) $$\frac{I_a}{I_c} \simeq \frac{N_a}{N_c}$$

In terms of mole fractions this may be written as

eq(7) $$\frac{I_a}{I_c} = \frac{x_a}{x_c} = \frac{x_a}{1-x_a}$$

Thus if suitable bands can be found in the Raman spectrum, I_c/I_a provides a measure of the crystallinity of a material. Comparisons between Raman spectra for different preparations of PTBD single crystals and samples with different thermal histories at room temperature and above the phase transition temperature should render these bands identifiable.

Part I of the present investigation involves the acquisition of Raman spectra for PTBD crystals grown from dilute solution under differing conditions and which have been subjected to different thermal and mechanical treatments. Comparisons are made between the spectra in order that amorphous and crystalline bands can be identified, and used to obtain further crystallinity data for PTBD.

STATEMENT OF THE EXPERIMENTAL PROBLEM

The experimental work to be described had four objectives which are listed below.

1. To obtain Raman spectra for various preparations of crystalline PTBD at room temperature, and to obtain Raman spectra for heptane grown PTBD crystals at various temperatures between room temperature and 80°C.
2. To determine if amorphous-crystalline band pairs analogous to the 1335, 1350 cm^{-1} band pair exist in the Raman spectrum, and to use them to compute crystallinities or various PTBD crystal preparations.
3. To determine if relationships exist between crystallinity and the frequencies of skeletal and lattice vibration bands.
4. To interpret changes in the appearance of the spectrum in the neighborhood of the crystal transformation temperature.

EXPERIMENTAL PROCEDURES

PTBD samples

The samples of PTBD-K used in the present study were obtained by Prof. M. Takayanagi from Ube-Kasan Co., Ltd. of Japan. The physical characteristics of this polymer were reported earlier(22). The trans content of the sample was found by infrared analysis to be greater than 95%. The as received polymer was reported to have a number average molecular weight of 8670($\pm$10%). The number average molecular weight for a sample of PTBD crystals precipitated from n-heptane was found to be 36900($\pm$10%). The number average molecular weight was measured by Debell and Richardson Co., Inc. with an Hitachi-Perkin-Elmer vapor phase osmometer.

Single Crystal Preparation

Single crystals of PTBD-K were precipitated from dilute solutions of n-heptane or toluene following procedures adapted from those given in references 22-25 and 32. The procedure for each type of preparation is given below.

H23, H43, and H63 crystals

0.06 gm of PTBD-K bulk material was dissolved in 500 ml of n-heptane by heating the mixture with constant stirring to 80°C. The solution was filtered hot through an all glass filter into a second flask, and the solution was then chilled to 0°C in an ice-water bath. After standing for one hour at 0°C the mixture was reheated to 73°C or the point at which the mixture just clears. This solution was then put in a constant temperature bath of 63°, 43° or 23°C for H63, H43, or H23 crystals respectively. The crystals were allowed to precipitate for several hours.

When the crystals have settled most of the supernatant solution was removed and fresh heptane was added. The crystals were allowed to resettle, and the process of renewing the heptane was repeated. Single crystals examined under an optical microscope had the normal hexagonal appearence(22,32)

T23 crystals

0.1 gm of PTBD-K bulk material was dissolved at 50°C in 500 ml of reagent grade toluene. The mixture was maintained at 50°C in a water bath with constant stirring for one hour. The solution was then filtered hot through a glass filter into a second flask. It was then cooled in an ice-water bath to about 0°C where it was allowed to sit for an hour while pre-precipitation occured. The mixture was then reheated to 50°C with stirring and immersed in a 21°C thermostatted bath. These crystals were examined using a Phillips 300 electron microscope and showed the normal hexagonal shape(22,23). Only the initial preparations were examined. When the precipitate had settled the toluene was renewed by the same procedure outlined in the section on H crystal preparation.

Crystal Mats

1 cm disk shaped mats of crystals were prepared by filtering the above preparations through Millipore Corp. filters held in plastic filter holders. Filtering was facilitated by aspiration. Enough precipitate was filtered to produce a mat approximately 0.2 mm thick.

H63A crystals(annealed crystals)

The set-up for annealing a crystal mat is shown in fig. 1(a). A mat of H63 crystals was placed on the aluminum disk on the right. The temperature was maintained between 80° and 90°C for up to 12 hours. The temperature was monitored by a thermometer seated in the metal disk on the left. To minimize oxidation, reduced pressure was maintained throughout annealing. After annealing the system was allowed to cool while reduced pressure was maintained.

H63M crystals(melt recrystallized crystals)

The set-up in fig. 1(a) was also used for this preparation. However the mat was heated to 140°C for about one hour. The sample was then allowed to cool slowly to room temperature.

H63MQ crystals(melted then quenched crystals)

The set-up in fig. 1(b) was used for this preparation. After heating to 140°C for one hour under reduced pressure the sample holder was plunged into liquid nitrogen. Fig. 1(c) depicts an exploded view of the sample holder. The washer prevents the mat from sticking to the upper aluminum disk.

Raman Spectroscopy

The instrument used to obtain all spectra was a Spex Ramalog 3 Raman spectrometer. The exciting radiation source was a Coherant Radiation Inc. Model 52B argon laser equipped with an etalon. The useful frequencies were 5145 and 4880 A. The detector was an ITT model FM-130 photomultiplier tube, certified for photon counting. The PM tube was maintained at -20°C in order that background shot noise could be

minimized. The photocell output was converted to intensity vs. wavenumber traces by a photon counting accessory.

Experimental Set-ups

The opaque sample holder depicted in fig. 2 was used for all crystal mat spectra. The metal disk was not part of the original equipment, but was added to hold the sample flush against the face of the sample holder and to give the mat added support. Since the sample diameter was approximately 0.25 cm smaller than the opening of the sample holder a washer with an outside diameter of 1 cm and an inside diameter of 1.5 cm was used to hold the specimen flat against the metal disk. The incident laser beam was focussed onto the mat at an angle of 30°.

The assembly for the high temperature experiments is illustrated in fig. 3. The metal disk was heated by a 1 cm heating tape obtained from the Brisco Mfg. Co. of Columbus, Ohio. The temperature was regulated by a rheostat with a range of 0 to 120 volts, and monitored by a Fenwal Electronics Inc. precision thermistor embedded in the metal disk. The thermistor resistance was measured by an impedence bridge, and this quantity was converted to temperature through the calibration curve depicted in fig. 4. The calibration curve was prepared by the author against a glass bulb thermometer with a precision of $\pm \frac{1}{2}$ degree immersed in a water bath.

Room Temperature Spectra

Raman spectra of the preparations decribed above were

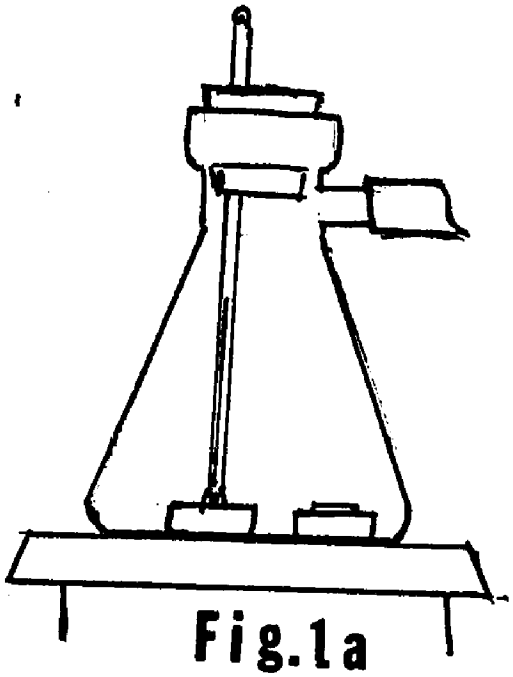

Fig.1a

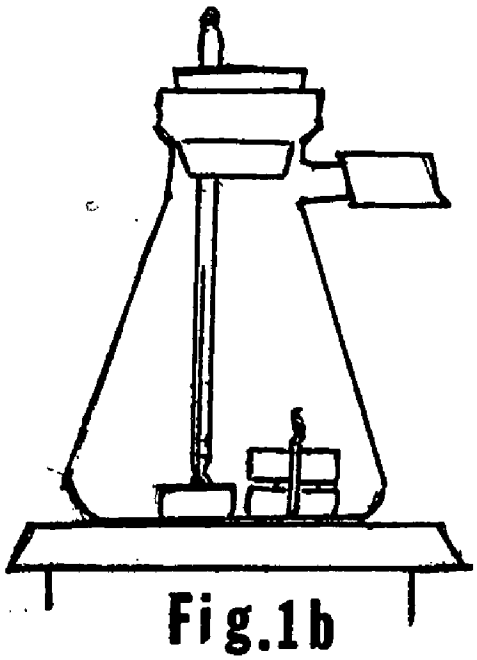

Fig.1b

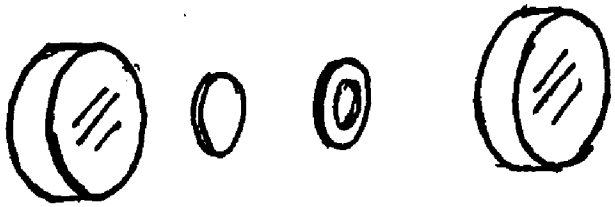

Fig.1c

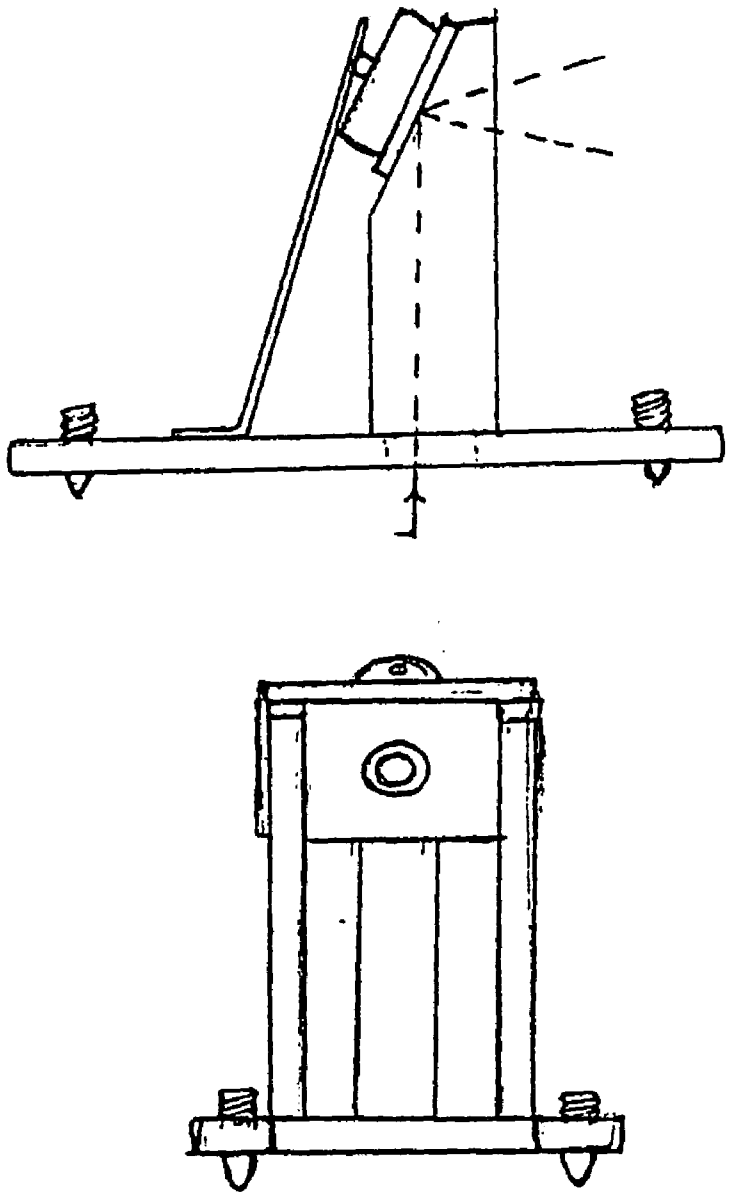

Fig. 2

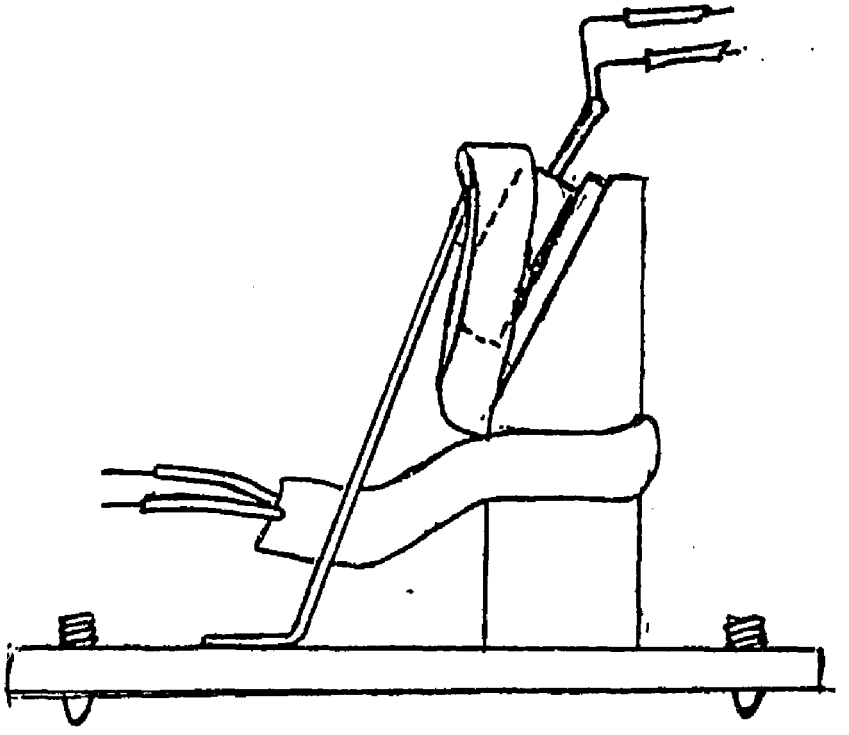

Fig.3

FIG.4

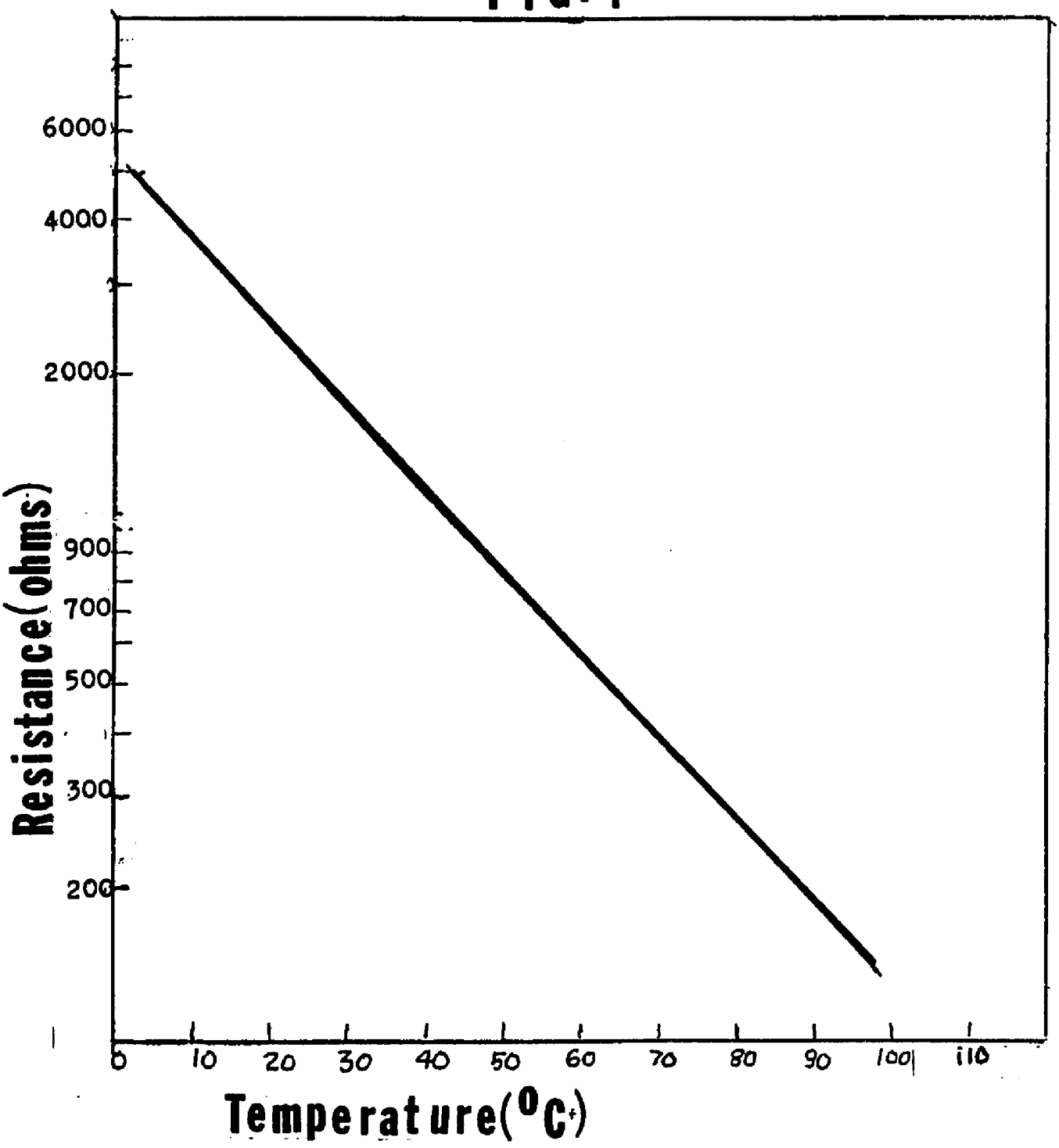

Resistance vs. log(temperature) curve for the thermister probe

obtained between 0 and 3200 cm^{-1} at room temperature. The entrance and exit slits were usually set at 100 microns (approximately 2 cm^{-1} band width), and the central slit was set at 120 microns. The scan rate was set such that

$$RATE \leq 60\,S/4RC$$

as recommended by the operating manual where s is the slit width in cm^{-1} RC is the time constant in seconds in the photon counting mode. The rate was in cm^{-1}/min. For all spectra the 4880 A laser line was used. The exciting light intensity was usually set at about 400 milliwatts.

For high resolution spectra the slit was set as narrow as 1 cm^{-1} and the scan rate as slow as 5 cm^{-1}/min.

High Temperature Spectra

High temperature spectra taken of PTBD samples fell into two categories. The first category were survey spectra taken between 0 and 3200 cm^{-1} and 80°C which is above the crystal phase transformation temperature. The second category were spectra of individual features in the spectrum at different temperatures near the phase transition temperature. High temperature spectra were usually more noisy than their room temperature counterparts so that these were usually run with longer time constants and larger slit widths. The temperature was controlled to within ±1°C, and enough time was given for the sample to equilibrate with the disk between runs.

Spectra for H63 and H63P* mats were obtained between

*H63 mat compressed under 25000 psi pressure in a hydraulic press

50 and 300 cm^{-1} at different temperatures between 25° and 80°C. Spectra were also obtained in the 1300 to 1350 cm^{-1} and 2700 to 3100 cm^{-1} regions.

RESULTS

Figs. 5 - 11 depict typical Raman spectra for different preparations of crystalline PTBD at room temperature. No bands occur in the 1700 - 2700 cm^{-1} range so this region has been omitted. The spectrum of H63 crystals at 77°C is shown in fig. 12. The frequencies of the spectra mentioned above as well as those of T23 and T23A crystals and those given by Cornell and Koenig for PTBD rubber are tabulated in Tables I and II. The above crystalline spectra are in substantial agreement with those given by Hsu et al(20).

Generally for H63 crystals the bands at 238, 761, 1150 and 1437 cm^{-1} are found to undergo substantial reduction in height relative to the constant 1666 cm^{-1} band upon annealing, melt recrystallization, melting and quenching in liquid nitrogen and compression under 25000 psi pressure. A 40% reduction in the height of the 238 cm^{-1} band is observed. Similar reductions in the intensities of the 238, 761, 1150 and 1437 cm^{-1} bands are also observed for crystals precipitated from toluene at 23°C.

The ratio of the 1331 cm^{-1} band height to that of 1311 cm^{-1} band, which has recently been used as a measure of order(20) is tabulated in Table III. The I_{1331}/I_{1311} ratio is 1.2 for H63 crystals and ranges from 1.4 to 1.8 for all of the previously mentioned preparations. Hsu et al(20) have also reported that the 529 cm^{-1} band sharpens upon annealing. A high resolution scan of this band is shown in fig.13.

The 946 cm^{-1} band which occurs in the H63, H43, H23

and T23 spectra as well as the bands in the 1050-1090 cm^{-1} range of H63, H43, and H23 spectra disappear when these crystals are annealed, compressed or recrystallized from the melt. The lattice vibration band which occurs at 70 cm^{-1} in the H63 spectrum shifts to 63 and 55 cm^{-1} in the H43 and H23 spectra respectively.

Considerable changes occur in the PTBD Raman spectrum as the sample is heated from room temperature to above the transition temperature(viz. 71 -76°C). Figs. 14 - 16 show changes which occur in the 50 - 300, 1300 - 1350 and 2800 - 3050 cm^{-1} regions as the sample is heated above the transition temperature. The bands at 1437, 1311, 238 and 90 - 120 cm^{-1} shift to lower frequencies at temperatures above 50 - 65°C while bands at 761 and 529 cm^{-1} shift to higher frequencies. The 2900, 2930 and 2946 cm^{-1} bands merge to form a broad band at 2908 cm^{-1} with a higher frequency shoulder. Above the phase transition temperature the bands at 946, 967, 1050 - 1090, and 1150 cm^{-1} disappear. The bands at 761 and 529 cm^{-1} become so diffuse that their frequencies cannot be determined. The 238 and 90 - 120 cm^{-1} bands become merged with the background forming a broad continuum between 0 and 200 cm^{-1}. The band heights of all the bands tend to decrease above the transition temperature with accompanying increases in band width(see fig 11)

Table I

Rubber[a]	H(63)	H(43)	H(23)	H(63)A	H(63)MR	H(63)P[b]	H(63)MQ
	70	63	55	73	70	70	67
	80	85	83	85	85	83	80
	100	100	100	100	100	100	100
	116	116	116	120	115	117	120
221	238	238	238	238	238	238	238
	529	529	529	532	529	529	529
537						534	
761	761	761	761	761	761	761	761
	946	946	946				
969	968	967	967	967	967	967	965
1011	1016	1016	1016	1016	1016	1015	1015
		1063	1050				
		1090	1090				
1124	1150	1150	1150	1152	1150	1152	1150
1267	1270	1270	1270	1270	1269	1270	1267
1301	1311	1311	1311	1310	1310	1311	1310
1324	1331	1331	1331	1330	1330	1331	1330
1431	1437	1437	1437	1436	1437	1437	1437
			1640	1640	1640		1640
1664	1666	1666	1666	1666	1666	1666	1666
2846	2839	2839	2837	2837	2838	2839	2838
2876	2879	2879	2878	2878	2878	2882	2880
2898	2899	2900	2898	2898	2897	2899	2899
		2908					
	2920	2920	2920	2918	2918	2920	2920
2932	2947	2947	2944	2943	2843	2947	2946
3003	2998	2999	2999	2997	2997	3000	2999

Raman spectral frequencies for various preparations of PTBD. Frequencies are in $cm.^{-1}$

a. taken from reference 36

b. H63 crystals compressed under 25000 psi pressure

Table II

T(23)	T(23)A	H(63)at 77°C	Assignments*
		0-300	Rotational -translational lattice vibrations
	85	continuum	
100	95		
	103		
235	238		C-C torsion, C-C st.
530	529		CCC def., O.P. CH bend
761	761		CH rock, O.P. def.
946			
967	967		CH rock, C-C st., CCC def
1018	1017	1014	C-C st.
1150	1152		C-C st.,CH rock, CCC def.
1270	1270	1270	CH wag,CH bend,CC st.
1310	1311	1305	CH_2 twist, CH_2 wag, CH i.p. bend
1330	1331	1338	
1435	1435	1430	CH_2 bend
1640	1640		
1666	1666	1666	C=C st., CH i.p. def, CC st.
2838	2839	2843	CH_2 sym. st.
2878	2879	2879	
2898	2899		CH_2 assym. st. overtones and combinations
2918	2918		=CH st.
2944	2946	2905	
2998	3000	2999	

Raman spectral frequencies for various preparations of crystalline PTBD. Frequencies are in $cm.^{-1}$

*Based on single chain normal vibration calculations by Neto and di Lauro(18)

Table III

H63	H43	H23	H63A	T23A
1.19	1.62	1.52	1.73	1.55

H63P	H63MQ	H63MR	T23A
1.62	1.85	1.84	1.55

I_{1331}/I_{1311} ratios for various preparations of crystalline PTBD

Captions for Figs. 5-12

Raman spectra for various preparations of crystalline PTBD

5. H23 crystals

6. H43 crystals

7. H63 crystals

8. H63P - H63 crystals pressed under 25000 psi pressure

9. H63A - H63 crystals annealed at 80°C

10. H63MQ - H63 crystals melted then quenched in liquid nitrogen

11. H63MR - melt recrystallized H63 crystals

12. H63 crystals at 77°C

In all cases the 1700-2700 cm^{-1} region is not shown because no bands occur in this region.

G = grating ghost

FIG.5a

H23

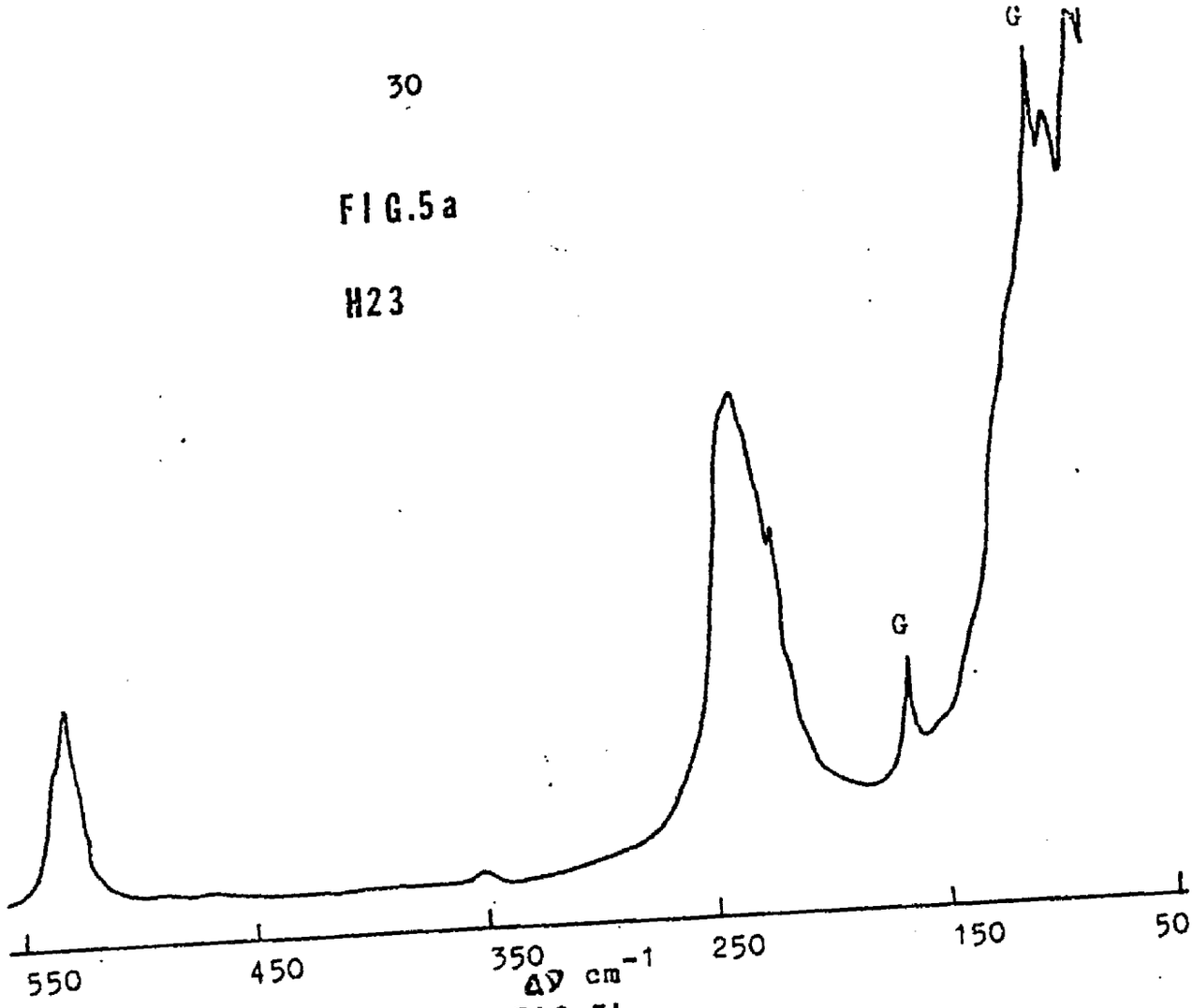

FIG.5b

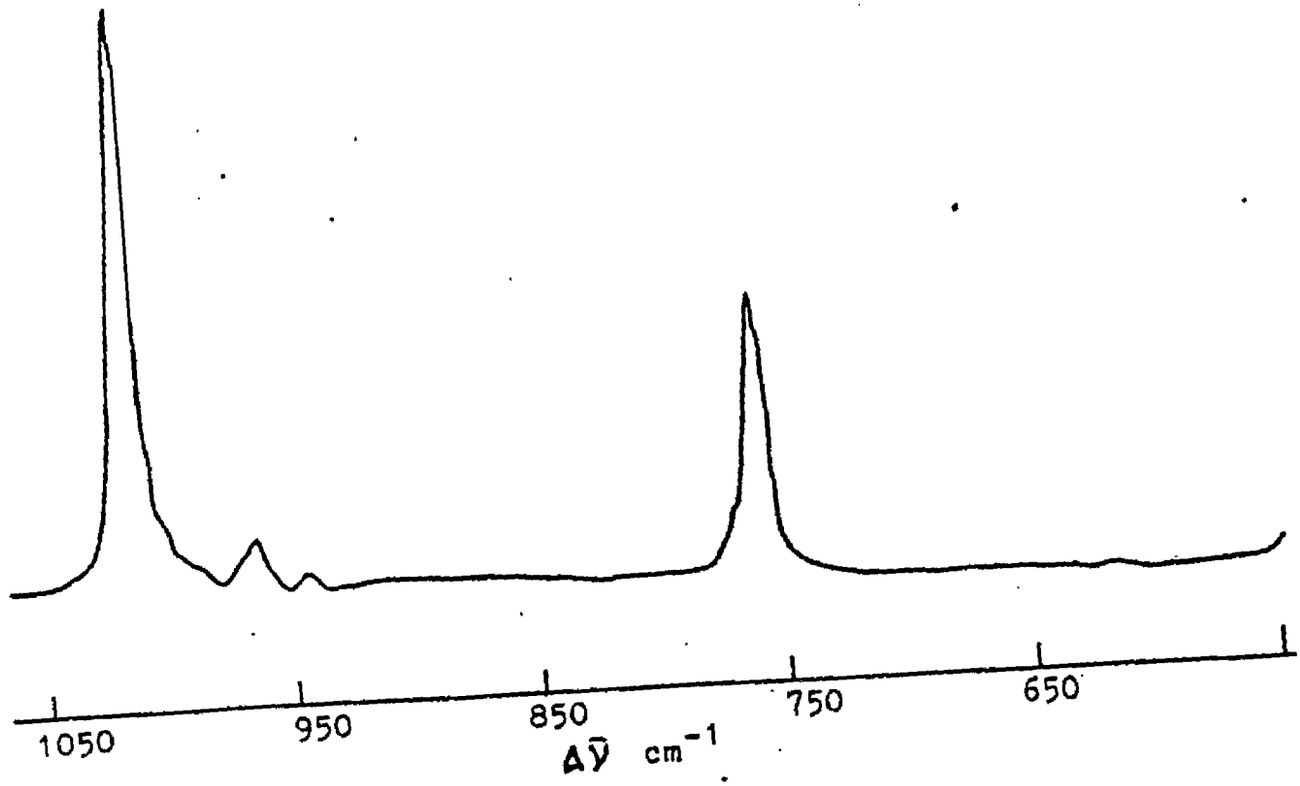

FIG.5c

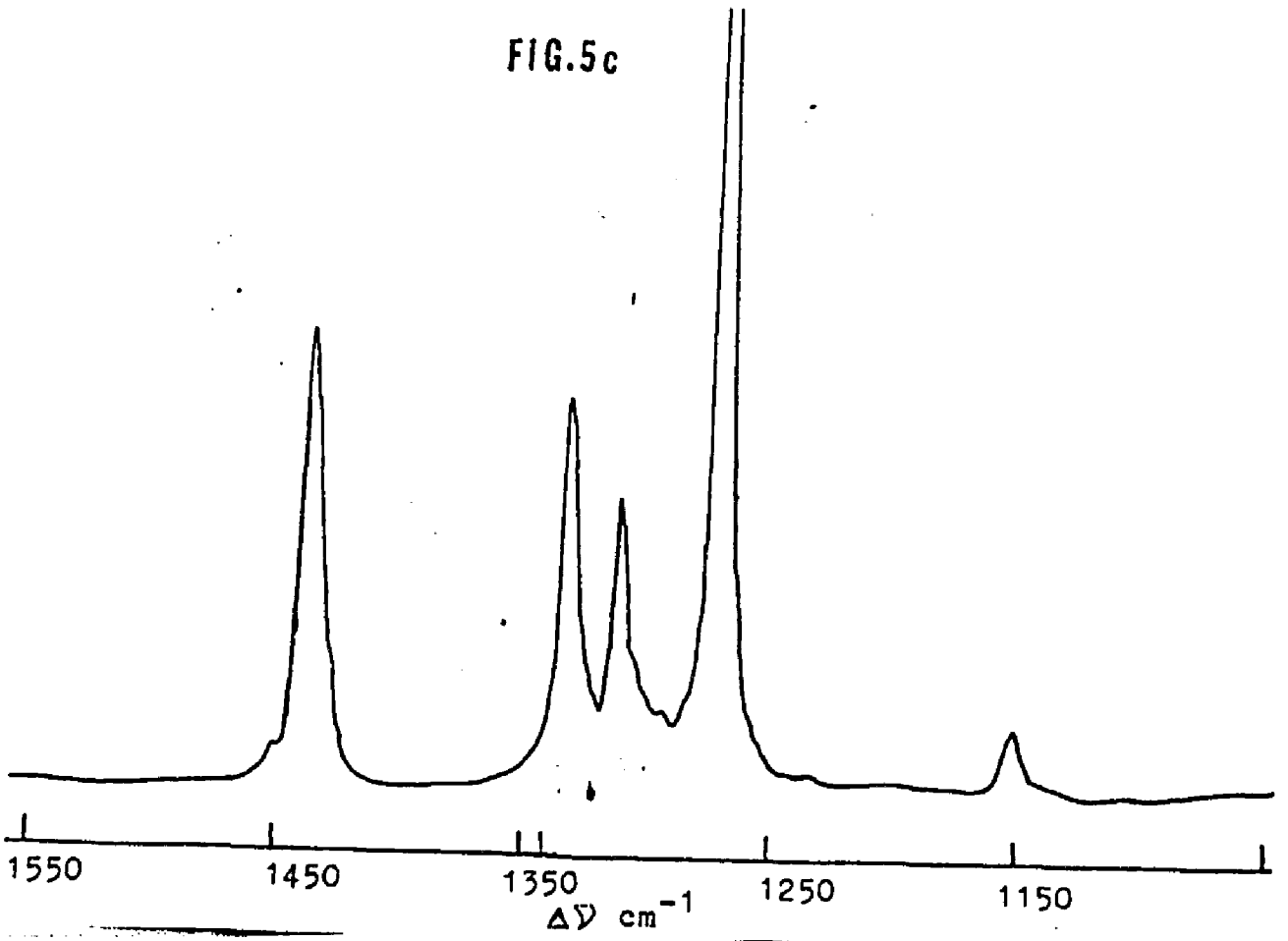
1550
1450
1350
1250
1150
Δν̃ cm-1

FIG.5d

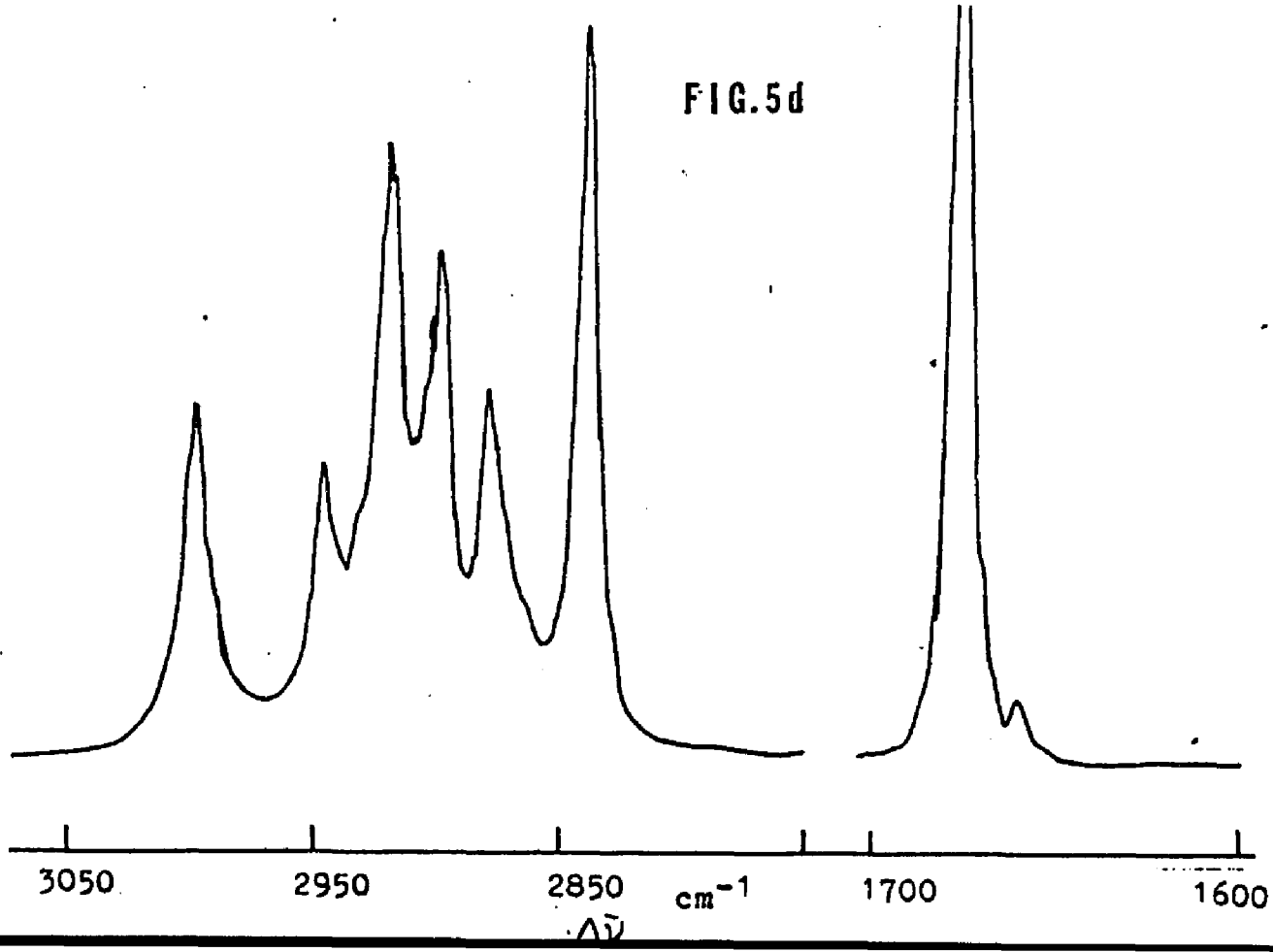
3050
2950
2850
cm-1
1700
1600
Δν̃

FIG. 6a
H43

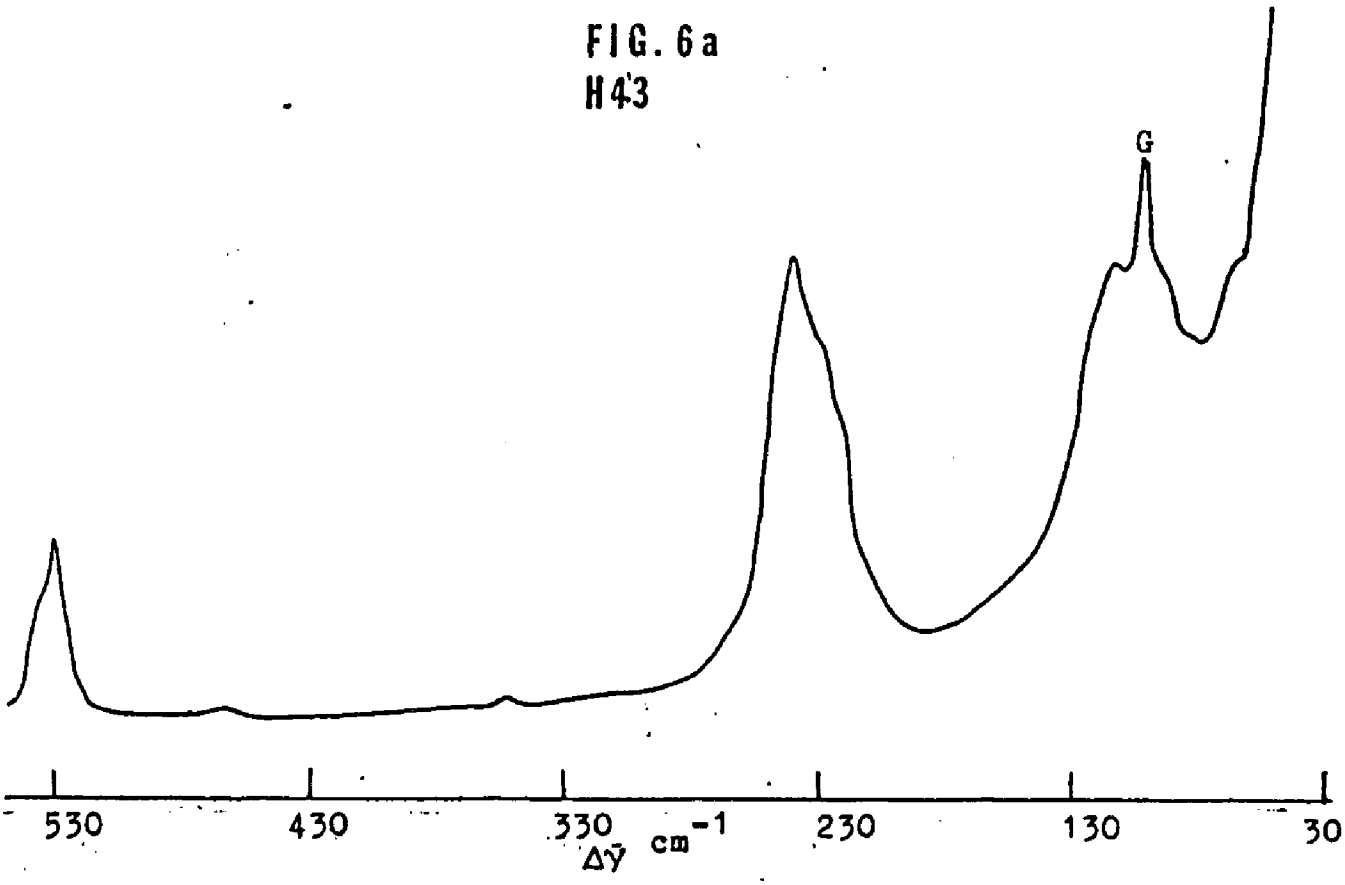

FIG. 6b

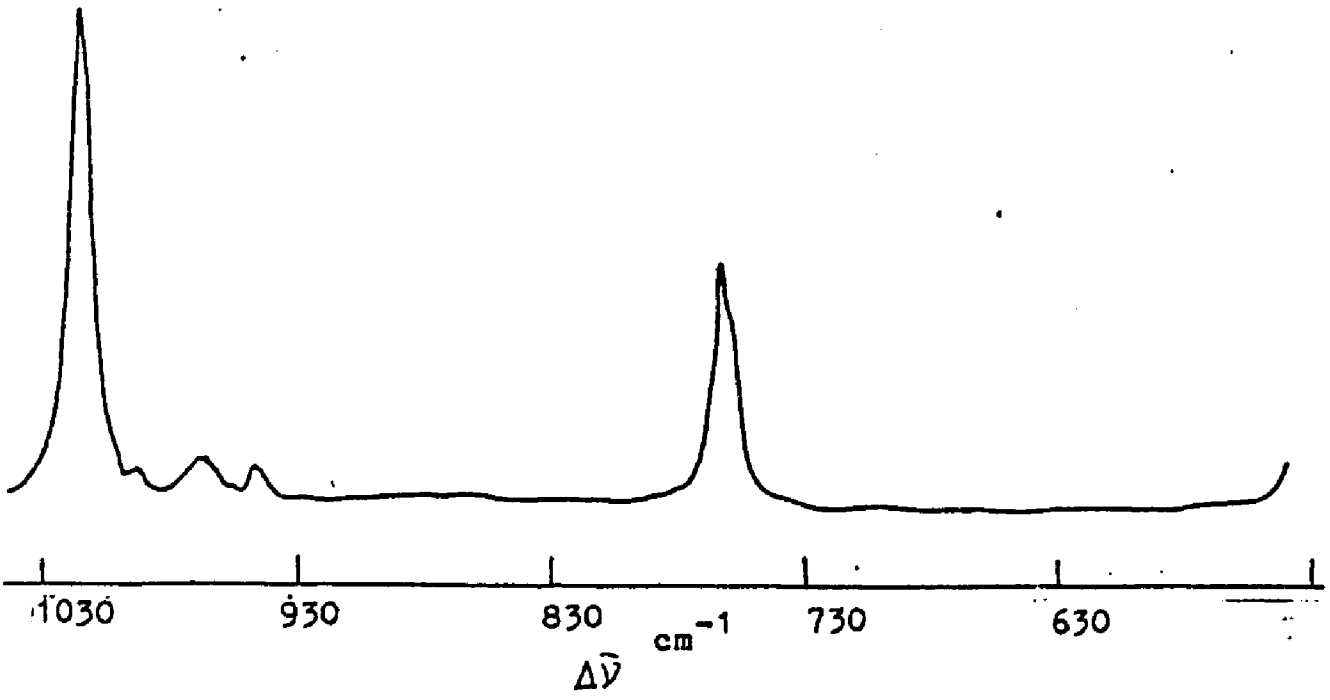

FIG.6c

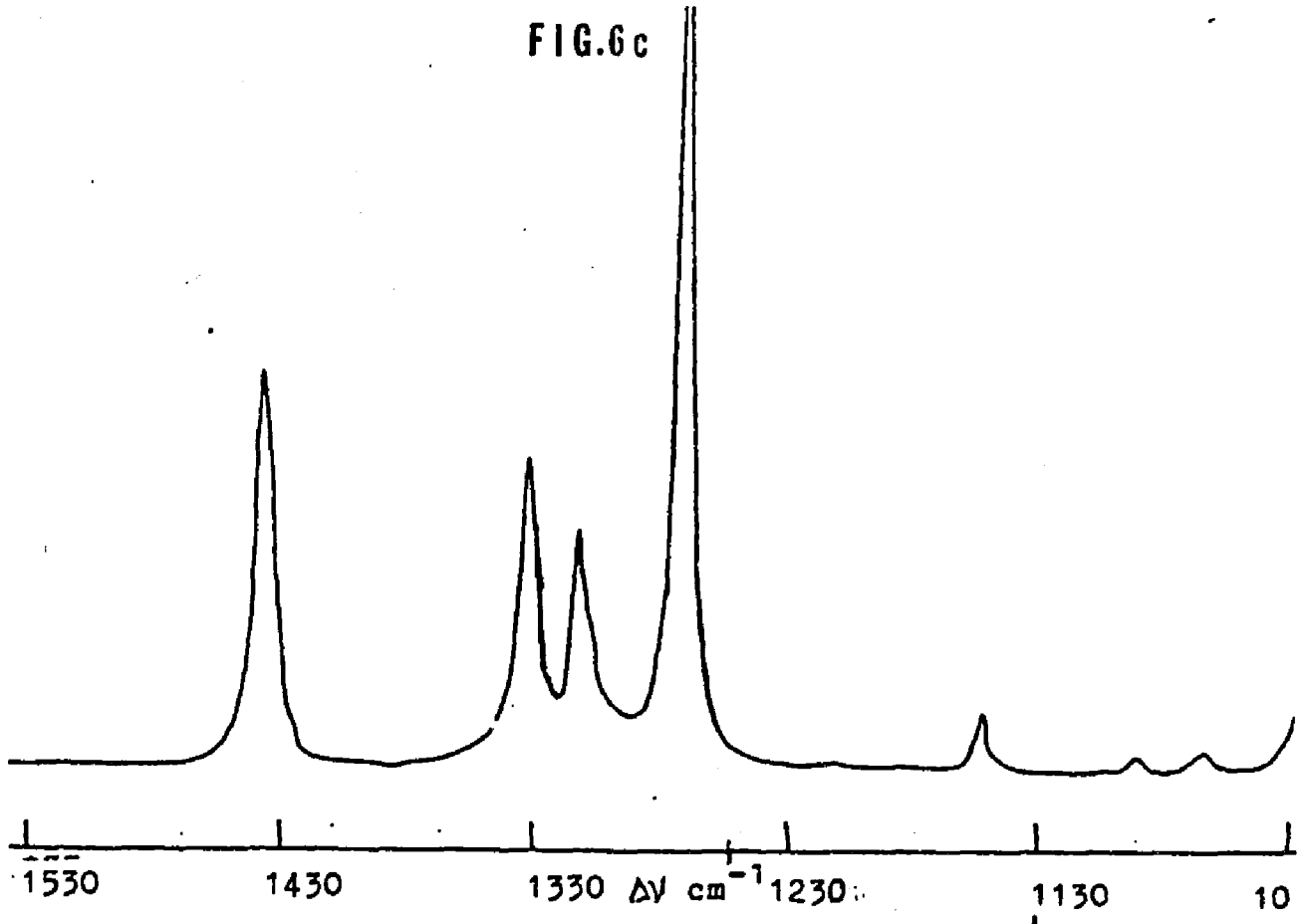
1530
1430
1330
Δν cm⁻¹
1230
1130
10

FIG.6d

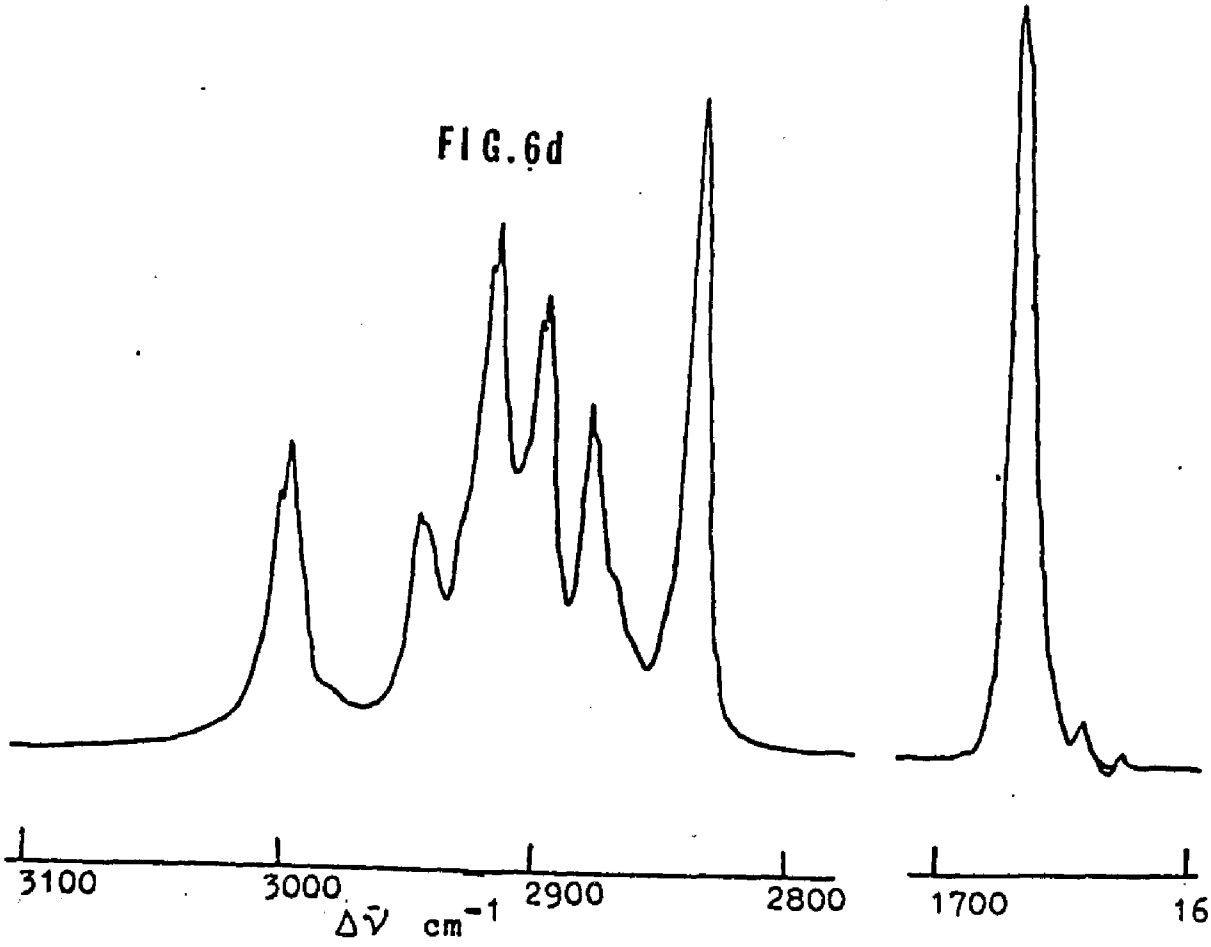
3100
3000
2900
2800
Δν̃ cm⁻¹
1700
16

FIG.7a
HG3

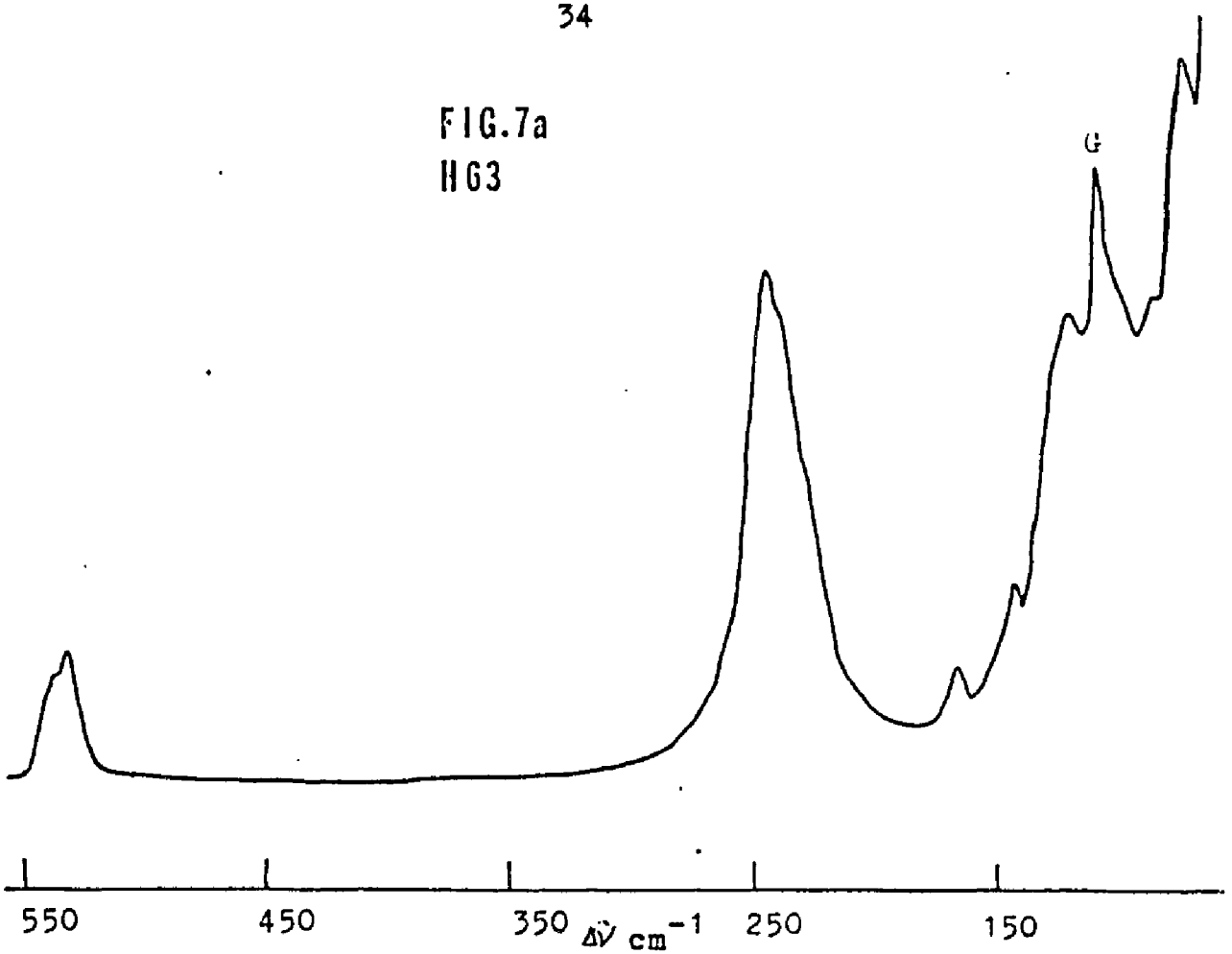

FIG.7b

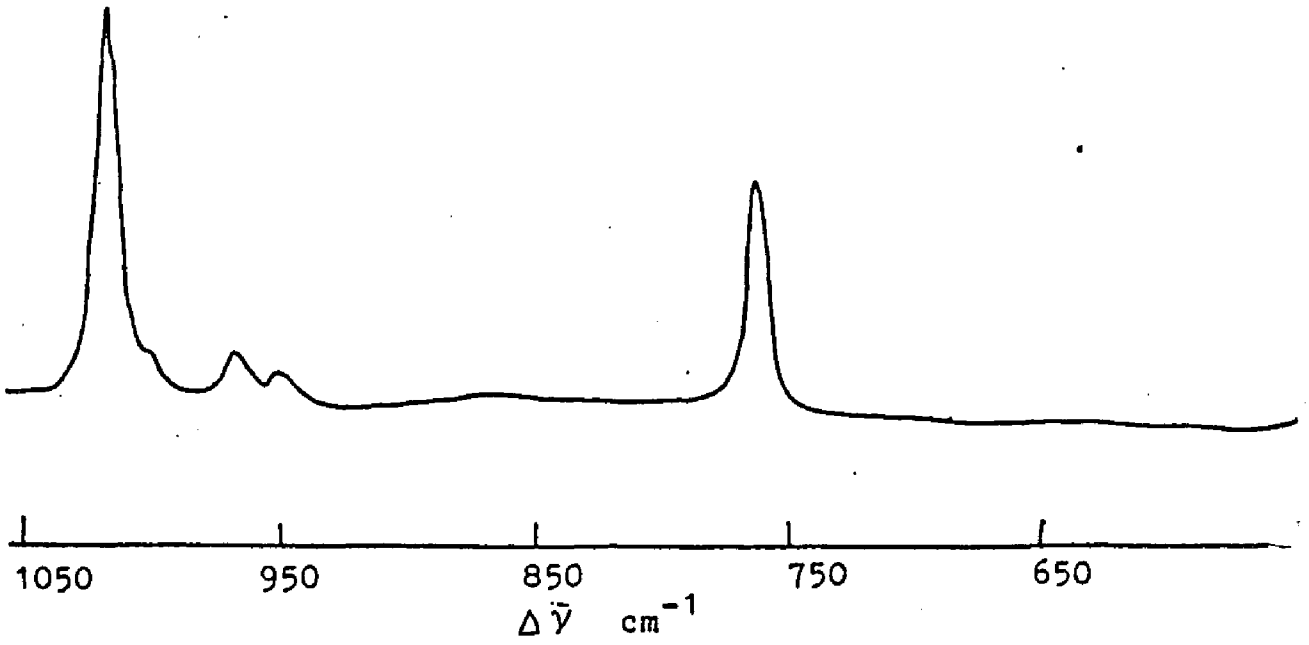

FIG.7c

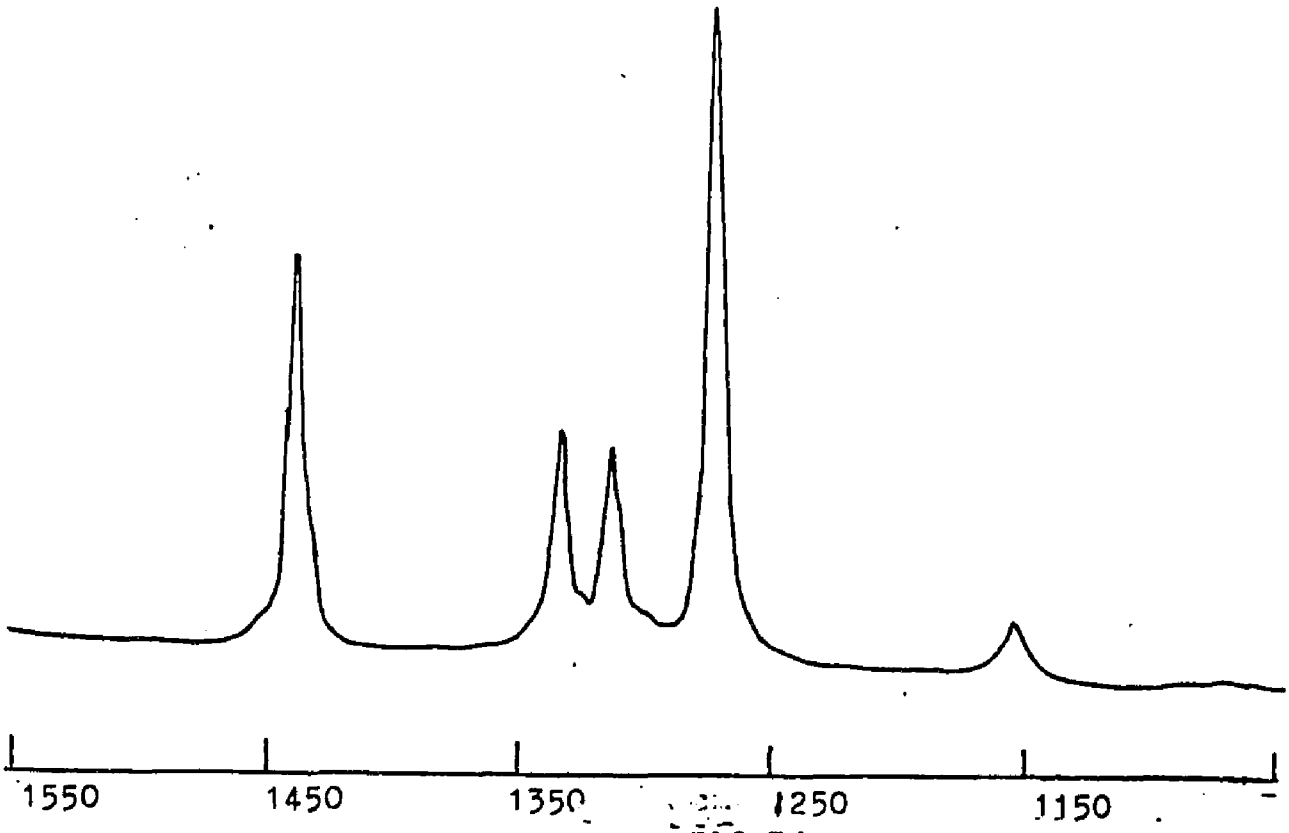

FIG.7d

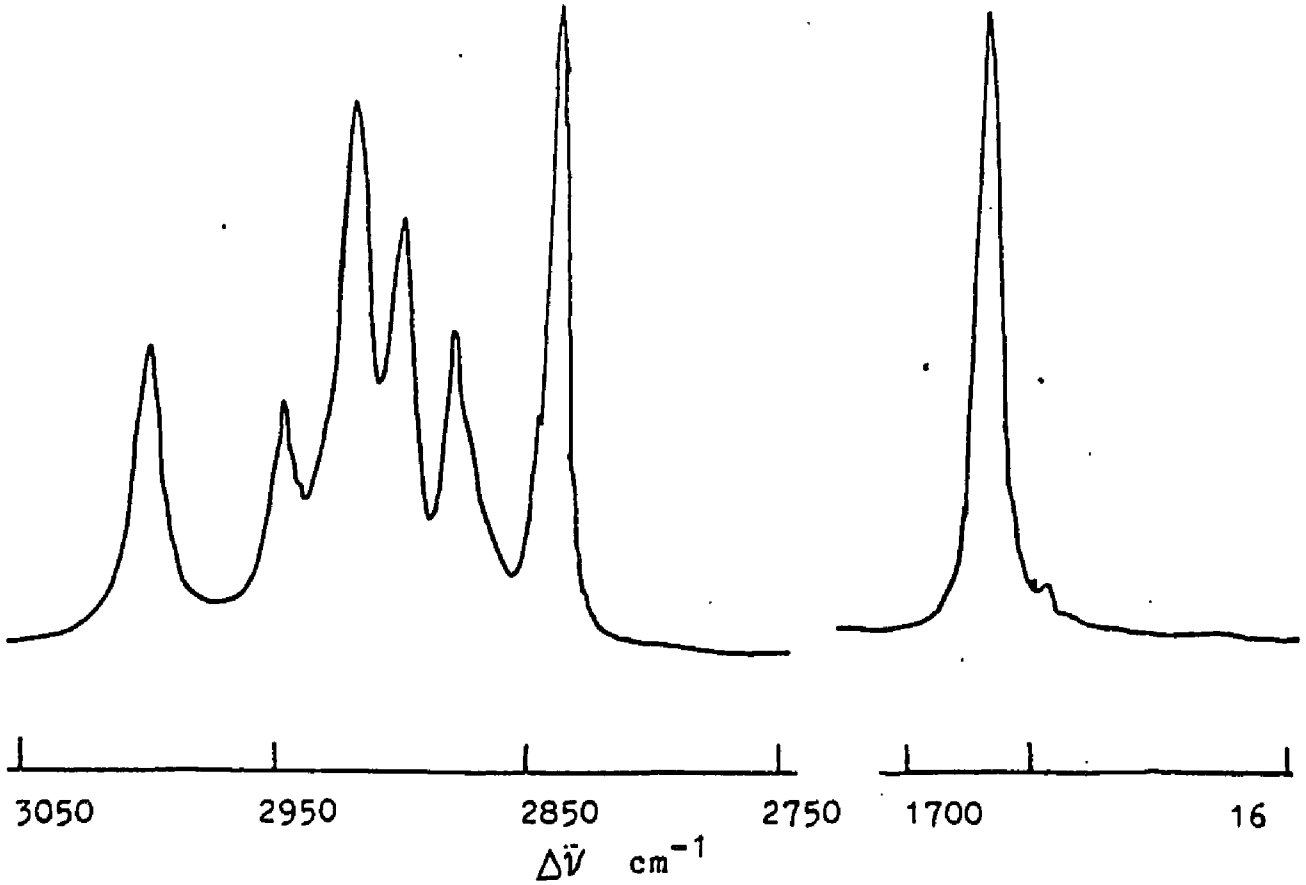

FIG.8a
H63P

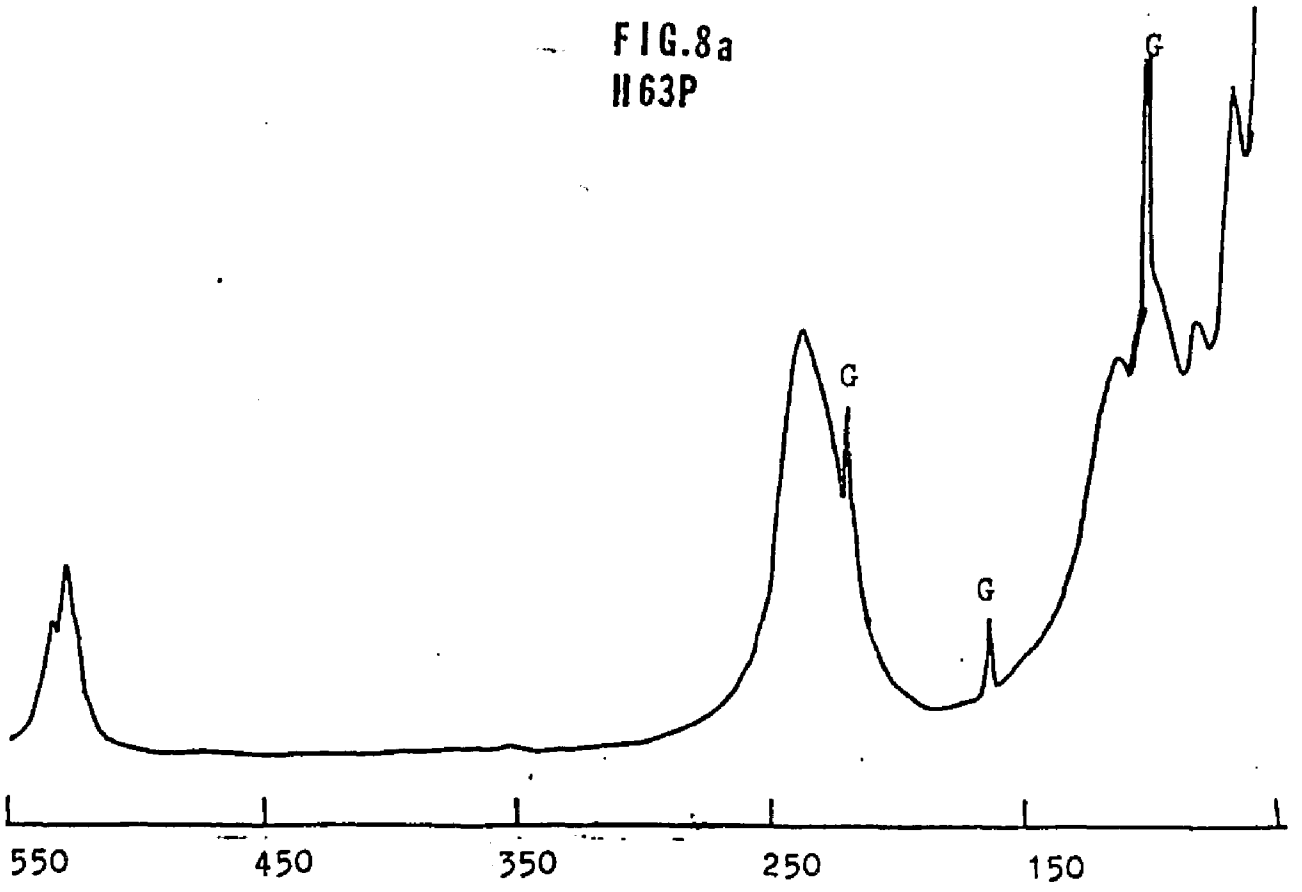

FIG.8b

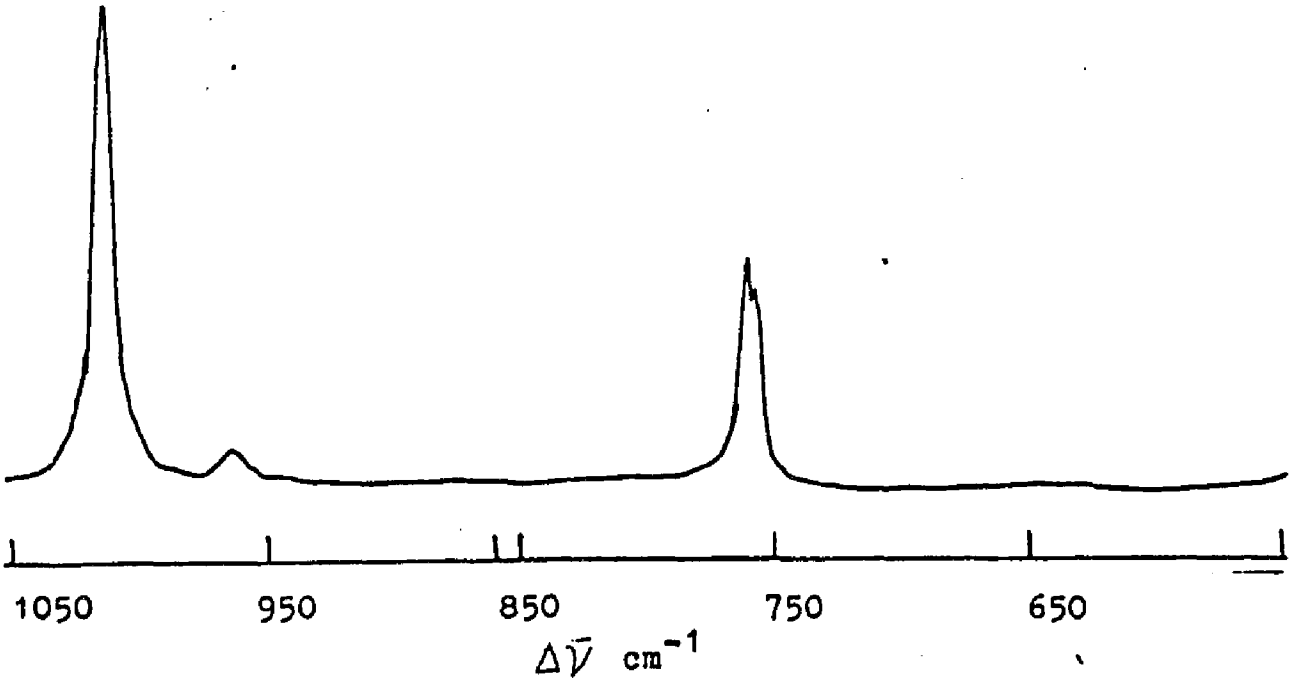

FIG.8d

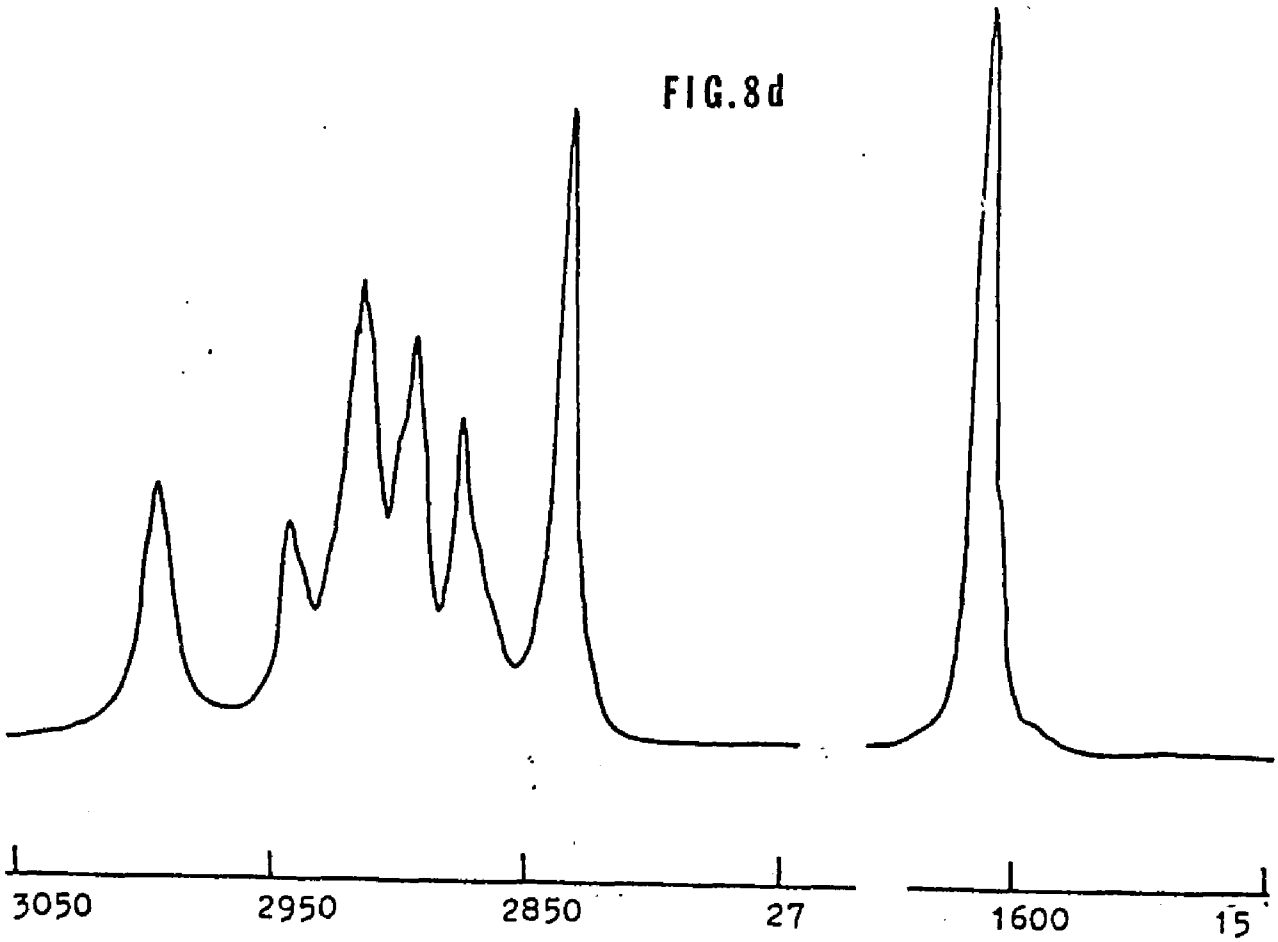

FIG.8c

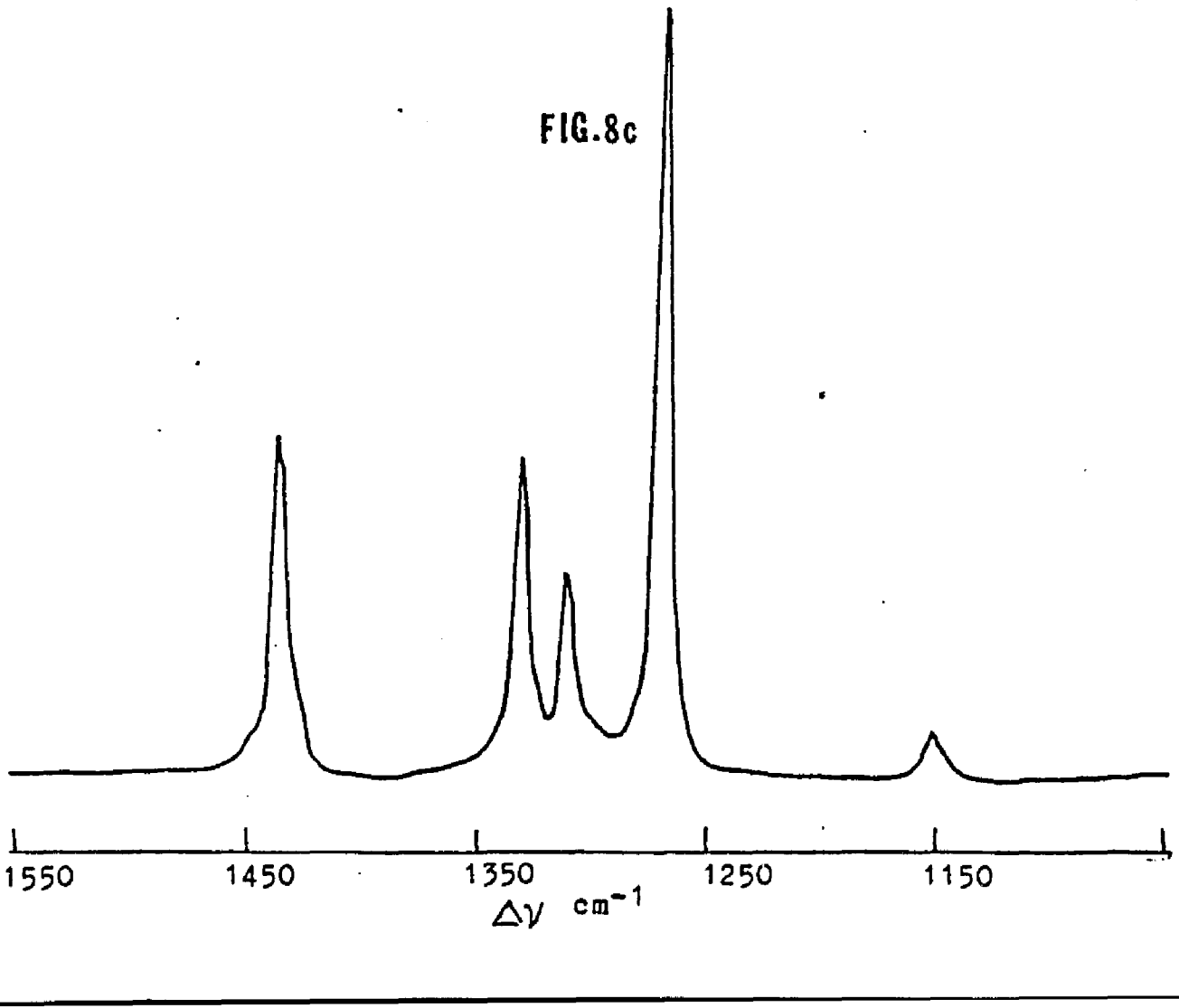

FIG.9a

H63A

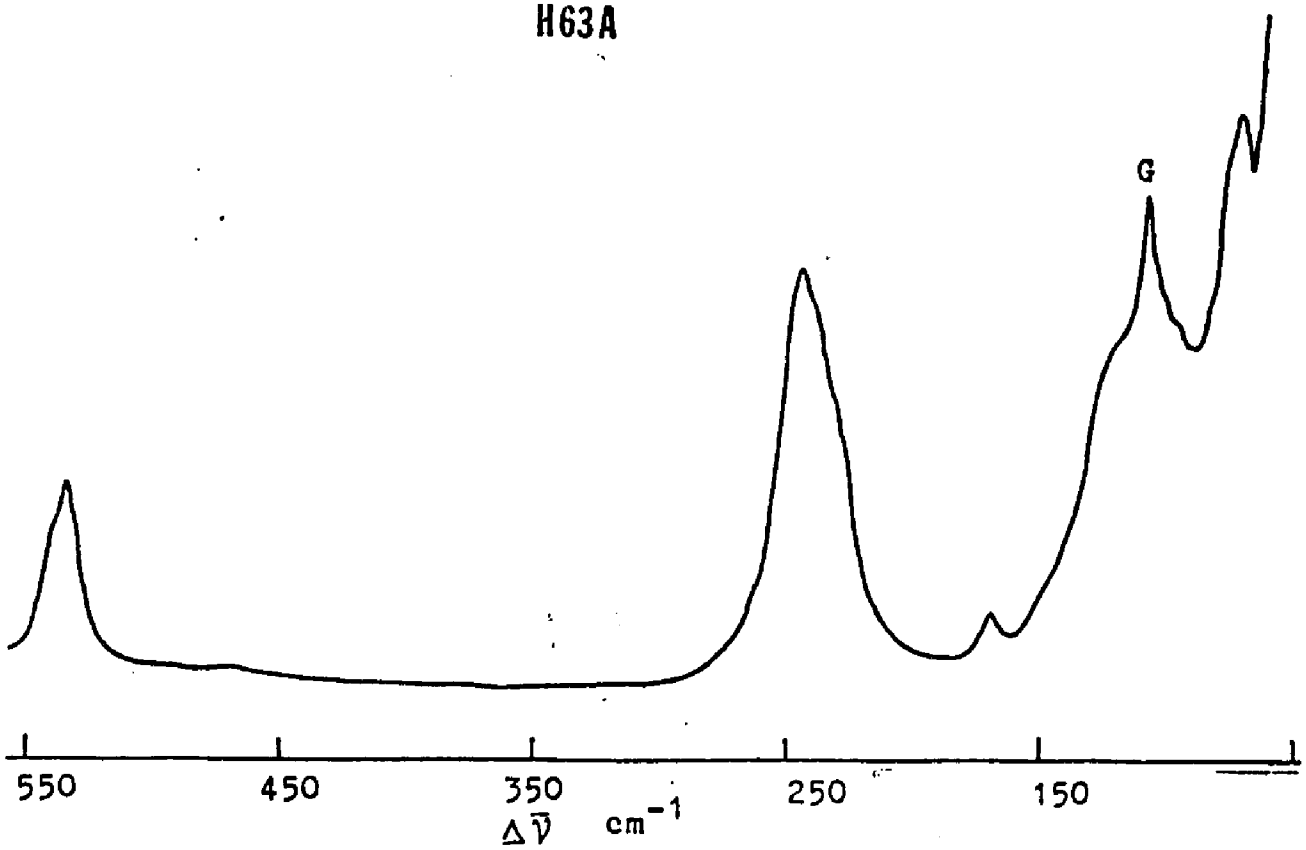

FIG.9b

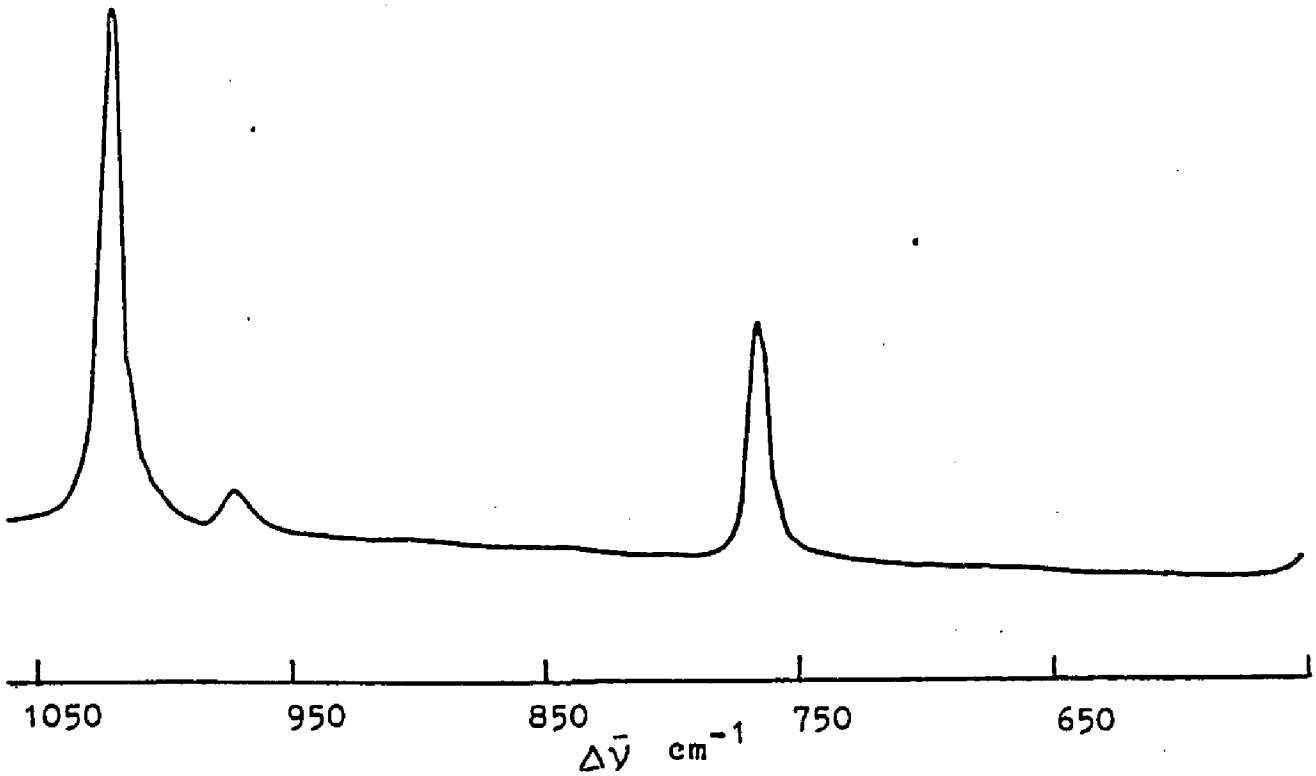

FIG.9c

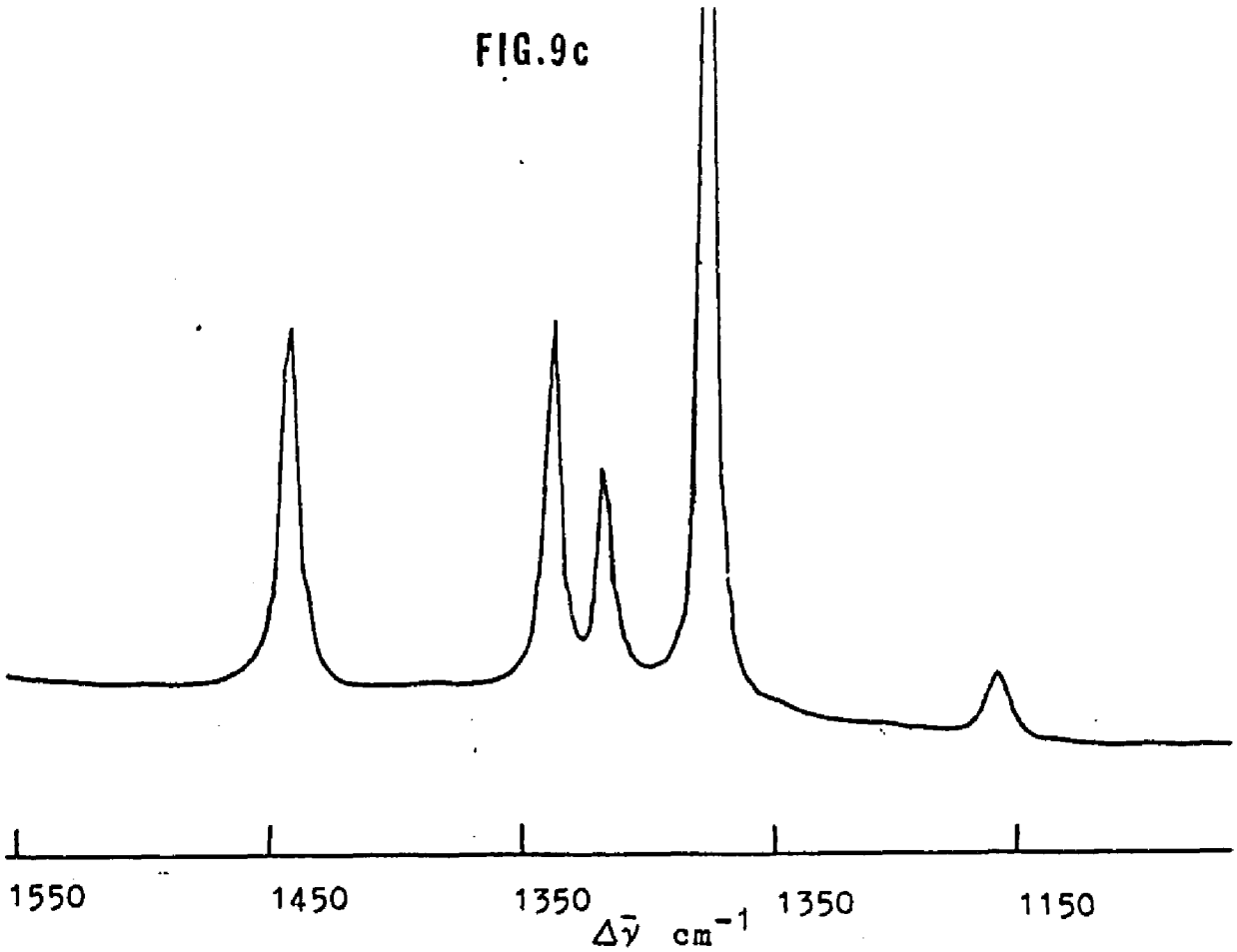
1550
1450
1350
1350
1150
$\Delta\bar{\nu}$ cm^{-1}

FIG.9d

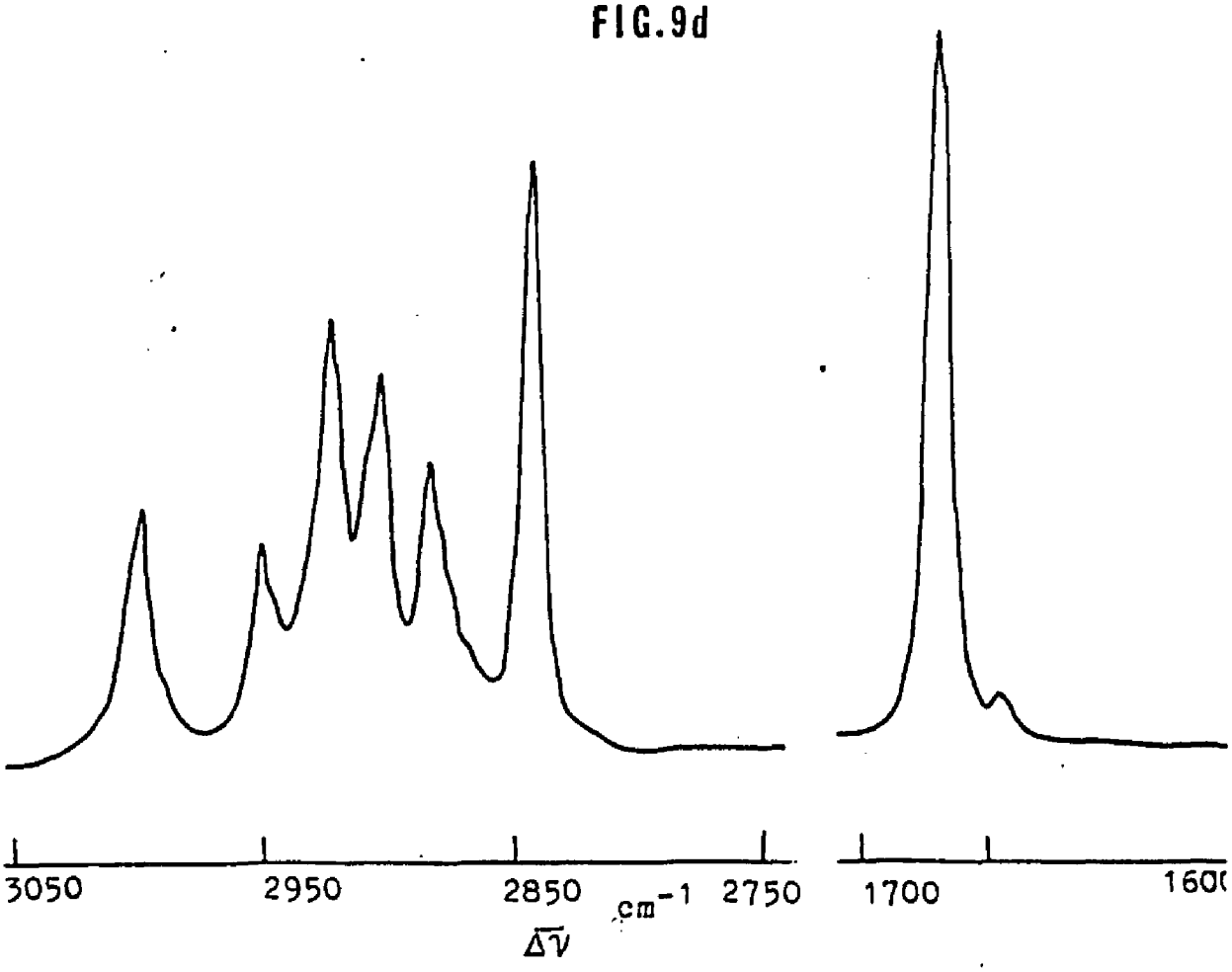
3050
2950
2850
2750
cm^{-1}
$\Delta\bar{\nu}$
1700
160(

FIG.10a
H63MQ

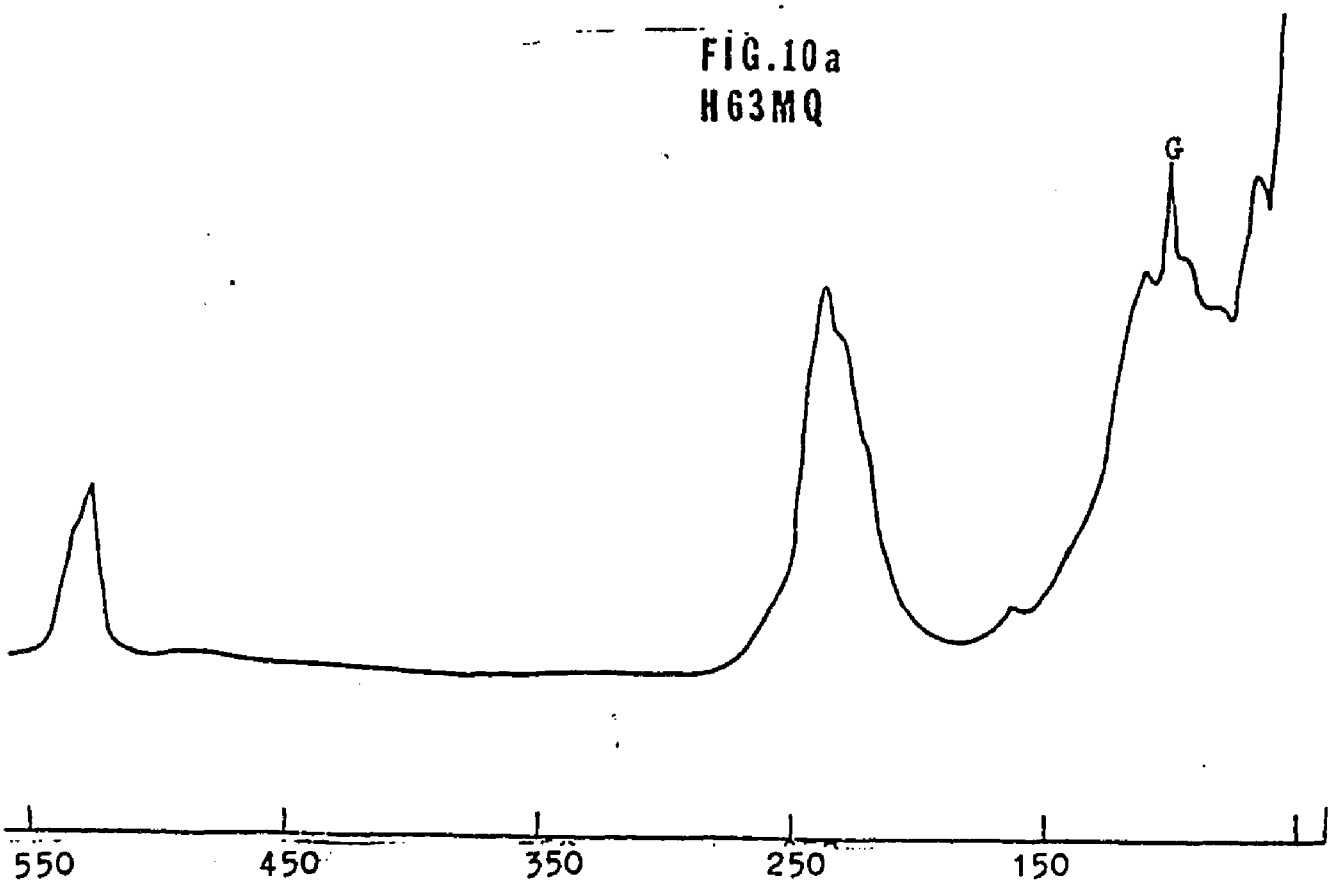

FIG.10b

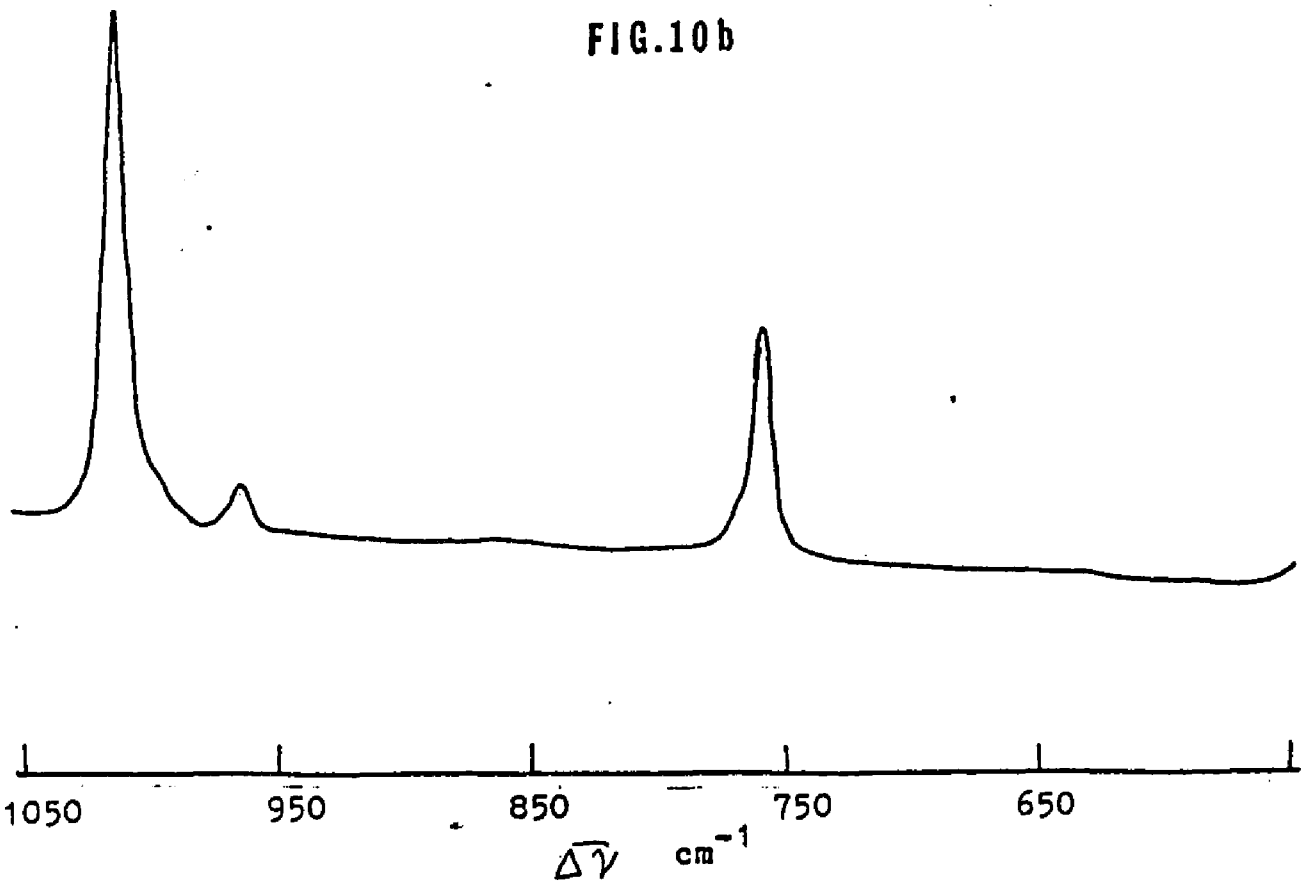

FIG.10c

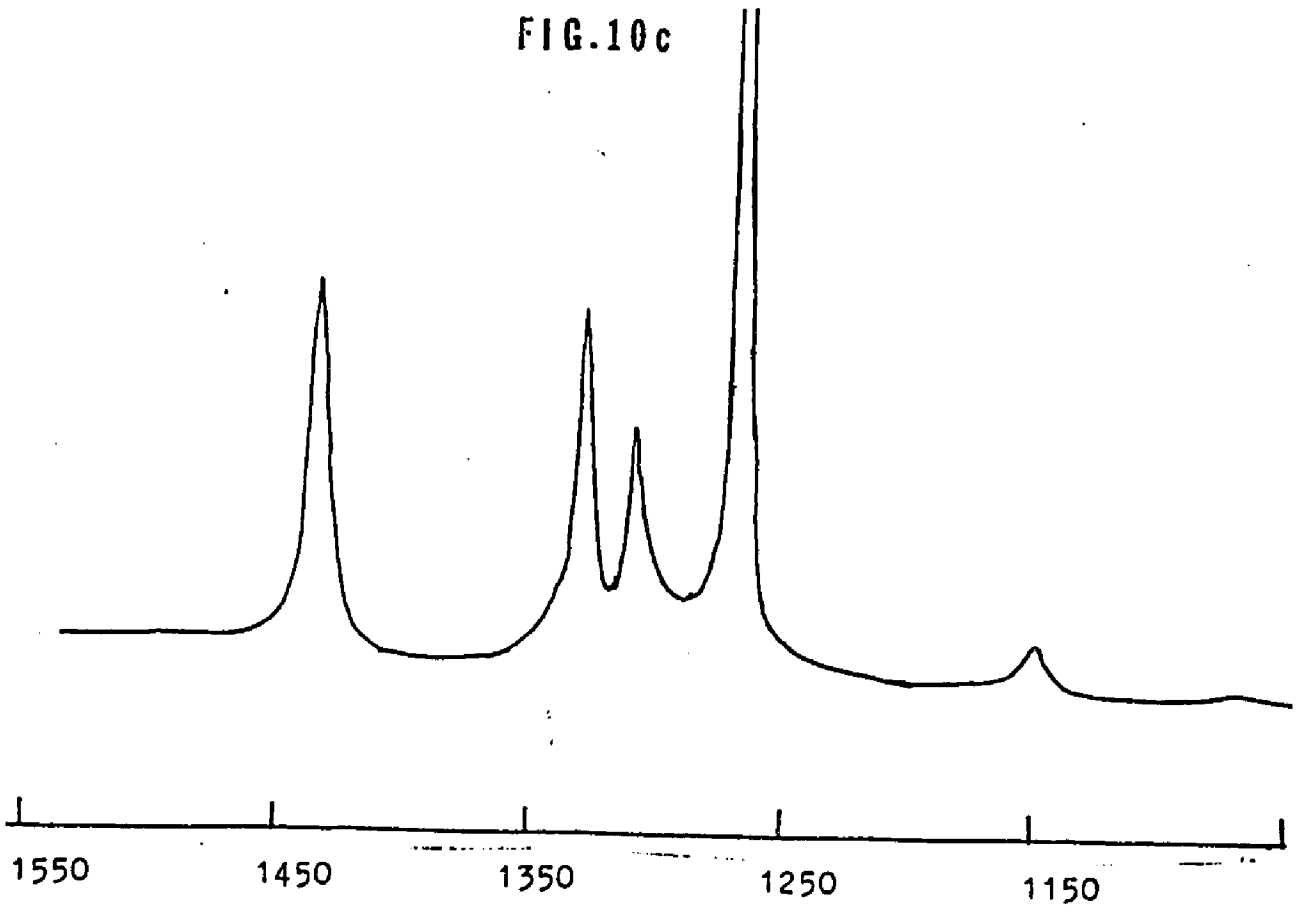

FIG.10d

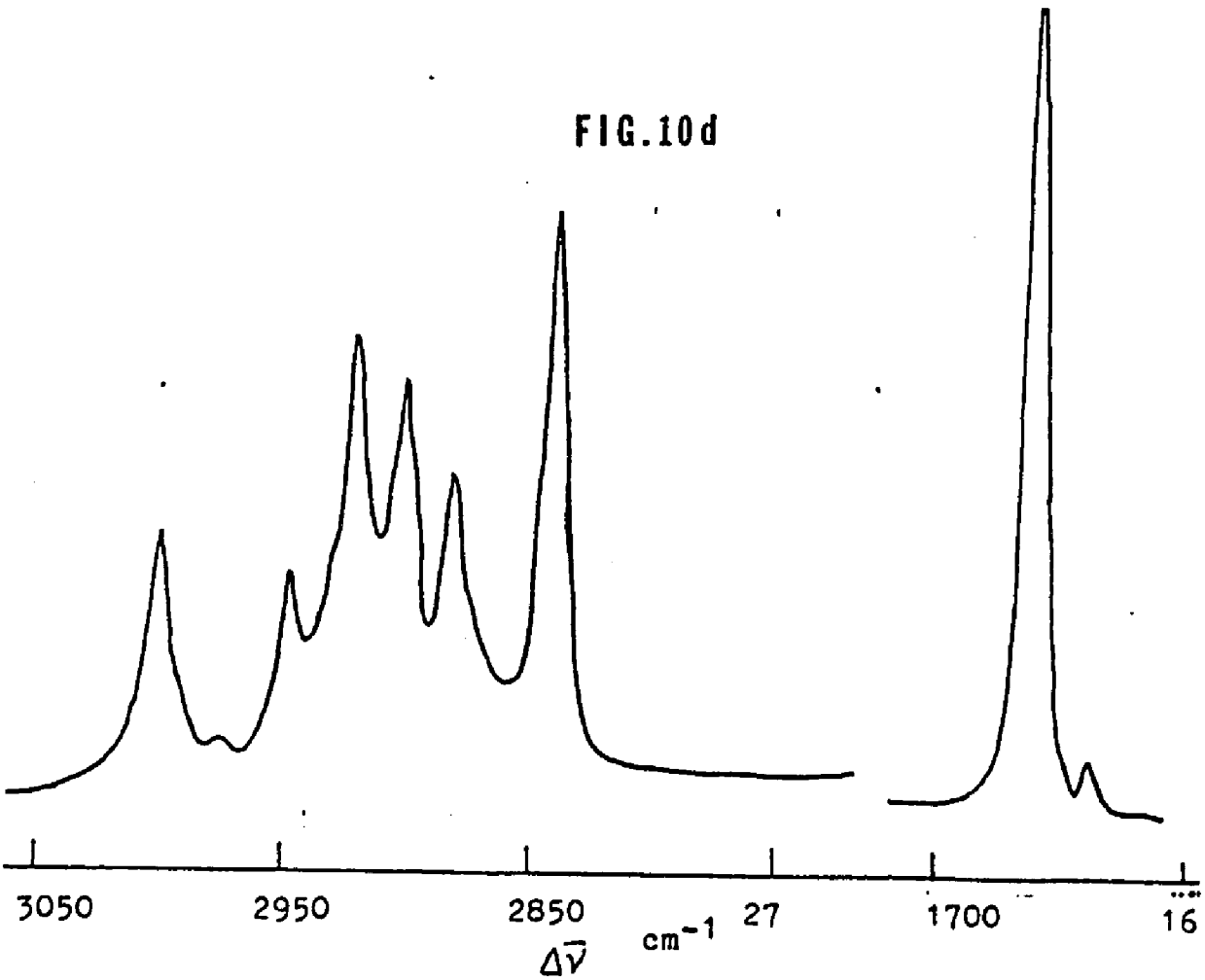

FIG.11 a
H63MR

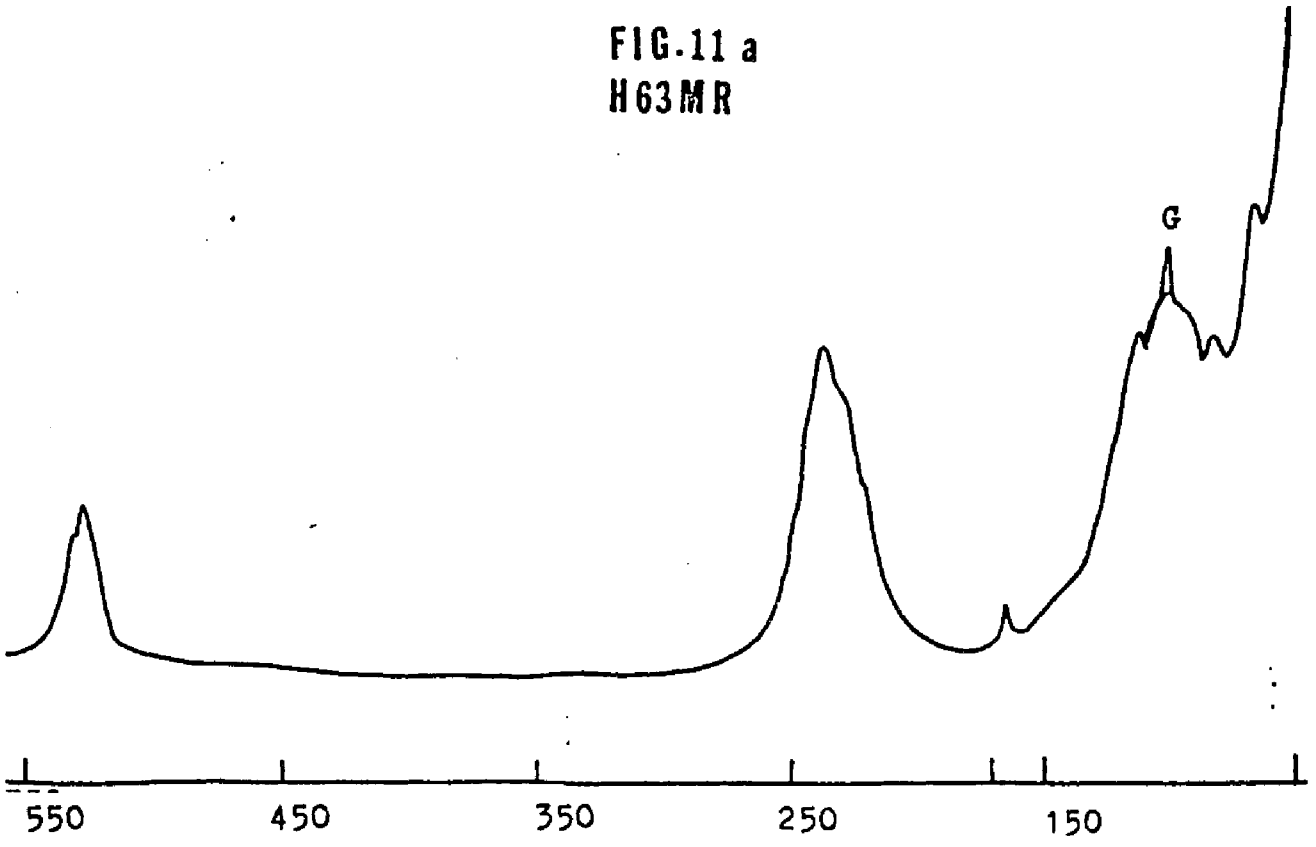

FIG.11b

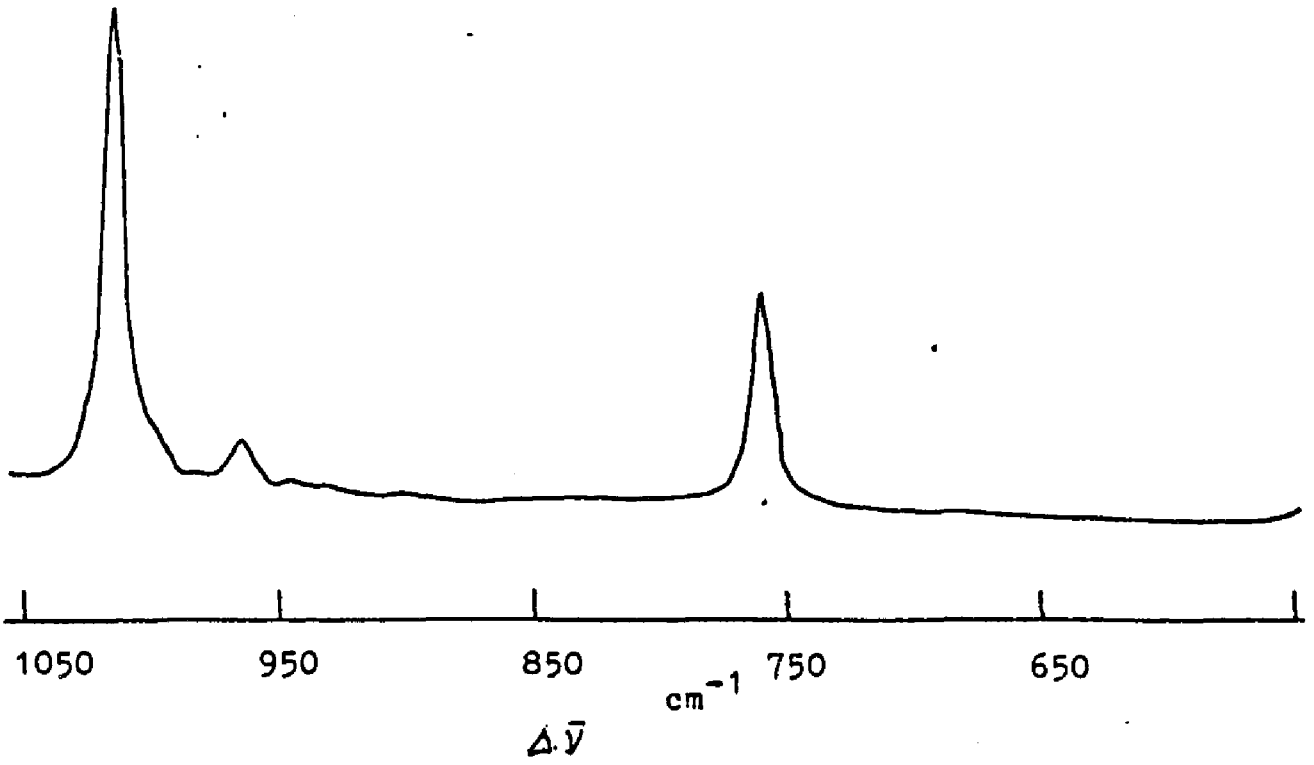

FIG.11c

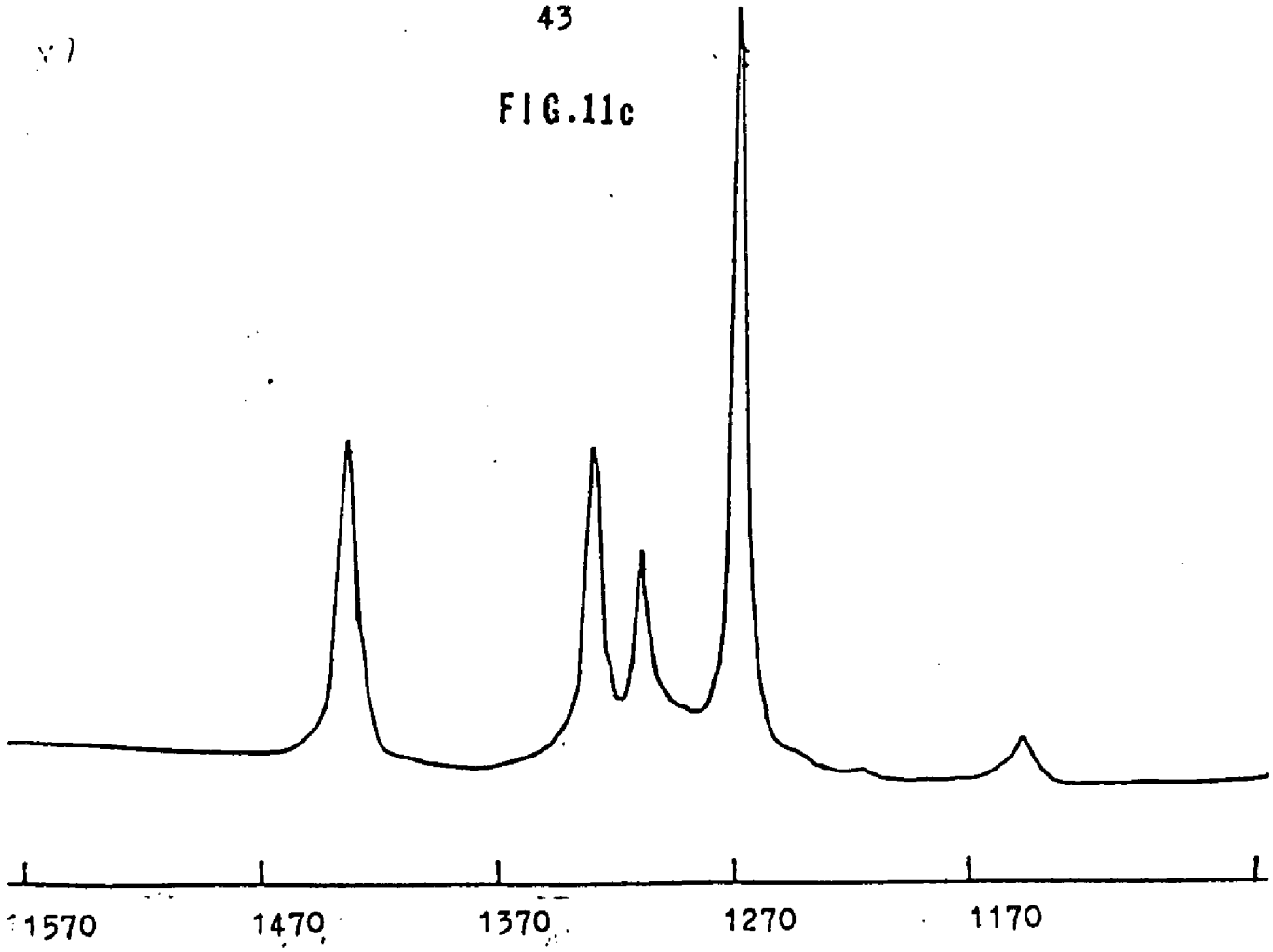

FIG.11d

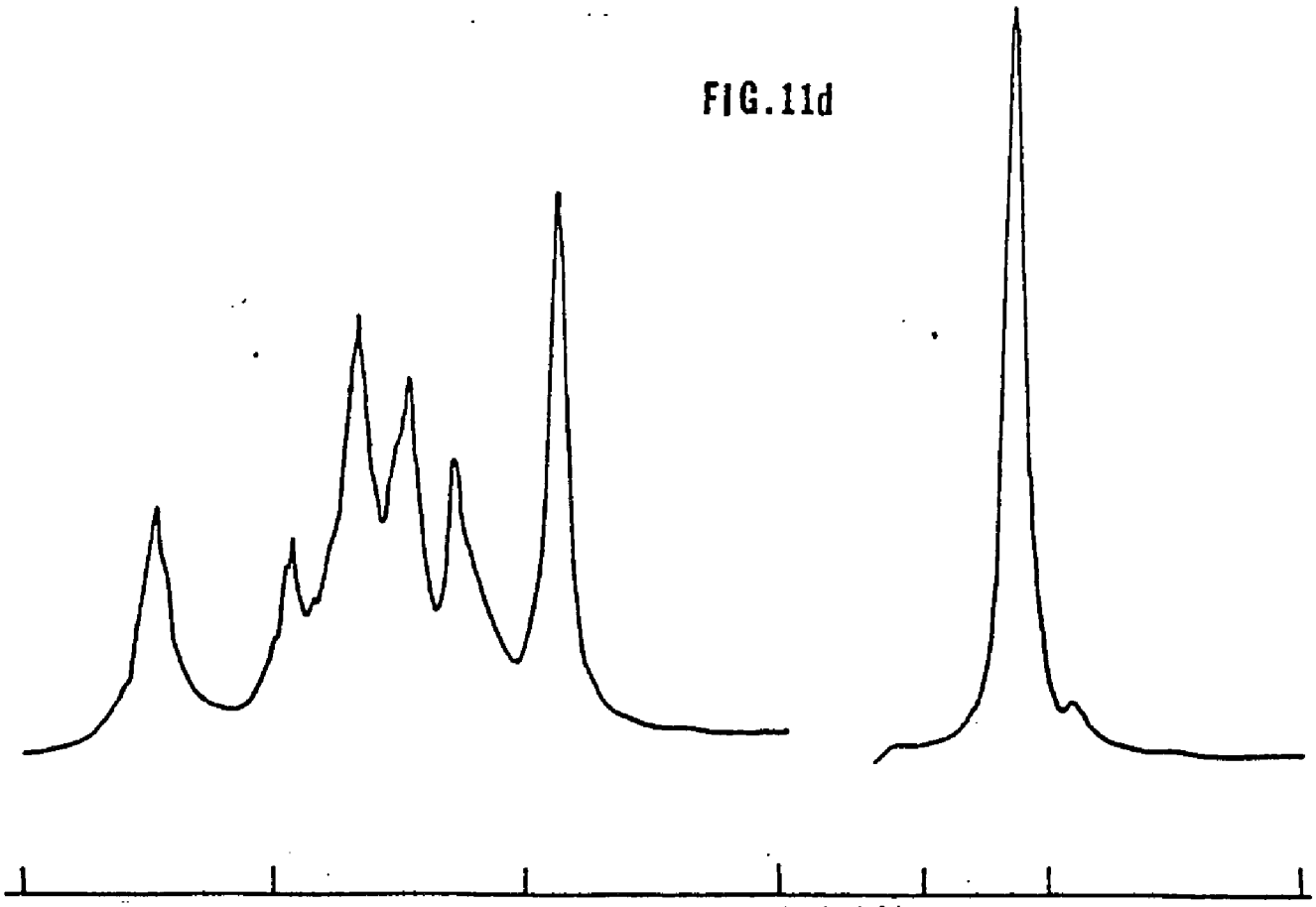

FIG.12a
H63 at77°C

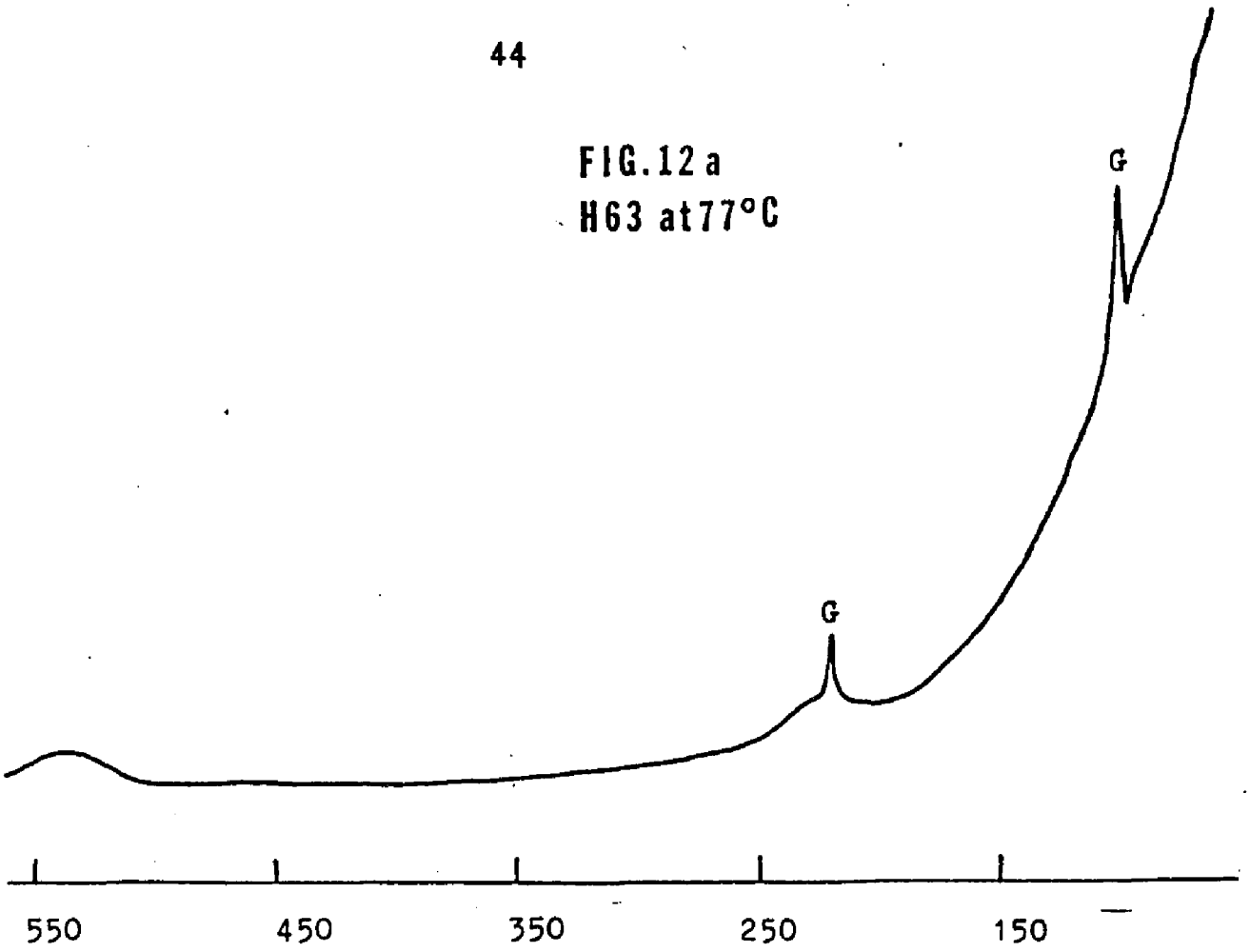

FIG.12b

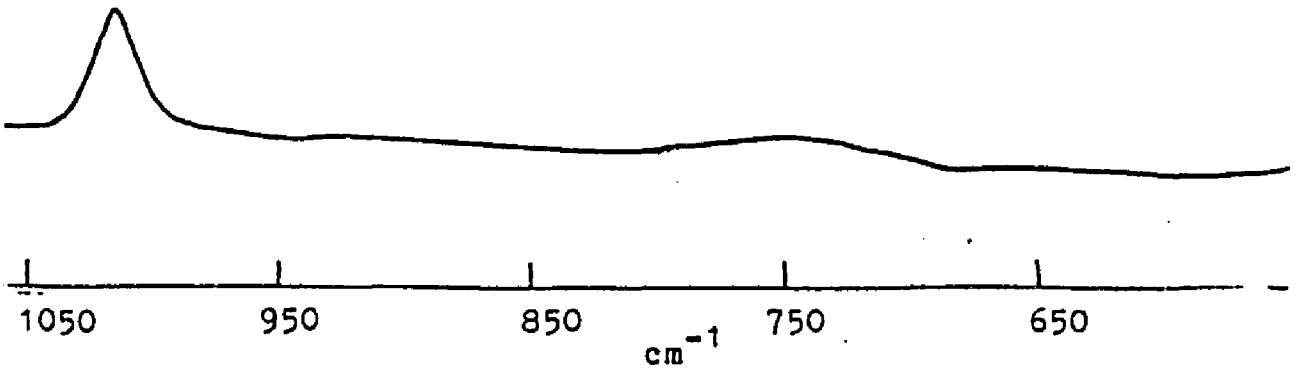

FIG.12c

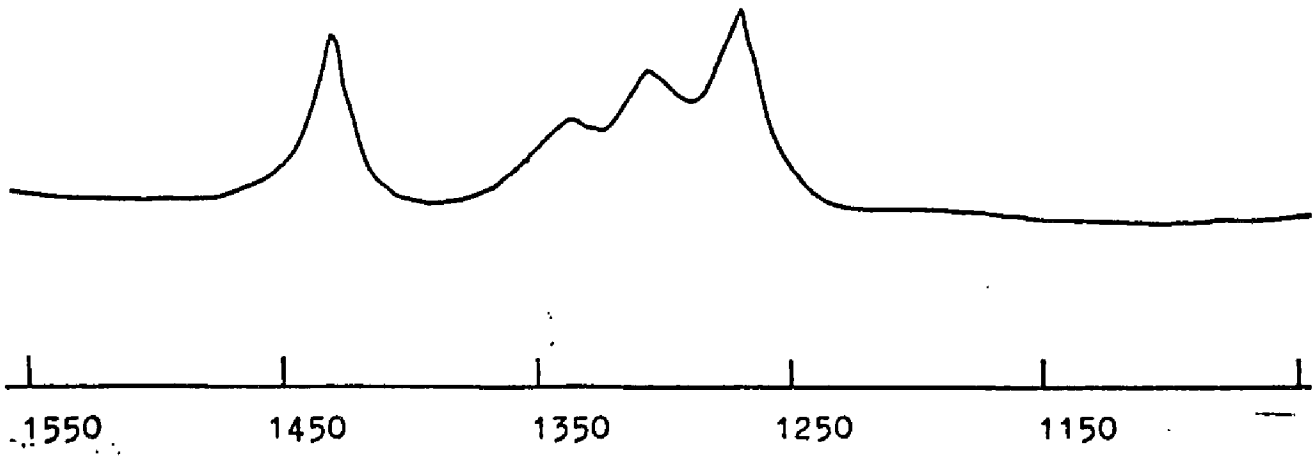

FIG.12d

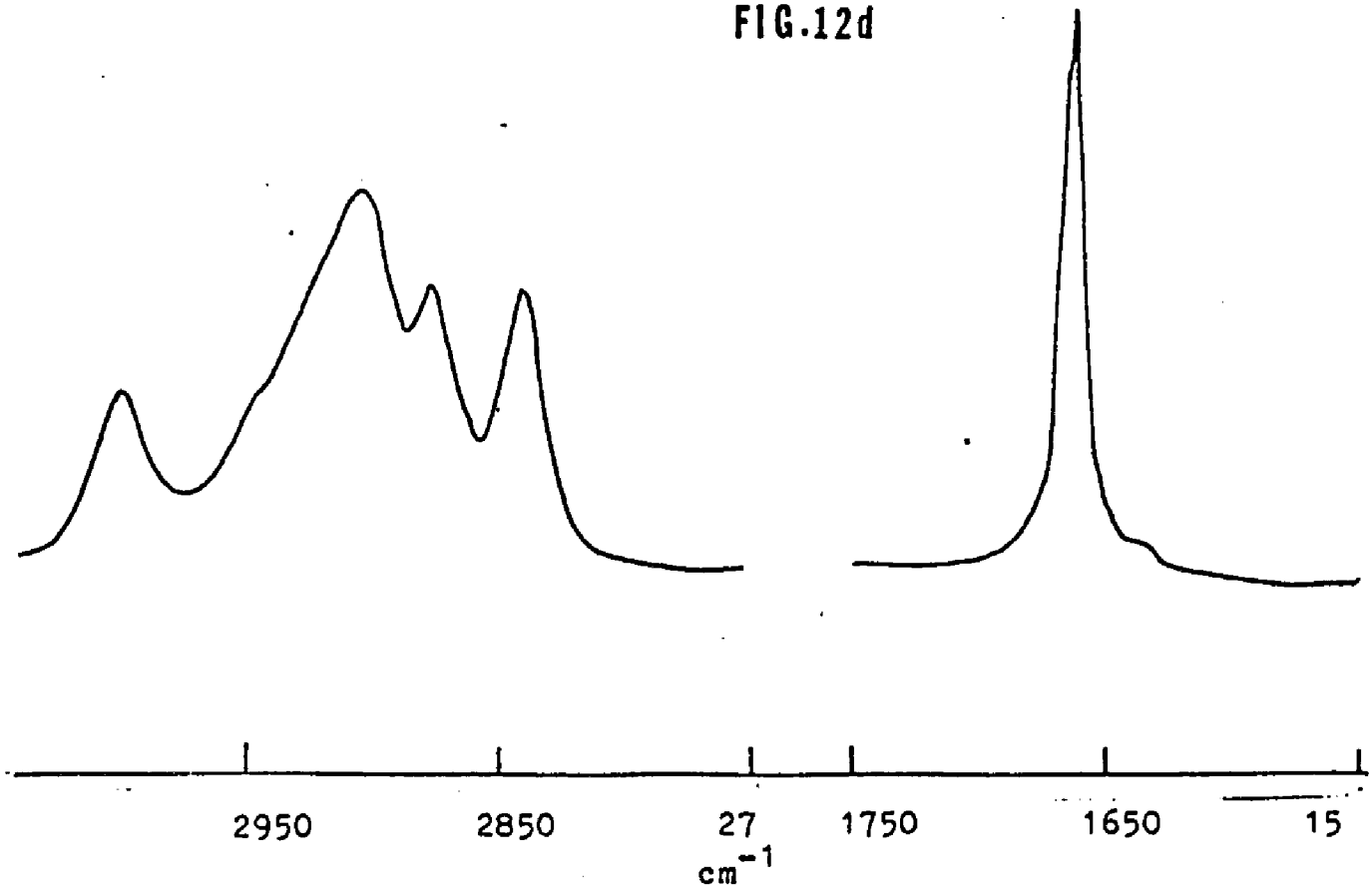

Fig. 13

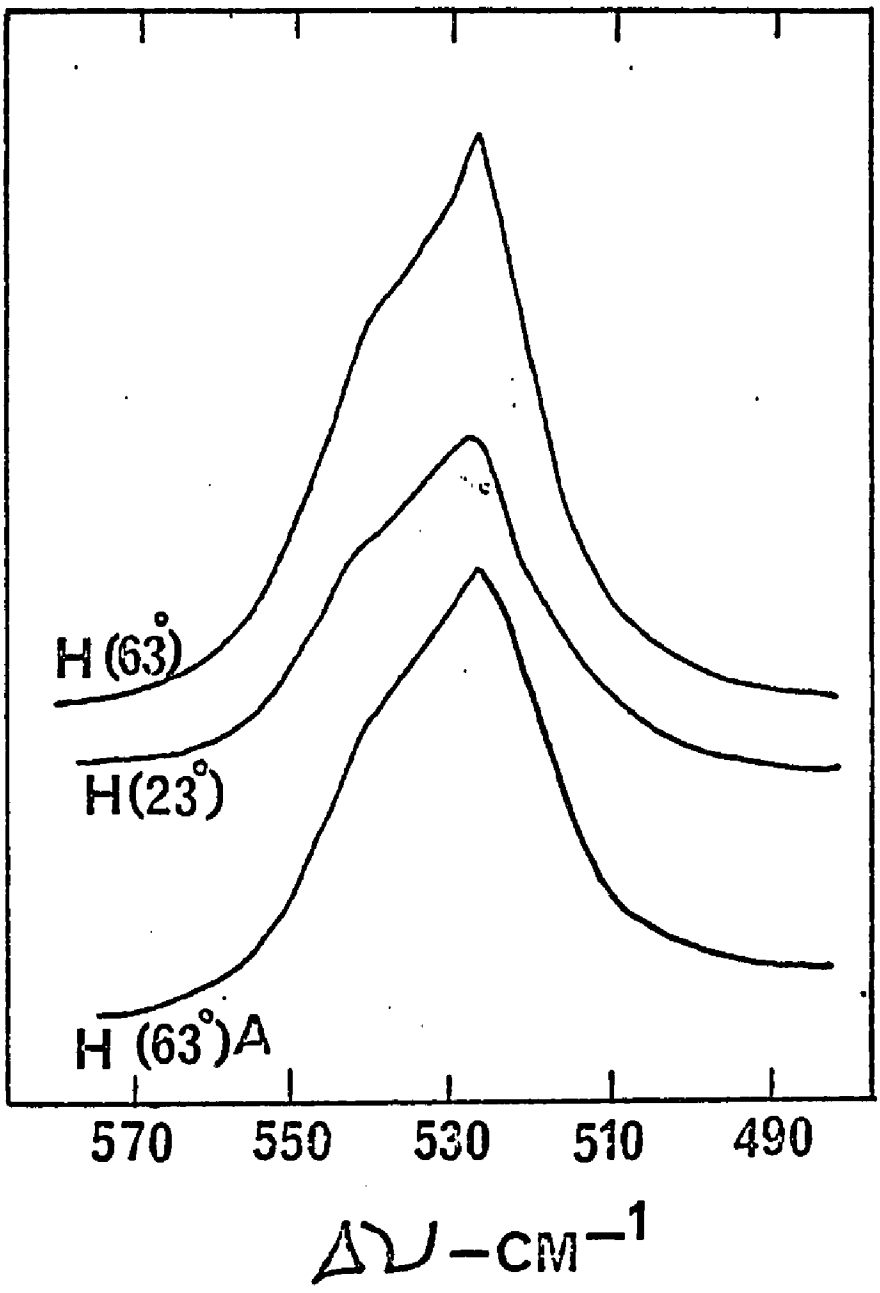

High resolution scan of the 529 cm^{-1} band

Captions to Figs. 14-16

14. Raman spectral scans between 50 and 300 cm^{-1} at temperatures between 25° and 78°C

15. a. Raman scans of the 1300-1350 cm^{-1} region for different crystalline PTBD preparations at room temperature

    b. Raman scans of 1300-1350 cm^{-1} region for H63 crystals at 45°, 65°, 71°, and 75°C

16. Raman scans of the 2800-3050 cm^{-1} region for H63 crystals at 45°, 65°, 71° and 75°C

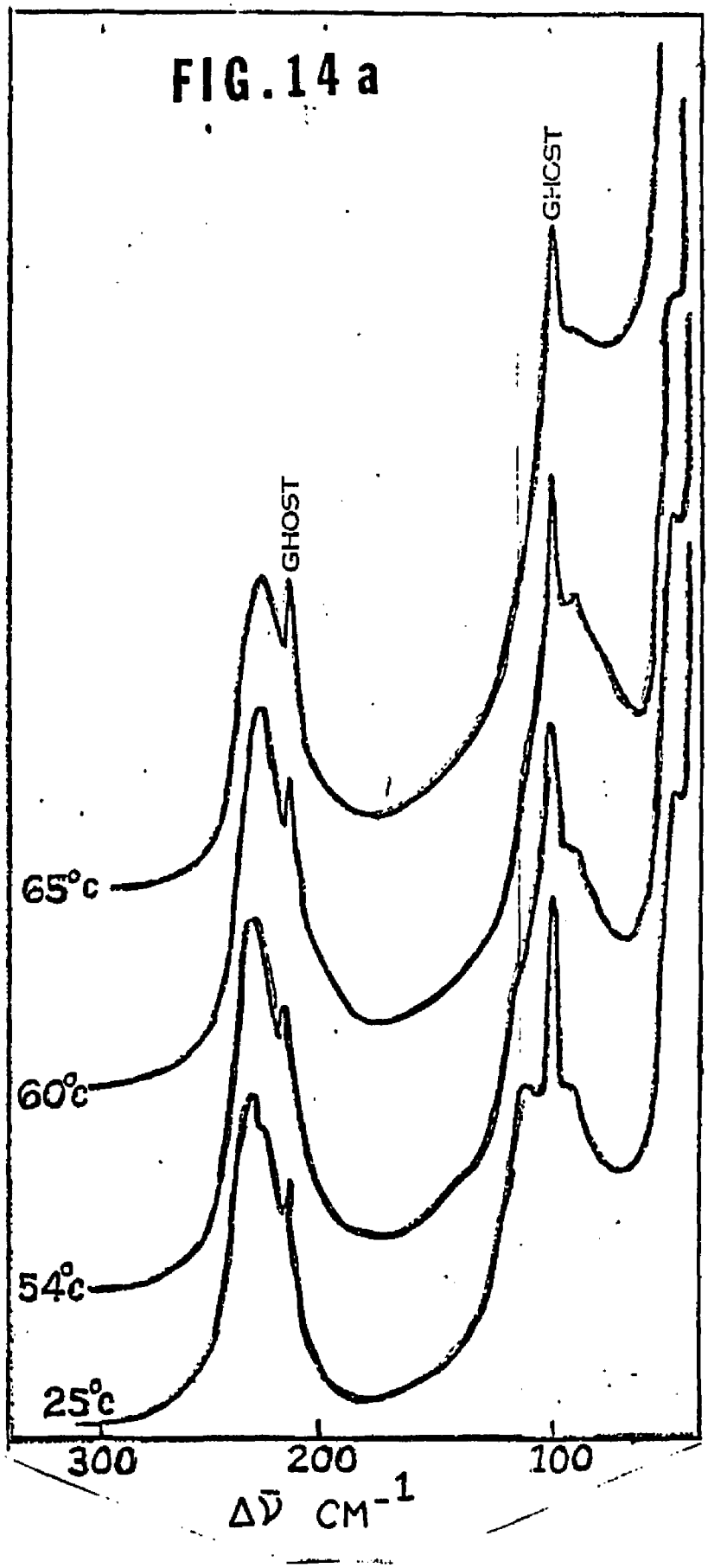
FIG. 14 a
GHOST
GHOST
65°c
60°c
54°c
25°c
300
200
100
Δν̄ CM⁻¹

FIG. 14b

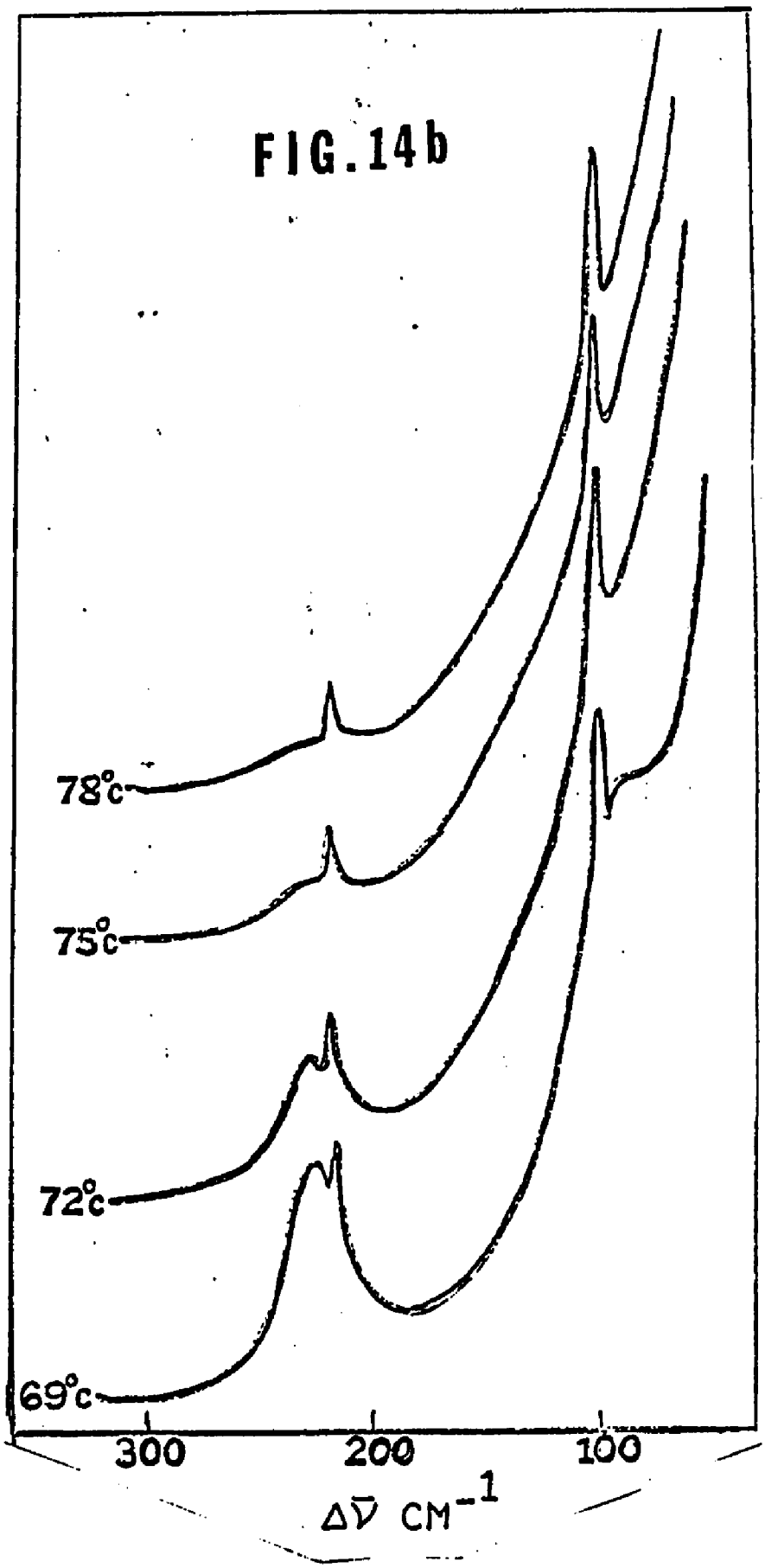

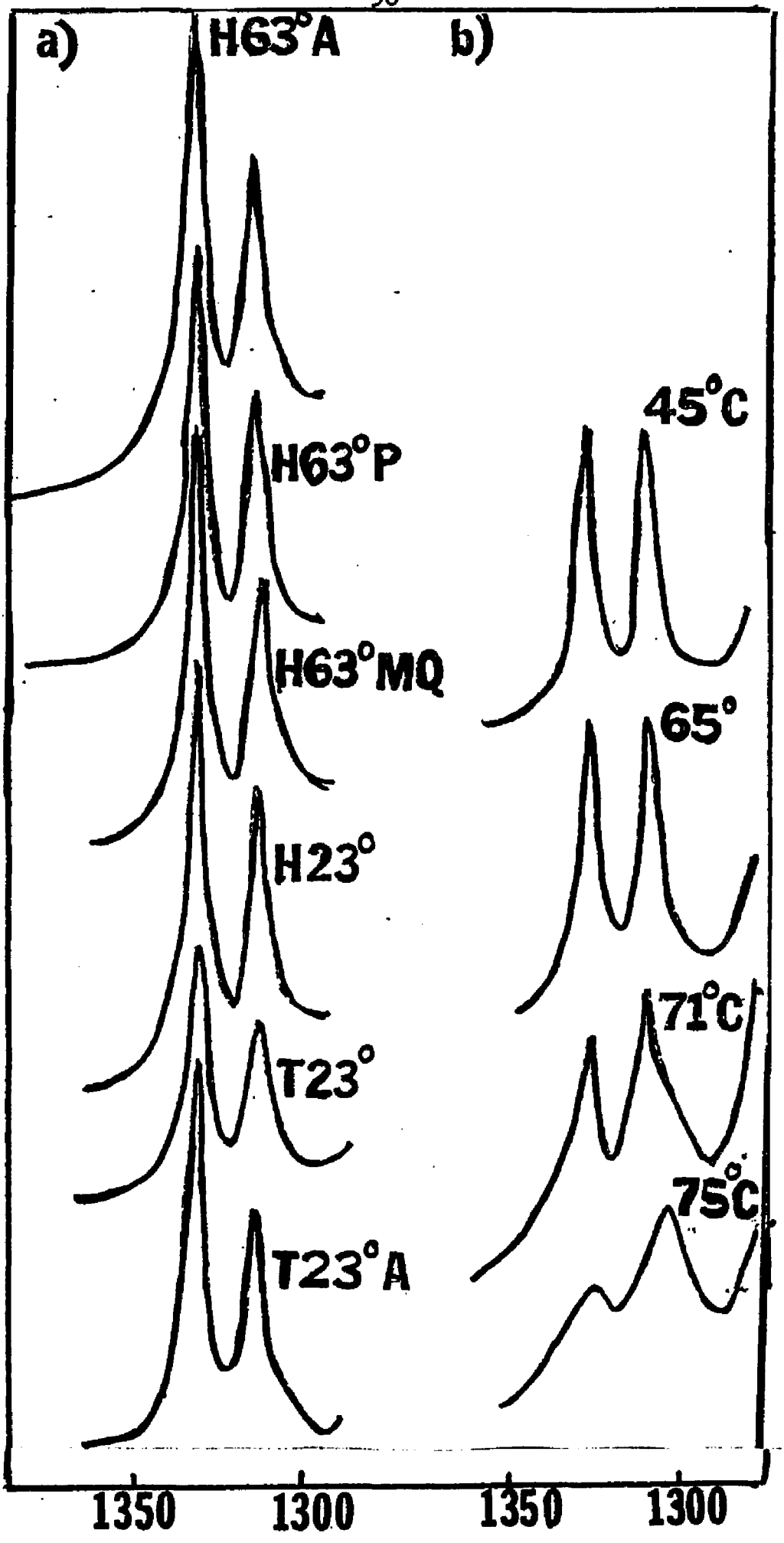
a)
H63°A
b)
H63°P
H63°MQ
H23°
T23°
T23°A
45°C
65°
71°C
75°C
1350
1300
1350
1300
ABSCISSA IN CM⁻¹

FIG.15

FIG.16

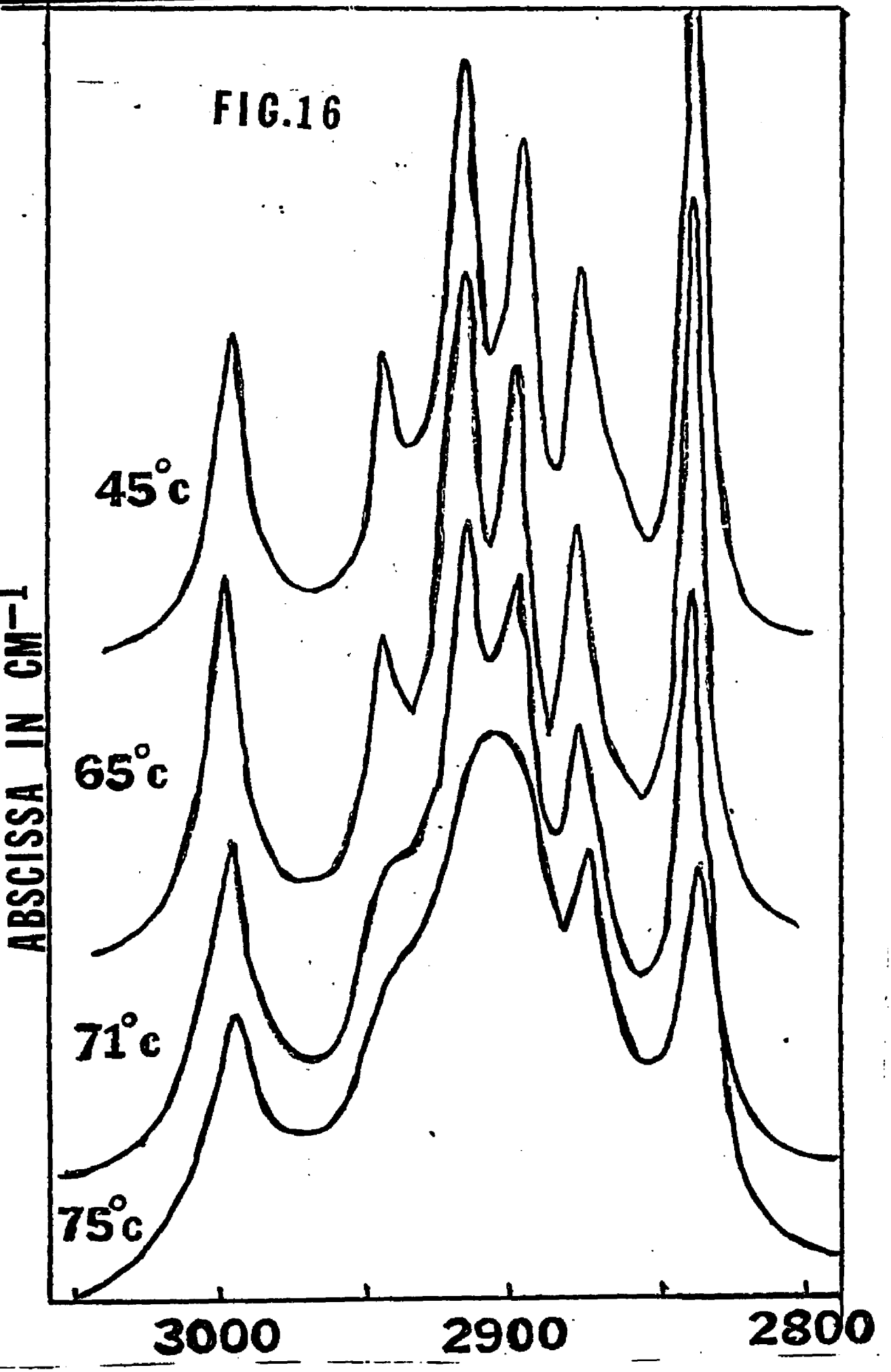

DISCUSSION

Two Raman band parameters are examined here to determine their relationship if any to the crystallinity; these are the band height and the frequency. Hsu, Moore and Krimm (20) have given the high frequency part of the 529 cm^{-1} band a noncrystalline assignment. This assignment is based in part on the sharpening of this band upon annealing at an unspecified temperature. In the present work this band was not found to sharpen upon annealing at $80^{o}C$(see fig. 13). Also, the shape of this band was not found to vary significantly between preparations with two or three fold differences in amorphous content.

A second indication of increased crystallinity cited by Hsu et al(20) was an increase in the I_{1331}/I_{1311} ratio. In the present work the ratio does increase for preparations which are expected to have high crystallinities(viz. H63A, H63MR, H63MQ and H63P). However I_{1331}/I_{1311} is also higher for T23 crystals which have been found to have lower crystallinities than H63 crystals(15,22,23,25,32). For H43, and H23 crystals, which are expected to have lower crystallinities than H63 crystals I_{1331}/I_{1311} is also higher. The failure of the I_{1331}/I_{1311} ratio to follow the expected trend in crystallinity implies that factors other than crystallinity determine this ratio. Both the 1331 and 1311 cm^{-1} bands were given crystalline assignments by the normal vibration analysis of Hsu and coworkers(20) so that

eq(6) is not applicable. However the trends observed in this ratio can be discussed in terms of eq(5). For any closely spaced bands the ratio of the intensities is $I_1/I_2 = N_1\overline{\alpha_1^2}/N_2\overline{\alpha_1^2}$. The ratio of I_{1331}/I_{1311} is found to vary from 2.4 at 110°K(20) to less than 1 near the transition temperature. This indicates that as the temperature increases $\overline{\alpha^2_{1331}}$ decreases at a faster rate than $\overline{\alpha^2_{1311}}$. $\overline{\alpha^2}$ is anisotropic so that it should be sensitive to changes in molecular geometry. The increase in conformational motion as the temperature increases lowers the effective values of $\overline{\alpha^2}$ which results in lowered scattering intensity. The more radical changes in molecular geometry which accompany the phase transition as well as the associated increases in chain motion is evidenced by the change of the I_{1331}/I_{1311} ratio to a value below 1. This is further evidence that $\overline{\alpha^2_{1331}}$ decreases with increasing conformational motion faster than $\overline{\alpha^2_{1311}}$.

If a relationship between $\overline{\alpha^2_{1331}}/\overline{\alpha^2_{1311}}$ and crystallinity does exist it is probably not a simple one.

Hsu and coworkers(20) have reported the disappearence of bands at 1078 and 1202 cm^{-1} upon annealing. In the present work no band at 1202 cm^{-1} was observed; however bands at 946, 1050, 1068 and 1090 cm^{-1} in the H63, H43 and H23 spectra are observed to disappear when these samples are annealed. If the PTBD spectrum at 77°C is examined, none of the peaks which disappear upon annealing increase in height above the transition temperature. In addition, none

of the bands in the 77°C spectrum were found to have higher ratios when compared to the 1666 cm^{-1} band than in the spectra at room temperature. Therefore no bands analogous to the 1335 and 1350 cm^{-1} crystalline PTBD are found in the Raman spectrum.

The transformation of form I to form II at 71°C brings about significant changes in the $=CH-CH_2-$ dihedral angle(14). This change is expected to cause shifts in some of the Raman bands. The single chain normal vibration calculations of Hsu et al(20) correctly predicts the shifts of the 1018, 761, and 529 cm^{-1} bands, but not the 238 cm^{-1} torsion band which decreases in frequency near 71°C. The torsion band is also lower in frequency in PTBD rubber which is considered to be amorphous(see Table I).

The shift of the 238 cm^{-1} band to lower frequencies with increasing temperature implies that this shift cannot be explained solely in terms of changes in molecular geometry. The torsion potential energy is sinusoidal. As the temperature increases the average amplitude of the vibration increases. This larger amplitude is accompanied by increased anharmonicity which lowers the frequency(90). The increase in interchain spacing brought about by thermal expansion also lowers the effective potential energy which contributes to the lowering of the frequency of vibration.

Of interest is the variation in frequency of the 70 cm^{-1} band in H63 crystals as a function of preparation. This band occurs at 73, 63, and 55 cm^{-1} in H63A, H43 and H23 preparations respectively which suggests that the frequency of this band is dependent on crystallinity. Unfortunately this

band is not observed in the T23 spectrum.

The diffuseness of the bands below 1000 cm^{-1} and the broadening of those above 1000 cm^{-1} in the 77°C spectrum comes about as a result of increased conformational motions of the molecules above the transition temperature. This disorder is also evident in the C-H stretching region where splitting of bands in this region decreases.

The C-H stretching frequencies do not change significantly between the single chain analysis of Neto and Di Lauro(18) and the unit cell calculation of Hsu, Moore and Krimm(20) which suggests that the six bands in this region can be attributed to the intramolecular vibrational coupling. Hsu and Krimm(28) have suggested that the frequency assignments in this region are complete. However in the opinion of this author the =CH stretching bands, which are 3013 and 3030 cm^{-1} in the analysis of Hsu et al (20), form a degenerate band at 2999 cm^{-1} in the Raman spectrum. If this band is in fact degenerate, then one of the other five bands in the C-H stretching region may be an overtone or combination band. This was suggested by Hsu and coworkers(20) earlier but later recanted(28). The 2946 band almost vanishes above the transition temperature. This behavior suggests that this band results from the combination of two bands whose ability to couple is disrupted by the disorder above the tranition temperature. The 2899 and 2920 cm^{-1} bands are apparently coupled. This coupling is disrupted above 75°C so that the bands merge to form one broad band at 2905 cm^{-1}.

The disappearence of the 238 cm^{-1} band(see figs. 14a and b) has two possible interpretations. (1) no equilibrium value exists for the dihedral angle so that the motion is no longer a true vibration.(2) The vibration has become mixed with low frequency lattice vibrations which no longer exist as individual bands. The increase in the intensity of the scattering between 0 and 200 cm^{-1} suggests that the second explanation is probably the case.

No new bands appear in the spectrum above the transition temperature which suggests that the selection rules of form I still apply in form II; therefore the average crystal geometry of form II is still probably monoclinic with the $P2_1/a$ factor group.

Finally the disappearence of bands at 946, 1050-1090, and 1202 cm^{-1}* and the failure of these bands to increase in intensity above the phase transition temperature suggests that these bands are associated with a metastable modification of PTBD I which exists in solution grown single crystals, but transforms to the more stable predominent form when the crystals are annealed above T_{tr}. Dilatometric measurements by Takayanagi and coworkers, as early as 1967(29), suggested the presence of a metastable modification in PTBD single crystals. More recent favorable evidence is offered by DSC measurements by Marchetti and Martuscelli (30,31). The theoretical implications of these findings are discussed in part II of this dissertation.

*1202 cm^{-1} band observed by Hsu et al(28)

CONCLUSIONS

(1) No crystalline/amorphous band pairs analogous to those observed in the infrared spectrum of crystalline PTBD were found in its Raman spectrum.

(2) The merging of bands in the hydrogenic stretching region results from decoupling of these modes brought about by molecular conformational motion in the high temperature form of PTBD.

(3) The failure of new bands to appear above the transition temperature suggests that the crystal structure is still monoclinic with the $P2_1/a$ space group.

(4) The disappearence of certain bands upon annealing, melt recrystallization or compression of solution grown PTBD under 25000 psi pressure indicates that a metastable modification of PTBD I exists below the transition temperature, but transforms into the more stable predominant form when subjected to the above thermal and mechanical treatments.

INTRODUCTION TO PART II

The availability of crystal structure data for both the high and low temperature forms of crystalline PTBD(14, 16) provides an opportunity for the theoretician to relate the macroscopic properties of PTBD to its microcrystalline structure. Stellman, Woodward and Stellman(17) have attemted to do just this. In that investigation the conformational energy per monomer unit was minimized with respect to the a and b lattice parameters in form I and with respect to the interchain spacing, σ, for form II in order to predict the most stable crystal structures for these two forms. The procedure was fairly successful in predicting the constants for form I, but was unsuccessful when applied to the proposed structure for form II. The enthalpy and entropy of transition were computed as well as the specific heat of form II. These were found to differ significantly from the experimental values. Examination of the procedures of Stellman and coworkers(17) by this author reveals that the differences between the computed and experimental results are due in part to computational errors as well as inadequate mathematical modelling. These flaws are discussed below along with changes introduced in the present work.

The Crystal Lattice Model

The lattices used in the calculations of Stellman et al(17) were the monoclinic lattice given by Iwayanagi et al(14) for form I and a 'hexagonal' lattice hypothesized by Stellman and coworkers(41) for form II. It is the 'hexagonal' lattice with which issue is taken here. The 'hexa-

gonal' lattice proposed by Stellman and coworkers(41) was generated by a series of simple translations of a single central PTBD chain in the XY plane(41). In a lattice generated in the above manner $-CH_2-$ groups could occupy planes containing only other $-CH_2-$ groups. The same is true for the -CH= groups. This author believes that unfavorable steric interference between methylenes 'crowded' into common planes would exist in this lattice. In the monoclinic lattice the planes are occupied by a 50:50 mixture of $-CH_2-$ and -CH= groups. This can best be seen in the XZ and YZ projections of Fig.20. The X-ray diffraction experiments of Suehiro et al(16) and Iwayanagi et al(14) have shown that the PTBD monomer unit undergoes a change in fiber period corresponding to a change in the $CH_2CH_2CH{=}CH$ dihedral angle from 109° in form I to 80° in form II. Therefore this author proposes that monoclinic lattices with these dihedral angles be used for calculations of lattice geometries and energies for lattices of forms I and II of PTBD. Furthermore the molecular packing given by the X-ray diffraction studies(13,14,16) is pseudohexagonal; i.e.the chains are arranged in a hexagonal array around a single central chain. Consistent with this packing the conformational energy can be minimized with respect to the interchain spacing. This one-parameter calculation insures pseudohexagonal packing, and is thus more constrained than that of Stellman et al(17). However it should lead to lattice parameters which are consistent with those given by experiment.

The Calculation of the Specific Heat

Stellman and coworkers(17) computed the specific heat (C_p) from the slope of the U(conformational energy) vs $T = K\sigma$ curve where K is a constant which relates σ to T, the temperature. Both U and σ are linear functions of T over short intervals so that

$$\frac{1}{K}\frac{dU}{d\sigma} = \frac{dU}{dT} = C_p$$

This formulation neglects the contribution of molecular vibration to C_p so that the value of C_p computed by Stellman et al fell short of the experimental value by 70%. In the present treatment, an adaptation of the method of generalized frequencies due to Dobratz(47) is used to compute the specific heat of crystalline PTBD form II. A description of the method is given in a later section entitled 'The Method of Generalized Frequencies.'

Computational Errors

Computational errors were detected in the calculations of Stellman and coworkers(17) by this author. These will be discussed along with the results of the present work in the DISCUSSION section.

The Free Energy Function

The Gibbs free energy per mole is given by(42)

eq(8) $$G = E + PV - TS$$

where E, PV, and TS are the total energy, the pressure volume product and the temperature entropy product. For solids $\Delta(PV)$ is usually small so that the Helmholtz free energy is used.

eq(9) $$A = E - TS$$

if electronic and nuclear energies are excluded, since they are not expected to change significantly with changes in molecular geometry, then for crystalline hydrocarbons A can be written as

eq(10) $$A = E_o + E_{vib} + E_{TOR} - TS_{vib}$$

The terms in the above expression warrant some explanation. $E_o+E_{tor}=U$ represents the total conformational energy per monomer unit. E_o is the sum of all pairwise non-bonded interactions between atoms of one unit and all of the atoms in the lattice. E_o can be written

eq(11) $$E_o = \sum_{i=1}^{n} \sum_{j=i+1}^{N} V(r_{ij})$$

j runs from i+1 so that no pairs are counted twice and so that i=j terms are excluded. N and n are, respectively, the number of atoms in the lattice and the number of atoms in the monomer unit. $V(r_{ij})$ is an empirical potential energy function; usually chosen as a Lennard-Jones or Buckingham function and r_{ij} is the internuclear distance between atoms i and j. E_{tor} is the potential energy arising from threefold sinusoidal barriers present in the monomer unit, and is of the form

eq(12) $$E_{TOR} = \frac{V_o}{2}(1 + \cos(3\phi))$$

In the above expression, V_o is the height of the barrier and ϕ is the dihedral angle between planes formed by four

atoms bonded in the manner depicted in fig. 17.

Fig. 17

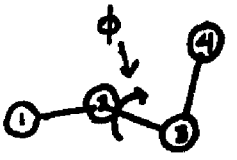

The definition of a Ø dihedral angle

E_{vib} is the energy resulting from internal and lattice vibrations of the molecules, and can be calculated from the vibrational partition function of the crystal. To a fair degree of approximation internal molecular vibrations are independent of the molecular packing in the crystal(6). Since internal vibrations are not expected to change significantly in the transition from form I to form II, from here on, unless otherwise noted, they(the internal vibrations) will be excluded from E_{vib}. What is needed is an approximation for Z_{vib}, the partition function.

A solid can be visualized as a giant molecule which vibrates with 3N-3 characteristic normal frequencies whose distribution and number determine the thermodynamic properties of the crystals at a given temperature(44). If $h\nu/kT$ is less than about 4, A, E, and S become independent of the exact nature of the frequency distribution(45) and almost any distribution with the same mean frequency as the true distribution should give satisfactory results. Under these circumstances the Einstein approximation, which assumes that every molecule in the solid is oscillating with the same lattice frequencies can be used. The partition function can be written(45)

eq(13) $$Z = Z_m^N$$

where Z_m is the molecular partition function and N is the of molecules in the lattice. For a system of harmonic oscillators Z can be written

eq(14) $$Z_m = \prod_i \left[\frac{e^{h\nu_i/kT}}{e^{h\nu_i/kT} - 1} \right]$$

where ν_i is the vibrational frequency.

The lattice vibrational contributions to the energy, heat capacity and entropy can be obtained from eq(13), and are given by the well known expressions(45)

eq(15) $$E_{vib} = \sum_i \left[\frac{Nh\nu_i}{2} + \frac{Nh\nu_i}{exp(h\nu_i/kT) - 1} \right]$$

eq(16) $$C_{vib} = \sum_i \left(\frac{h\nu_i}{kT} \right) \frac{e^{h\nu_i/kT}}{(e^{h\nu_i/kT} - 1)^2}$$

eq(17) $$S_{vib} = \sum_i \left[\frac{Rh\nu_i}{kT} (e^{h\nu_i/kT} - 1)^{-1} - R \ln (1 - e^{-h\nu_i/kT}) \right]$$

The frequencies of vibration in the X, Y, and Z directions and of libration around the molecular axis are likely to be differant, but their mean value ν_m can be used in place of ν_i in equations 15, 16 and 17.

By ignoring the effect of lattice vibrations Stellman and coworkers have equated U and A. For computing ΔH_{tr} and ΔS_{tr} this approximation is acceptable but if T_{tr}(the transition temperature)is to be predicted the vibrations must be included.

The Relationship Between Free Energy and Crystal Structure

If suitable potential energy functions are chosen, E_o can be computed from a knowledge of the molecular and crystalline structure. The expression for E_o was given earlier (viz. eq(11)).

An approximation which relates the vibrational mean frequency to the crystal structure will now be derived. If E_o is the energy per monomer unit at equilibrium then the force constant resulting from the displacement of this monomer unit as a rigid body in the X direction is given by

$$\text{eq(18)} \quad K_x = \left(\frac{\partial^2 E_o}{\partial x^2}\right)_{x_o} = \sum_{i=1}^{n} \sum_{n+1}^{N} \left[\frac{\partial^2 V(r_{ij})}{\partial x^2}\right]_{x_o} - K_{x_o}$$

The symbol x_o indicates that the above quantities are evaluated at the equilibrium x coordinates of the atoms composing the monomer unit. The summation in j is carried out from n+1 because the ij distances within the 'rigid' monomer unit are invariant with respect to displacement of the unit. The summations above do not account for the fact that the entire chain is considered to undergo rigid displacement in this approximation so that Kx_o which is the 'force constant' for the monomer unit being displaced relative to the rest of the chain, is subtracted. This is the long wave approximation. K_{x_o} can be negative or positive. The terms in the summation can be written

$$\text{eq(19)} \quad \left[\frac{\partial^2 V}{\partial x^2}\right]_{x_o} = \left[\frac{\partial^2 V}{\partial r_{ij}}\right]_{r_{ij}} \left(\frac{x_{ij}}{r_{ij}}\right)^2 + \left[\frac{r_{ij}^2 - x_{ij}^2}{r_{ij}^3}\right] \left(\frac{\partial V}{\partial r_{ij}}\right)_{r_{ij}}$$

In the above expression the derivatives are evaluated at the equilibrium value of r_{ij}.

The libration torque constant for a rigid body oscillating about a principle axis is given by

eq(20) $$H_\theta = \left[\frac{\partial^2 V}{\partial \theta^2}\right]_{\Delta\theta = 0}$$

where $\Delta\theta$ is the angle by which the body is rotated from equilibrium. Application of the above expression to the present system was found to yield an unwieldy expression and physically meaningless negative force constants. An alternative procedure for obtaining the libration is to equate it to the mean frequency of the x, y and z translational lattice vibrations. The frequency of this vibration is expected to lie in the neighborhood of the mean frequency of the low frequency lattice vibrations so that this procedure is not unreasonable.

After the force constants are obtained from eqs. 18 and 19 the frequencies are computed from

eq(21) $$\nu_x = \frac{1}{2\pi}\sqrt{\frac{K_x}{M}}$$

where M is the formula weight of the monomer unit.

The Method of Generalized Frequencies

At temperatures where no transitions are taking place and where the Einstein approximation applies E_{vib}, S_{vib}, and $C_p(vib)$ can be approximated by an adaptation of the method of generalized frequencies(43). This method was first introduced by K. Bennewitz and W. Rossner(46) for use with

gaseous organic compounds, and was later modified by Dobratz(47) to give more accurate results. The Dobratz equation is given below.

eq(22) $$C_p = 4R + \frac{a}{2}R + \sum_i n_i C_{\nu_i} + \sum_i \left[\frac{(3N-6-a-\Sigma n_i) n_i C_{\delta_i}}{\Sigma n_i} \right]$$

For gases, the first term in the above includes the rotational and translational contributions to C_p; $\frac{1}{2}R$ per degree of freedom. a is the number of internal free rotations in the molecule. ν_i and δ_i are generalized frequencies of bond stretching and bending respectively associated with the ith bond type. These frequencies have been compiled, averaged and tabulated by Stull and Mayfield(48, 49) and Dobratz(47) from spectroscopic data. n_i is the number of times the ith bond type appears in the molecule. C_{ν_i} and C_{δ_i} are the Einstein contributions of frequencies ν_i and δ_i respectively to the heat capacity. The term in brackets represents the ratio of the number of bending to the number of stretching vibrations, and is usually referred to as ϕ.

To adapt eq(22) for use with crystalline polymers, several assumptions are made. First $C_p = C_v$. This is a common approximation made for condensed phases. Second, all internal rotations are replaced with torsional vibrations having an average frequency of 250 $cm.^{-1}$ This frequency was computed from

eq(23) $$\bar{\nu}_{TOR} = \frac{1}{2\pi C}\sqrt{GF}$$

where G is the Wilson G matrix element(4) for torsional vibration around a C-C bond. F is the force constant given for hydrocarbon torsion barriers by Neto and di Dilauro(18). Torsional motions in the backbone of the polymer are considered to be combined with the skeletal bending vibrations; i.e., C_{ν_i} is assumed to be the same for backbone torsions as for bends. This approximation is reasonable since the molecular packing restricts the ability of the chains to twist thus raising their effective vibrational frequency, and encouraging mixing of torsional and skeletal bending modes.

Third the mean lattice frequency can be used as previously described to compute the lattice contribution to C_p. Even if the lattice vibration frequencies, which are usually less than 200 cm^{-1} in energy, are not available, a contribution of 1.9872 $cal.mole^{-1}.deg^{-1}$ can be used for each of the four low frequency lattice vibrational degrees of freedom. The equation resulting from the above assumptions is

$$\text{eq(24)} \quad C_p = 4C_{\nu_l} + \sum_i n_i C_{\nu_i} + \frac{(3N-4-a-\Sigma n_i)}{\Sigma n_i} \sum_i n_i C_{\delta_i} + a C_{\nu_{tor}}$$

where a is the number of side-chain torsions and $C_{\nu_{tor}}$ is the contribution of a torsion vibration to C_v. C_{ν_m} is the contribution of one degree of lattice vibrational motion to C_v, n_i, ν_i, δ_i, and N have the same meanings as in the Dobratz equation. The Dobratz equation has been found to be valid for a wide variety of gaseous hydrocar-

bons above 250K, so that similar performance is expected from eq(24) for hydrocarbon solids.

Finally, although eq(24) is derived for specific heats, equations of the same general form can be used to compute E_{vib}, and S_{vib}. In such cases the right side of eq(15) would replace the $C\gamma_i$ and $C\delta_i$ terms when E_{vib} is to be computed, and eq(17) would replace these terms when S_{vib} is desired.

STATEMENT OF THE THEORETICAL PROBLEM

The computer experimental work to be described had five objectives which are listed below.

1. To predict the interchain spacing for crystalline PTED forms I and II by finding the minimum potential energy as a function of interchain spacing. This has the simultaneous effect of testing the utility of the chosen empirical potential energy function for representing the potential energy of the system.
2. To compute the mean lattice vibration frequencies for the above lattices. These are the Einstein frequencies which are used in the approximate lattice partition function.
3. To compute H, S and G as functions of temperature for the forms I and II lattices with the potential energies and lattice mean frequencies computed above.
4. To compute phase transition thermodynamic properties for the above lattices.
5. To adapt the method of generalized frequencies of Dobratz (47) for computing heat capacities of crystalline polymers.

COMPUTATIONAL PROCEDURES

Description of PTBD Molecular and Lattice Geometries

In this section a mathematical description of the PTBD chain geometry will be presented. The procedures for generating the initial atomic coordinates from this geometry and the generation of the crystal lattice from these coordinates will be described. Subsequently the computer experiments performed on the crystal lattice will be described.

PTBD Chain Geometry

The structure of the PTBD repeat unit is depicted below in fig. 18

Fig. 18

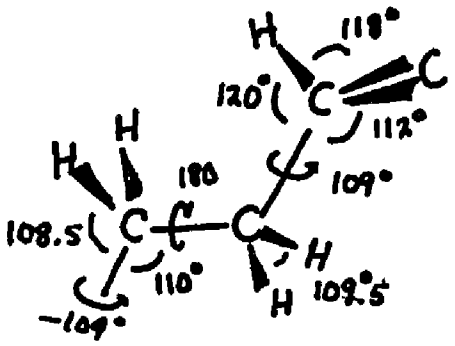

Bond	Lengths
C-C	1.54 A
C-H	1.08 A
C=C	1.32 A

The parameters in fig. 18 are the same as those used by Stellman et al(17) for form I. In form II the $CH-CH_2$ dihedral angle is changed from 109° to 80°.

Cartesian Coordinate Generation

The coordinates of a fourth atom can be constructed from the coordinates of a chain of three to which it is connected. Two types of construction are possible(see fig. 19 a and b). The coordinates of atom 4 are computed from those of atoms 1, 2, and 3 in two steps. First the coord-

CASE 1

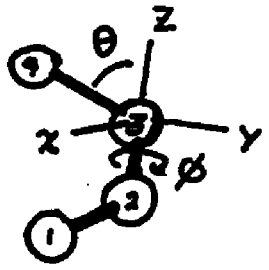

Fig.19(a)

CASE 2

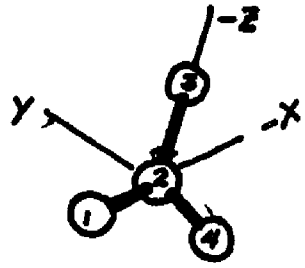

Fig.19(b)

inates of atom 4 in a coordinate system centered on atom 3 or 2 are computed. Second, these coordinates are transformed to the laboratory fixed coordinate system. The mathematical procedures for cases 1 and 2 are summarized below.

The local cartesian coordinate system can be expressed in terms of the well known i, j and k unit vectors. The definitions of these unit vectors for the two cases are given below.

	CASE 1	CASE 2
eqs(25)	$\vec{J} = \frac{\vec{u}_{23} \times \vec{u}_{21}}{\lvert \vec{u}_{23} \times \vec{u}_{21} \rvert}$	$\vec{J} = -\frac{\vec{u}_{23} \times \vec{u}_{21}}{\lvert \vec{u}_{23} \times \vec{u}_{21} \rvert}$
eqs(26)	$\vec{k} = \vec{u}_{23}$	$\vec{k} = -\vec{u}_{23}$
eqs(27)	$\vec{i} = \vec{J} \times \vec{k}$	$\vec{i} = \vec{J} \times \vec{k}$

$\vec{u}_{pq}$ is a unit vector directed from atom p to atom q. The definitions of the cartesian coordinates of atom 4 relative to the local coordinate axes defined by i, j and k are given below.

CASE 1

$x_{34} = r_{34} \cos\phi \sin\theta$

$y_{34} = r_{34} \sin\phi \sin\theta$

$z_{34} = r_{34} \cos\theta$

$\theta = \pi - 4234$

ϕ = 1234 Dihedral Angle

ℓ = 3 (Atom At Origin)

CASE 2

$x_{24} = r_{24} \cos\phi \sin\theta$

$y_{24} = r_{24} \sin\phi \sin\theta$

$z_{24} = r_{24} \cos\theta$

$\theta = \pi - 4324$

$$\phi = \frac{(\cos(4124) - \cos(4123)\cos(4324))}{(\sin(4324)\sin(4124))}$$

$\ell = 2$

The transformation to laboratory fixed coordinates can be accomplished via the following scheme taken from Kreyzsig(50). Let V_{L4} be the vector directed from atom L to atom 4.

$$\vec{V}_{L4} = x_{L4}\vec{i} + y_{L4}\vec{j} + z_{L4}\vec{k}$$

V_{L4} can also be expressed in a coordinate system whose origin is centered on the atom L, and whose axes are parallel to the laboratory fixed coordinates.

$$\vec{V}_{L4} = x'_{L4}\vec{i}' + y'_{L4}\vec{j}' + z'_{L4}\vec{k}'$$

The laboratory coordinates of atom 4 can be obtained by 'dotting' V_{L4} successively with $\vec{i}'$, $\vec{j}'$ and $\vec{k}'$, and adding to the resultant terms x_L, y_L and z_L.

$$x'_4 = x_{L4}\,\vec{i}\cdot\vec{i}' + y_{L4}\,\vec{j}\cdot\vec{i}' + z_{L4}\,\vec{k}\cdot\vec{i}' + x_L$$

$$y'_4 = x_{L4}\,\vec{i}\cdot\vec{j}' + y_{L4}\,\vec{j}\cdot\vec{j}' + z_{L4}\,\vec{k}\cdot\vec{j}' + y_L$$

$$z'_4 = x_{L4}\,\vec{i}\cdot\vec{k}' + y_{L4}\,\vec{j}\cdot\vec{k}' + z_{L4}\,\vec{k}\cdot\vec{k}' + z_L$$

note: $\vec{i}\cdot\vec{i} = \vec{j}\cdot\vec{j} = \vec{k}\cdot\vec{k} = 1$

$\vec{i}\cdot\vec{i}'$ etc. are the cosines of the angles between the local and laboratory fixed coordinate axes.

PTBD Chain Generation

The equal and opposite dihedral angles of the PTBD chains give the molecule translational symmetry so that the polymer chain can be generated via a series of unit translations of the initial monomer unit along the molecular symmetry axis. The unit of translation is the same as the molecule's fiber period, which is computed from the molecular geometry. The fiber period is the distance between atom i of a monomer unit and atom i in the immediate neighboring unit in the chain.

PTBD Unit Cell and Lattice Generation.

The xz, yz and xy projections of the unit cell for the monoclinic lattice are depicted below in fig.20.

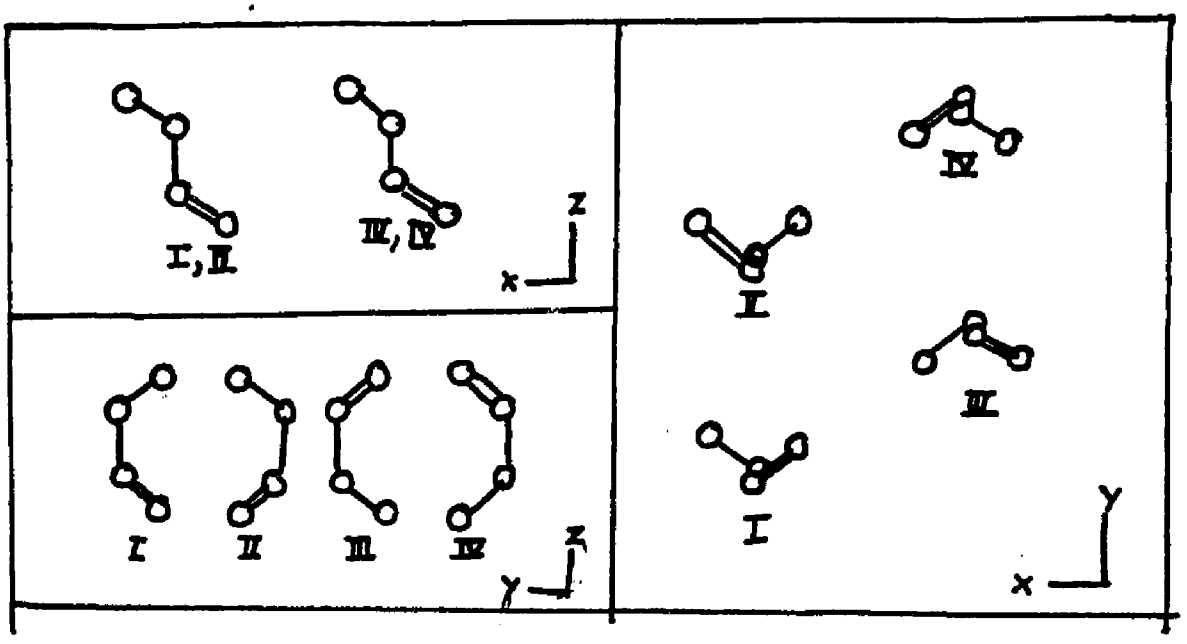

Fig.20

The monomer units have been numbered I - IV . Notice that molecule I eclipses molecule II and molecule III eclipses molecule IV. The relevant parameters for the unit cell of

of form I are given in Table IV.

Table IV

$a = 8.63$ A, $b = 9.11$ A, $c = 4.83$ A

θ = setting angle = 150°

$\beta = 114^{\circ}$ = the inclination of the molecular axis

$\sigma = 4.60$ A = the interchain spacing

Unit cell parameters for PTBD I(from ref. 16)

θ is defined for monomer unit I as the angle between the xy projection of the CH_2-CH_2 bond and the positive x axis.

The unit cell can be generated from an initial monomer unit through a series of operations which are summarized below.

Unit I

1. Transform the initial unit so that its symmetry axis coincides with the z axis. At this stage $\theta = 0^{\circ}$.
2. Rotate the unit 150° around the z axis to give $\theta = 150^{\circ}$.
3. Rotate the unit 24° counter clockwise around the Y or b axis to give $\beta = 114^{\circ}$, and unit I.

Unit III

1. Duplicate unit I at a position a/2 angstroms along the positive X axis from unit I.
2. Reflect the duplicate through the y=b/8 plane to yield unit III.

Unit II

1. Duplicate unit I at a position b/2 angstroms along an axis parallel to the positive Y axis away from unit I.
2. Rotate the duplicate 180° around the above axis to yield unit II.

Unit IV

1. Duplicate unit II at a position a/2 angstroms along the positive X axis from the position of unit II.
2. Reflect the duplicate unit through the y=5b/8 plane to yield unit IV.

The coordinates of atoms in the unit cell projections depicted in fig. 20 were actually generated in the above manner by the FORTRAN program in APPENDIX A.

The Monoclinic Lattice

To generate a lattice of 125 cells the above operations were applied to a five monomer unit PTBD chain yielding a stack of 5 unit cells. The lattice could then be generated by a series of simple translations of the unit cell stack. To simplify force and torque constant computations the lattice was oriented so that the chains were perpendicular to the XY plane. (see APPENDIX C for defining equations)

The 'Hexagonal' lattice

Following the dissertation of J.M. Stellman a 5 unit chain was subjected to a series of simple translations in the XY plane to yield the 'hexagonal' lattice of chains. (See APPENDIX C for defining equations.)

The Empirical Potential Energy Functions

The nonbonded potential energy function chosen for the present work was that of R.A.Scott and H.A. Scheraga(51). The function is a Lennard-Jones type function and has the form

eq(28) $$E(r_{ij}) = -\frac{a}{r_{ij}^{6}} + \frac{b}{r_{ij}^{12}}$$

The parameters for this function are given in Table V.

Table V

Atom Pair	$a(kcal\text{-}A^{6}\cdot mole^{-1})$	$b(kcal\cdot A^{12}\cdot mole^{-1})$
H...H	46.7	4460
C...H	128.	205000
C...C	370.	286000

Parameters for the Scott-Scheraga function

The a and b parameters are derived by first computing the value of a from the Slater-Kirwood equation for dispersion interactions(84,85,86)

$$a_{ij} = \frac{\frac{3}{2} e^2 \sqrt{a_o}\, \alpha_i \alpha_j}{\left[\sqrt{\frac{\alpha_i}{n_i}} + \sqrt{\frac{\alpha_j}{n_j}}\right]}$$

where a_o is the first Bohr orbit, 0.5292 A, α_i and α_j are the atomic polarizabilities of atoms i and j, n_i and n_j are the effective number of electrons in the outer shells of these atoms, and e is the fundamental electronic charge. Eq. 28 is then minimized with respect to r_{ij}, and evaluated at the value of the Van der Waals distance between atoms i and j, and solved for the value of b(51).

The Van der Waals radii were compiled from X-ray diffraction data by A. Bondi(87). At temperatures well below the transition temperature the Van der Waals radii are fairly insensitive to changes in temperature, so that interchain spacings computed in this study are valid for room temperature(20°) which is about 55°below the transition temperature. Near 75°C (the transition temperature) anharmonic effects become significant and thermal expan-

sion must be taken into account. In the present study the experimental thermal expansion coefficients for the interchain spacing reported by Suehiro et al(16) are used to convert the interchain spacings at 20° to those at 75°C.

The three fold sinusoidal potential energy function used in this study is given below.

eq(29) $E_{TOR}(\phi) = \frac{1}{2}V_o(1+\cos(3\phi))$ V_o=1.98 kcal/mole

The value of V_o is taken from reference 52.

Computer Experiments

A listing of the program used in these 'experiments' is given in APPENDIX A along with comments describing its operations.

Calculations of the conformational energy, minus torsion which is constant, vs. σ, the interchain spacing were carried out for the monoclinic lattices of forms I and II, and on the 'hexagonal' lattice with the form II dihedral angle. Force constants for the low frequency lattice vibrations were computed at the interchain spacings corresponding to the energy minima, and the experimentally derived interchain spacings. From these data the lattice vibration mean frequencies were computed and used to compute E_{vib}, S_{vib} and along with U to compute A.

Calculation of Phase Transition Thermodynamic Properties

To compute T_{tr}, linear regression analysis is applied to A(form II)-A(form I) as a function of T. T_{tr} is the temperature at which ΔA is zero.

ΔH_{tr} has two contributions. These are ΔU which is the

energy of crystal structure reorganization and ΔE_{vib} which is the change in the vibrational energy.

Application of the Method of Generalized Frequencies

The specific heat of crystalline PTBD was computed as a function of temperature between 75° and 139°C. $S_{139}-S_{75}$ was also computed for PTBD. The mean lattice vibration frequency computed from eqs. 18, 19, and 21 for a form II lattice with $\sigma = 4.95$ A was used to compute the lattice vibrational contribution to the lattice partition function. For an example outlining the application of eq(23) to computing C_p for PTBD at 80°C see appendix B. The generalized frequencies for each bond type are tabulated in Table VI.

To test the method's general utility, it was applied to the calculation of heat capacities of several other polymers at 25° or 0°C. Most of these were crystalline. A contribution of 1.9872 cal.mole^{-1}deg^{-1} was assumed for each degree of lattice vibrational freedom.

TABLE VIA

Generalized Frequencies for Hydrocarbon Bond Types*

Bond Type	$\gamma_i(cm^{-1})$	$\delta_i(cm^{-1})$
C-H(arom.)	3045	1318
C-H(aliph.)	2914	1247
C-C(aliph.)	989	390
C-C(arom.)	989	390
C=C(aliph,assym)	1664	421
C=C(aliph,sym)	1618	599
C≡C(arom.)	2215	333
C=C(arom.)	1618	844

* Taken from references 48 and 49

TABLE VIB

Generalized frequencies for Non-hydrocarbon Bond Types**

Bond Type	$\gamma_i(cm^{-1})$	$\delta_i(cm^{-1})$
C-I, S-S	500	260
C-Br	560	280
C-Cl,C-S	650	330
C-N, N-N	990	390
C-O, N-O	1030	205
C-F, C=S	1050	530
C=N	1620	845
C=O, N=O	1700	390
S-H	2570	1050
N-H	2920	1320
O-H	3420	1150

** Taken from reference 47

RESULTS

Crystal Lattice Constants

The lattice conformational energies of the form I and II monoclinic and of the 'hexagonal' form II lattices are listed as functions of σ, the interchain distance in Table VII. The torsion energy terms were excluded since they were held constant during the computations. The same data are displayed in graphic form in figs. 21, 22 and 23. The form I minimum occurs at σ=4.60 A which is the same as the experimental value given by Suehiro et al(16) at 20°C. The monoclinic form II lattice has its minimum at 4.85 A; however if it is assumed that 4.85 A corresponds to the value at 20°C, and the coefficient of thermal expansion for σ given by Suehiro et al(16)(viz. $2.8 \times 10^{-4} deg^{-1}$) is applied, a value of 4.92 A for the interchain spacing at 75°C is obtained. The minimum energy of the 'hexagonal' lattice occurs at 5.10 A; if this σ value is assumed to be that corresponding to 20°C, a value of 5.18 A at 75°C is obtained. The calculated and experimental lattice constants for various lattices at 20°C and 75°C are summarized in Table VIIIA. The a, b and σ lattice constants computed by Stellman and coworkers(17) are summarized in Table VIII B. σ is computed from a and b via the formulae in APPENDIX C so that two values of σ are given.

Mean Lattice Vibrational Frequencies

The values of $\bar{\nu}_x$, $\bar{\nu}_y$, and $\bar{\nu}_z$ calculated using eqs. 18, 19 and 21 and their mean value, $\bar{\nu}_m$ are listed in Table IX for the monoclinic lattices with the experimental and computed σ values. The expression for H_θ, the libration

Table VII

σ(A)	E_o(Form I)	E_o(Form II)	E_o(Hexagonal)
4.40	-10.105	0.611	
4.45	-10.855	-2.550	
4.50	-11.330	-4.895	
4.55	-11.599	-6.610	
4.60	-11.692*	-7.838	
4.65	-11.667	-8.689	
4.70	-11.546	-9.249	3.731
4.75	-11.355	-9.584	-0.995
4.80	-11.112	-9.747	-4.106
4.85	-10.831	-9.778*	-6.170
4.90	-10.524	-9.709	-7.498
4.95	-10.199	-9.511	-8.187
5.00	- 9.866	-9.367	-8.794
5.05			-9.023
5.10			-9.070*
5.15			-9.025
5.20			-8.888
5.40			-7.966

Lattice conformational energy(excluding torsion terms) as a function of interchain spacing form forms I and II monoclinic lattices and for the Stellman et al "Hexagonal" lattice(17)
Interchain spacing is expressed in angstroms.
Energy is in Kcal.mole^{-1}
*Energy minimum

Fig. 21

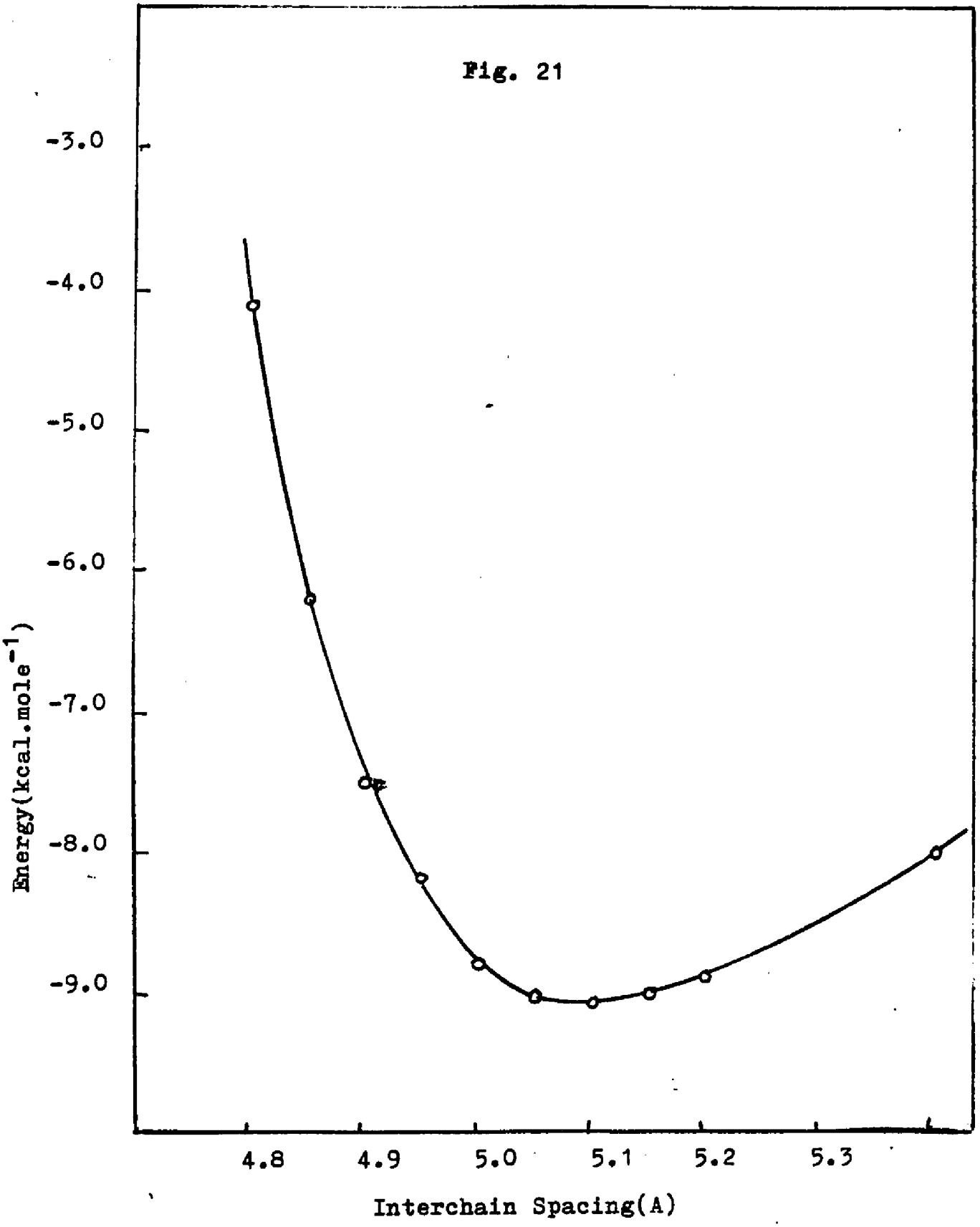

Energy vs. Interchain spacing for the 'Hexagonal' lattice

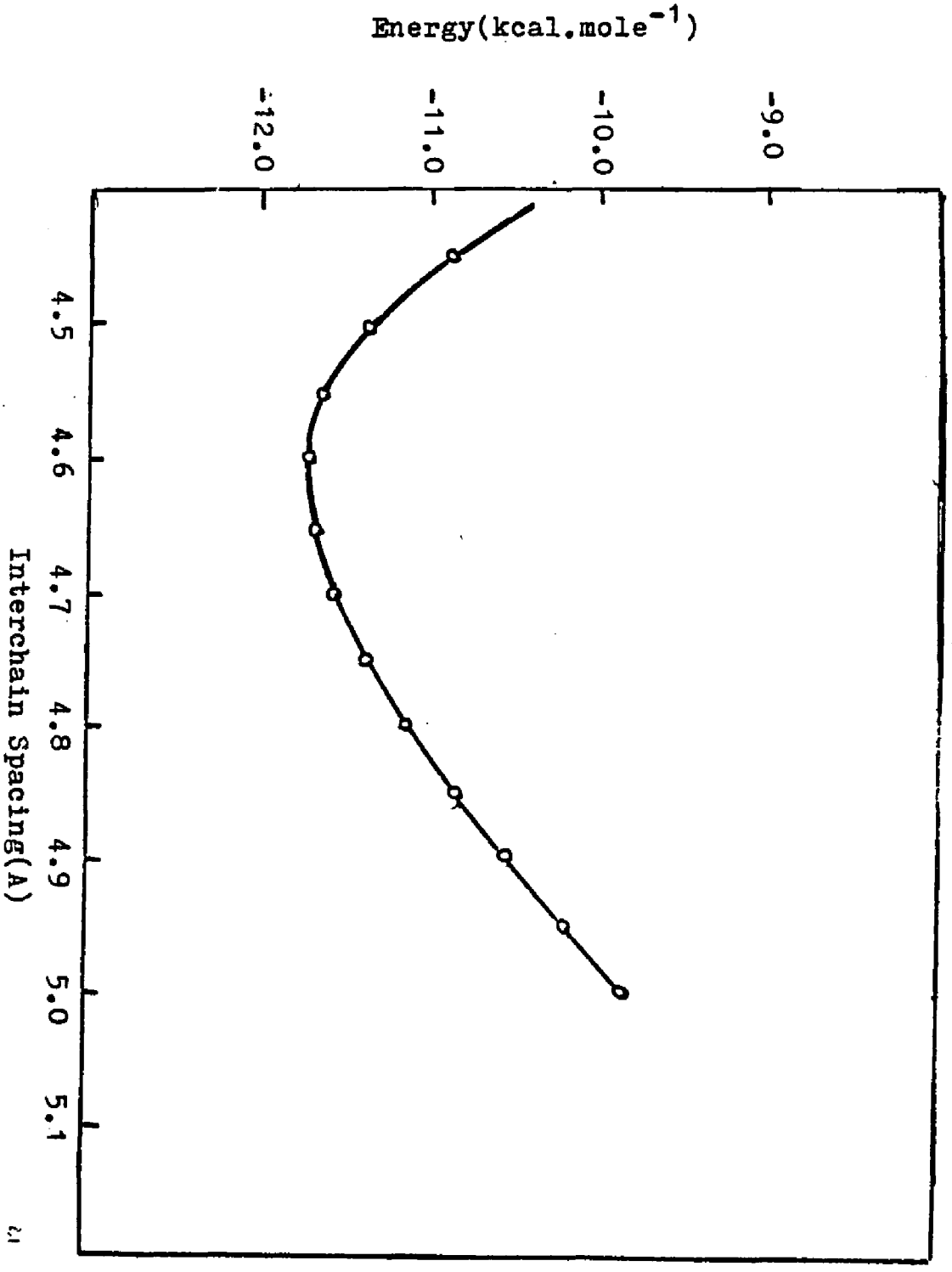

Fig. 22

Energy vs. Interchain Spacing for Form I PTBD Lattice

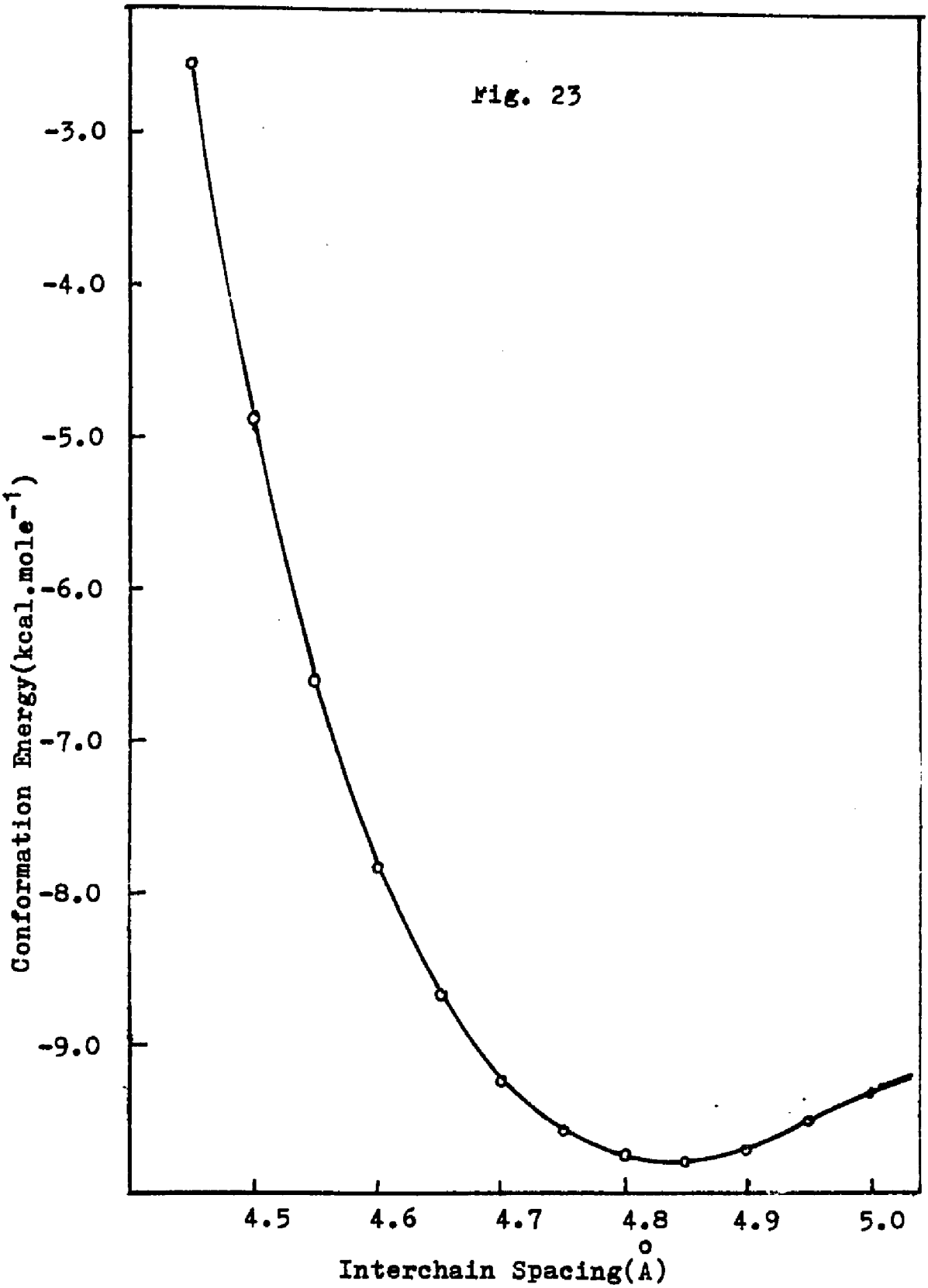

Energy Vs. Interchain Spacing for Form II PTBD lattice

Table VIII A

T(°C)	σ(A)	a(A)	b(A)	c(A)	Comment
20	4.55	8.63	9.11	4.83	Form I Ref(2) exp.
20	4.60	8.72	9.20	4.83	Form I Ref(6) exp.
75	4.67	8.85	9.34	4.83	Form I Ref(6) exp.
20*	4.60	8.72	9.20	4.83	Form II calc
75**	4.67	8.85	9.34	4.83	Form II calc
20*	4.85	9.20	9.70	4.66	Form II calc
75**	4.92	9.33	9.84	4.66	Form II calc
75	4.88	-	-	4.65	Form II Ref(1) exp.
75	4.95	-	-	4.66	Form II Ref(6) exp.
75	5.18	-	-	4.66	Hex. Lattice-calc

Calculated and experimentally derived lattice constants for various PTBD crystal lattices.
exp.- experimental constants
calc.- calculated constants
*Calculated value at 20°C
**Calculated from assumed value at 20°C with coefficient of thermal expansion for σ, the interchain distance given by Suehiro et al(16)

Table VIIIB

PTBD lattice constants computed by Stellman et al(17)

Lattice Form	a(A)	b(A)	σ(A)	Comment
I	8.70	9.60	4.59(4.80)[a]	SS function[b,d]
I	8.65	9.50	4.56(4.75)[a]	K function[c]
II	9.85	8.50	5.20(4.25)[a]	SS function
II	9.70	8.50	5.12(4.25)[a]	K function
'Hexagonal I'[e]	-	-	4.60	K function
'Hexagonal II'[f]	-	-	4.67	K function

a. Values of σ computed from a and b respectively

b. Scott Scheraga function

c. Kitaygorodski function

d. Value of b_{HH} may have been in error

e. 'Hexagonal' lattice with dihedral angle equal to 109°.

f. 'Hexagonal' lattice with dihedral angle equal to 80°.

Table IX

$T(^{o}C)$	σ(A)	$\bar{\nu}_x$	$\bar{\nu}_y$	$\bar{\nu}_z$	$\bar{\nu}_m$	Comment
20	4.60*	43	96	45	61	Form I
75	4.67*	31	85	46	54	Form I
75	4.92**	28	70	35	44	FormII
75	4.95*	26	65	32	41	FormII

Calculated lattice vibrational frequencies for various forms of PTBD.

*Experimental interchain distances(see Table VIII)

**Calculated interchain distances(see TableVIII)

constant yielded physically meaningless negative values so that $\bar{\nu}_m$ was substituted for $\bar{\nu}_\theta$. This procedure was discussed earlier(p.64).

Computed Thermodynamic Quantities

E_{vib}, TS_{vib} and A which are respectively the energy of vibration, the temperature entropy product of vibration and the Helmholtz free energy are listed as functions of temperature in Tables X and XI for monoclinic lattices having the theoretical and experimental σ values. To simplify analysis, the conformational energy, U, was held constant at the value corresponding to the 75°C interchain spacings. ΔA is listed in the last column. Linear regression analysis was applied to the ΔA vs. T data. For the theoretical transition, viz.(σ=4.67 A, ϕ = 109°)→(σ=4.92A, ϕ = 80°) a slope of -1.802 cal.deg^{-1} and an intercept of 192.8 cal were obtained. These give a T_{tr} of 107°. ΔA vs. T data calculated from experimental lattice geometries, viz. (σ=4.67 A, ϕ=109°)→(σ=4.95A, ϕ=80°) yielded a slope of -2.182 cal.deg^{-1} and an intercept of 175.5 cal. These give a T_{tr} of 80.4°C. The transition thermodynamic properties of these two models are summarized in Table XII along with experimentally derived properties.

Results from the Method of Generalized Frequencies

The specific heats of several crystalline hydrocarbon polymers are listed for 25°C in Table XIII. The specific heats of these polymers calculated from eq(24) are also listed. Eq.(24) was also applied to one noncrystalline

Table X

T(°C)	E_{vib}(I)	E_{vib}(II)	TS_{vib}(I)	TS_{vib}(II)	A(I)	A(II)	ΔA
25	2382	2377	5560	6097	-14845	-14697	148
35	2461	2456	5827	6382	-15033	-14903	130
45	2540	2536	6096	6670	-15223	-15111	112
55	2619	2616	6368	6960	-15416	-15322	94
65	2699	2694	6643	7253	-15611	-15536	75
75	2778	2773	6920	7548	-15809	-15536	57
85	2859	2853	7199	7848	-16007	-15969	38
95	2936	2932	7480	8144	-16211	-16189	22
105	3015	3011	7764	8446	-16416	-16412	4
115	3094	3091	8049	8750	-16622	-16636	-14
125	3174	3170	8337	9056	-16830	-16863	-33
135	3253	3250	8627	9364	-17041	-17091	-50

Case I

Thermodynamic properies as functions of Temperature for the transformation (σ=4.67A, ϕ=109°)→(σ=4.92A, ϕ=80°)

E_o(I)= -11619 cal.mole^{-1} $\quad\quad$ $\bar{\nu}_I$= 54 cm^{-1}

E_o^o(II)= -9652 cal.mole^{-1} $\quad\quad$ $\bar{\nu}_{II}$=44 cm^{-1}

ΔE_{tor}= -1325 cal.mole^{-1}

Energy units are in cal.mole^{-1}

Table XI

$T(^{o}C)$	$E_{vib}(I)$	$E_{vib}(II)$	$TS_{vib}(I)$	$TS_{vib}(II)$	A(I)	A(II)	ΔA
25	2382	2376	5560	6209	-14796	-14669	121
35	2461	2456	5827	6498	-14978	-14878	100
45	2540	2532	6096	6790	-15168	-15091	77
55	2619	2614	6368	7084	-15361	-15306	55
65	2699	2694	6643	7380	-15556	-15522	34
75	2778	2773	6920	7679	-15754	-15742	12
85	2859	2852	7199	7980	-15952	-15964	-12
95	2936	2931	7480	8283	-16156	-16188	-32
105	3015	3011	7764	8589	-16361	-16414	-52

CaseII

Thermodynamic properties as functions of Temperature for the transformation (σ=4.67A, ϕ=109^{o})$\rightarrow$(σ=4.95A, ϕ=80^{o})

$E_o(I)$= -11619 cal.mole^{-1} $\quad \nu_I$ = 54 cm^{-1}

$E_o(II)$= -9511 cal.mole^{-1} $\quad \nu_{II}$= 41 cm^{-1}

ΔE_{TOR}=-1325 cal.mole^{-1}.

Energy units are cal.mole^{-1}

Table XII

Sample	$\Delta H(cal.g^{-1})$	$\Delta S(cal.g^{-1}deg^{-1})$	$T_{tr}(^{o}C)$	Reference
Case I	12.3	0.032	107*	calculated
Case II	14.4	0.041	80.4**	calculated
H60	27.5	-	-	55
H43	19.5	-	-	55
H18	23.0	-	-	55
H63MR	27.	0.079	71	7,26
H63	26.	0.075	73	26
T23	19.	0.058	55	26
B8***	18.	0.053	65	26

Phase transition thermodynamic properties of Several preparations of crystalline PTBD.

*Predicted from ΔA vs. T data in Table X

**Predicted from ΔA vs. T data in Table XI

***Crystals precipitated from benzene at $8^{o}C$

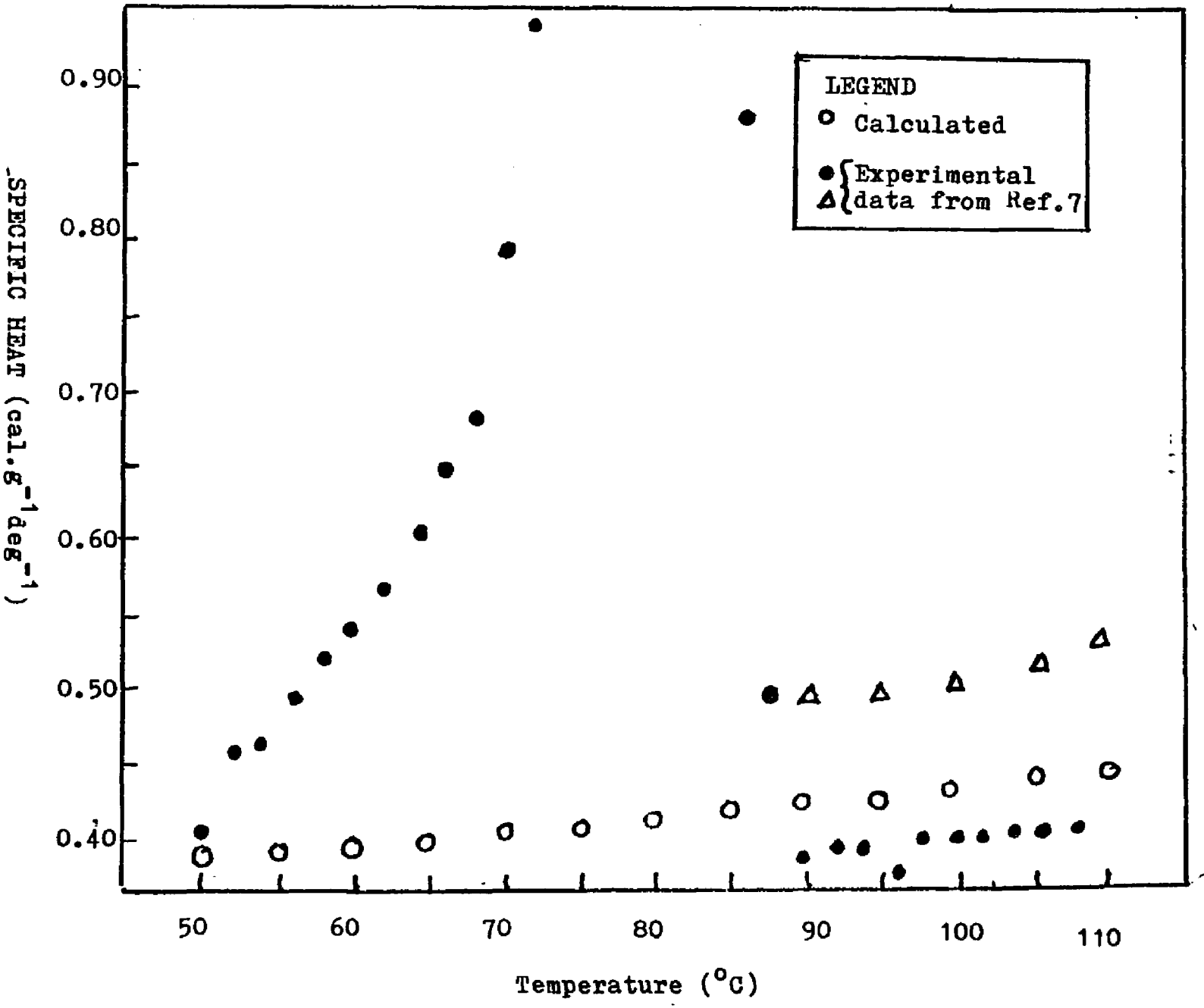
LEGEND
Calculated
Experimental
data from Ref.7
0.90
0.80
0.70
0.60
0.50
0.40
SPECIFIC HEAT (cal.g^{-1}deg^{-1})
50
60
70
80
90
100
110
Temperature (°C)

Fig. 24

Table XIII

Polymer	Monomer Unit	C_p(calc)	C_p(exp)	References
Polyethylene	$(-CH_2CH_2-)$	13.64	12.44	67,69,70 71,76,77 78,81
Poly-1-butene(i,c)	$(CH_2CH(CH_2CH_3)-)$	24.10	23.91	68,83
Polystyrene(i,c)	$(CH_2CH(C_6H_5))$	30.41	30.37	66,68,72
Poly-4-methyl-1 pentene(i,c)	$(CH_2CH(CH_2CH(CH_3)_2))$	34.55	34.70	73,74
Polypropylene(i,c)	$(CH_2CH(CH_3))$	18.87	18.00	66,72
Polypropylene(s,c)	same as above	18.87	18.15	66,75,82
Poly-1,4 trans butadiene(c)	$(CH=CHCH_2CH_2)$	22.66	23.	17
Polyethylene terephthalate	$(OCH_2CH_2OCOC_6H_4CO)$	43.97	50.66	79,80
Polyoxytrimethylene(c)*	$(CH_2CH_2CH_2O)$	20.53	25.58	88
Polyoxymethylene(c)	(CH_2O)	12.32	8.71	37,65
Polyisobutylene	$(CH_2C(CH_3)_2)$	24.10	26.12	89

Heat capacities of various polymers computed with equation 24. i = isotactic, c = cystalline, l = linear, s = syndiotactic.

Heat capacity units are cal.mole.$^{-1}$deg^{-1}

*Measured at 0^0C

and to three polymers containing oxygen with considerably less success. The specific heat of PTBD computed with eq(24) as a function of temperature is plotted in fig. 24 along with experimental data derived by Stellman et al(17).

$S_{139}-S_{73}$ for PTBD was also computed by the method of generalized frequencies and was found to be 0.077 cal.deg^{-1} g^{-1}The mean specific heat of PTBD-II measured by Stellman and coworkers(17) was 0.45 cal.deg^{-1}.g^{-1} $S_{139}-S_{73}$ derived from this value works out to be 0.079 cal.deg^{-1}g^{-1} which compares quite favorably with the value computed with eq(24).

DISCUSSION

Crystal Structure and Phase Transition Properties

In the Introduction it was stated that certain computational errors existed in the work of Stellman, Woodward and Stellman(17). Before discussing the results of the present work, these flaws will be discussed.

First, the b_{HH} constant for the Scott-Scheraga function was listed in the dissertation of J.M. Stellman as 44.60 kcal.$A.^{12}mole^{-1}$ instead of the correct value of 4460 kcal. $A.^{12}mole^{-1}$ given in reference 51. Single chain energy calculations carried out by this author with the erroneous value gave the same values as those reported by Stellman et al(17), which indicates that the erroneous value might have been used throughout the work.

Stellman and coworkers(17) computed the enthalpy of transition by taking the energy difference between two 'hexagonal' lattices with interchain spacings corresponding to the experimental form I value and to to the 'hexagonal' unit cell energy minimum in form II. For form II the hexagonal lattice is questionable, and for form I it is definately incorrect since it is known from experimental work to be monoclinic.

In the present work the minimum energy for the 'hexagonal' lattice of Stellman et al(17) occurs at 5.10A which is assumed by this author to be valid at 20°C. At 75°C the coefficient of thermal expansion of σ gives 5.18 A which exceeds the experimental value given by Suehiro and coworkers(14) by 0.23A. In contrast the monoclinic form II lattice has a minimum at 4.85 A, assumed to be the value at 20°C; this changes to 4.92 A at 75°C which is in excellent agree-

ment with the value given by Suehiro et al at 20°C, but exceeds that given by Natta and Corradini(13) by 0.05A. In any case the Scott-Scheraga function does give good agreement between calculated and experimental interchain spacings if it is assumed that the Van der Waals radii from which the potential energy functions are parametrized are valid for 20°C.

The lattice constants given by Stellman et al(17) are listed in Table VIIIB. It is of interest to compare the values of these constants to the lattice constants given in the present calculation. However, before comparisons are made, two important differences between the present work and that of Stellman and coworkers(17) should be pointed out. First, the calculation of Stellman et al was carried out by freely varying the two lattice parameters a and b, while in the present work only the interchain distance was varied. This procedure guarantees a constant ratio of a and b. It also guarantees a pseudohexagonal molecular packing which is consistent with references 13, 14 and 16. A second difference is in the function used. Earlier it was pointed out that the b_{HH} constant of the Scott-Scheraga function may have been in error in the Stellman calculation so that the lattice constants predicted by the Stellman et al function are suspect. Lattice constants computed in the present work will be compared with those derived by Stellman et al with the Kitaygorodsky(K) function.

The values of σ in the fourth column of Table VIII are derived with the equations of APPENDIX C. As can be

seen the values of the σ derived from the a and b values in that table are divergent. The differences between values computed from a and b values in the lattices range from 0.19 to 0.95 A. These divergent values of σ give rise to lattices which are substantially different from the pseudo-hexagonal molecular packing given by X-ray diffraction experiments. It is note worthy that the relative magnitudes of a and b computed by Stellman and coworkers are reversed in form II relative to form I. The reversal of magnitudes can be interpreted in an interesting way. The differences between σ(II) and σ(I), the interchain spacings of forms II and I, respectively are given below. The values due to Stellman et al are averages of the σ's computed from a and b. All of the values are uncorrected for thermal expansion, and all are for monoclinic lattices.

σ(II)-σ(I)	Function	Reference
0.18 A	SS	17
0.03 A	K	17
0.25 A	SS	Table VIIIA

The change in the PTBD molecular geometry decreases the fiber period of the molecule resulting in an increase in the effective radius of gyration of the molecule about its symmetry axis. The repulsion between the different molecular chains is not isotropic in the plane perpendicular to the molecular axes so that the increased repulsion in form II is accommodated by a shift of the molecules in the direction which relieves the maximum stress. In the work of

Stellman et al(17) the increased stress is relieved by a decrease in b and an increase in a. As can be seen above σ computed with the K function does not increase significantly. σ computed with the SS function is suspect. In the present work, a and b are constrained to change in the same ratio so that increased repulsion guarantees an increase in σ. The largest increase in σ, viz. 0.25 A is observed in the present work. Constraining a and b to vary in a constant ratio is somewhat artficial but is consistent with the experimental results.

Dilatometric experiments by Takayanagi et al(29) and DSC measurements by Marchetti et al(30,31) indicate that solution grown PTBD crystals are composed of two coexisting metastable crystalline forms below 75°C. It is possible that the parameters of these forms can be found in the form of minima in the U vs. σ and ϕ surface where ϕ is the $CH-CH_2$ dihedral angle. The Scott-Scheraga function would be a good function to start with because of its success in predicting the lattice constants of form I.

Phase Transition Thermodynamic Properties

As might be expected from the crudeness of the present model the phase transition thermodynamic properties are somewhat less than satisfactory. Comparison of ΔH_{calc} with ΔH_{tr} for H60 heptane crystals shows that only 50% of the enthalpy of transition has been accounted for by the model. Depending on which case in Table XII is examined, the value of T_{tr} is more or less gratifying, and indicates that the

model shows promise. Several factors contribute to the success or failure of the model,and these should be considered when the results are examined. First the internal vibrations were treated as invariant between forms I and II. Examination of the H63 Raman spectra at 25° and 77°C show that this is not the case. It should also be pointed out that the SS function was derived for saturated hydrocarbons. A function which is more specific to thecase of unsaturated hydrocarbons such as the Williams 6-exp(91) might perform better.

The Method of Generalized Frequencies

Because the present method uses the Einstein harmonic oscillator approximation to compute thermodynamic functions, several limitations must be observed. First, the motions of the molecules should approximate harmonic oscillations. Second the substances in question should not be at temperatures near phase transitions. The method is not expected to work for amorphous or glassy materials since they often undergo second order phase transformations which occur over wide ranges of temperature. The method should not be used below approximately 250 K where the Debye method tends to be more accurate. Finally the method is limited by the availability of generalized frequencies which can be applied to the system of interest.

All of the hydrocarbons in Table XIII are partly crystalline except polyisobutylene which is amorphous. The agreement between theory and experiment within this group is good (viz. $\pm$0.50 cal.mole^{-1}). Agreement among the oxygen

containing polymers is poorer. This is expected since the generalized frequencies for this group are not as well established as those of the hydrocarbons. However the large deviations observed in this group (see Table XIII) suggests that there are other factors contributing to C_p in these cases. Amorphous polymers tend to have higher observed C_p's than their crystalline counterparts. A notable exception to this rule of thumb is polystyrene whose amorphous C_p is 29.74 $cal.mole^{-1}deg^{-1}$(81,83,87) compared to 30.37 $cal.mole^{-1}deg^{-1}$ for the crystalline material. Another case of interest is polyoxymethylene whose computed C_p is significantly higher than the experimental value. Such a discrepency indicates that the contributions from low frequency modes, which are not as well established as their high frequency counterparts, are not as large as the calculated result suggests. This may be particularly true for lattice vibrations which have been assigned a contribution of 1.9872 $cal.mole^{-1}deg^{-1}$ per degree of freedom.

CONCLUSIONS

(1) The Scott-Scheraga (SS) non-bonded potential energy function predicts the correct interchain spacing for PTBD I at 20°C, and in conjuction with the coefficient of thermal expansion given by Suehiro et al(16) only slightly underestimates(4.92A compared to 4.95A(16)) the interchain spacing of form II at 75°C when monoclinic lattices are considered.

(2) The 'hexagonal' lattice overestimates σ for form II by 0.23A when the Scott-Scheraga function is used. This discrepency is attributed to methylene crowding inherent in this lattice.

(3) The SS function accounts for only 50% of the enthalpy of transition of crystalline PTBD. Better results can be expected from other functions and if the present crude model for the free energy is improved.

(4) The method of generalized frequencies provides a promising technique for estimating non-transition thermodynamic properties of crystalline polymers.

APPENDIX A

The following pages list the FORTRAN computer program used to perform computer experiments in the present work. A brief explanation of each segment is given below.

(1) MAIN PROGRAM - This segment computes the x, y, and z coordinates of a molecule and uses them to construct a unit cell. It also carries out the energy and force constant computations. Most of this is done via the calling of the succeeding subroutines.

SUBROUTINES

(1) FUNCTION ENERGY carries out necessary summations to compute the values of E_o and the force constants.

(2) FUNCTION E is the function being summed by FUNCTION ENERGY.

(3) ASSIGN-copies x, y, and z coordinates from registers NI to NF to NI+J to NF+J.

(4) SHIFT shifts X, Y, and Z from registers NI+DI to NF+DI and increments their values by DX, DY and DZ respectively.

(5) TRSFRM carries out the coordinate system transformation of x, y, and z to x', y', and z' on page 71.

(6) REFLECT reflects x, y and z coordinates in registers NI through NF into registers NI+DI to NF+DI through a plane parallel to the XY, XZ or YZ plane.

(7) ROTATE rotates X,Y and Z coordinates around an axis parallel to the X, Y or Z axis by angle PHI.

(8) SUBROUTINE TAB prints out X, Y and Z coordinates from registers NI to NF.

(9) CROSS computes vector cross product.

(10) UNIT generates a unit vector from coordinate input.

(11) CRTSN constructs cartesian coordinates of a molecule from molecular geometrical input.

```
      $JOB          JADE,TIME=600
      INTEGER WORDS(18)
      DO 100 I=1,500
      READ(5,101)WORDS
      WRITE(7,102)WORDS,I
100   WRITE(6,103)WORDS,I
101   FORMAT(2OA4)
102   FORMAT(18A4,I8)
103   FORMAT(' ',18A4,I8)
      STOP
      END
```

```
      $DATA
      INTEGERCHAR,CASE,DI
      DOUBLE PRECISION R,RE,PHEE,FE,DCOS,DSIN,DARCOS,DSQRT,RP,PI,PHIP,EX
     1(2),WHY(2),ZEE(2),REW,DX,DY,DZ,XI,YI,ZI,XJ,YJ,ZJ,XK,YK,ZK,CTHETA,
     1THETA ,PHI,DABS,X,Y,Z,PI2,DZEE
      DOUBLE PRECISION A,B,C,CBETA
      DOUBLE PRECISION JX,JY,JZ
      COMMON/CART/X(200 ),Y(200 ),Z(200 )/LENGTH/RE(22)/ANGLE/FE(40)/IND
     1EX/IRE(22),JRE(22),IFE(40),JFE(40),NRE,NFE/ELEMT/CHAR(400 )
      COMMON/Q/JX(400 ),V(400 ),W(400 )
      PI=DARCOS(-1.00)
      PI2=2*PI
C INPUT MOLECULAR GEOMETRY
      READ,NRE,NFE,NATOM
      PRINT,'                    LENGTH      I       J'
      DO 1 I=1,NRE
      READ(5,2)RE(I),IRE(I),JRE(I)
1     WRITE(6,2)RE(I),IRE(I),JRE(I)
      PRINT,'                    ANGLE       I       J'
      DO 3 I=1,NFE
      READ(5,2)FE(I),IFE(I),JFE(I)
3     WRITE(6,2) FE(I),IFE(I),JFE(I)
2     FORMAT(F9.6,2I2)
20    FORMAT(' ',20X,F9.5,2I5)
      READ(5,6)(CHAR(I),I=1,NATOM)
6     FORMAT(40I2)
C     CONSTRUCT INITIAL MOLECULAR COORDINATES
C*****************************CARTESION COORDINATE CONSTRUCTOR
      READ,N1,N2,N3
      RP=R(N2,N3)
      PHEE=PHI(N1,N3) *PI2/360
      X(N1)=0.00
      Y(N1)=0.00
      Z(N1)=0.00
      X(N2)=R(N1,N2)
      Y(N2)=0.00
      Z(N2)=0.00
      X(N3)=X(N2)+RP*DABS(DCOS(PHEE)+0.00)
      Y(N3)=RP*DSIN(PHEE)
      Z(N3)=0.00
      IF(NATOM.LT.4) GO TO202
      DO 14 I=4,NATOM
      READ(5,5)I1,I2,I3,I4,CASE,PHIP
      CALL CRTSN(I1,I2,I3,I4,CASE,PHIP,PI)
14    CONTINUE
5     FORMAT(4I2,I1,F6.3)
202   PRINT,'INITIAL MOLECULAR COORDINATES'
      CALL TAB(1,NATOM)
```

```
C   DEFINE MOLECULAR AXIS
      READ,N1,N2,N3,N4
      EX(1)=(X(N2)+X(N1))/2
      EX(2)=(X(N3)+X(N4))/2
      WHY(1)=(Y(N1)+Y(N2))/2
      WHY(2)=(Y(N3)+Y(N4))/2
      ZEE(1)=(Z(N1)+Z(N2))/2
      ZEE(2)=(Z(N3)+Z(N4))/2
C   TRANSFORM MOLECULAR AXIS TO Z AXIS
      REM=DSQRT((EX(2)-EX(1))**2+(WHY(2)-WHY(1))**2+(ZEE(2)-ZEE(1))**2)
      DX=-EX(1)
      DY=-WHY(1)
      DZ=-ZEE(1)
      CALL SHIFT(1,NATOM,DX,DY,DZ,0)
      DO 21 I=1,NATOM
      X(I)=U(I)
      Y(I)=V(I)
21    Z(I)=W(I)
      CALL TAB(1,NATOM)
      XK=(EX(2)-EX(1))/REM
      YK=(WHY(2)-WHY(1))/REM
      ZK=(ZEE(2)-ZEE(1))/REM
      DX=X(N2)-X(N1)
      DY=Y(N2)-Y(N1)
      DZ=Z(N2)-Z(N1)
      CALL   AXB(DX,DY,DZ,XK,YK,ZK,XI,YI,ZI)
      REM=DSQRT(XI*XI+YI*YI+ZI*ZI)
      XI=XI/REM
      YI=YI/REM
      ZI=ZI/REM
      CALL AXB(XK,YK,ZK,XI,YI,ZI,XJ,YJ,ZJ)
      PRINT,XI,YI,ZI
      PRINT,XJ,YJ,ZJ
      PRINT,XK,YK,ZK
      CALL TRSFRM(XI,YI,ZI,XJ,YJ,ZJ,XK,YK,ZK,1,NATOM)
      PRINT,'REORIENTED MOLECULAR COORDINATES'
      CALL TAB(1,NATOM)
      DZ=Z(11)-Z(9)
C     SPECIAL INSTRUCTIONS
C  SET SETTING ANGLE
      CALL REFLCT(1,2,1,NATOM,0.00,0)
      CALL ROTATE(150.00,3,1,NATOM)
      PRINT,'  CHAIN WITH 150 DEGREE SEETING ANGLE'
      CALL TAB(1,NATOM)
C CHAIN ENERGY AND FORCE CONSTANTS
C INSERT AFTER Z AXIS ORIENTATION OF MOLECULE
      UCHAIN=0.
      NATOM=10
      NC=7
      NQ=NC*NATOM
      NI=(NC-1)*NATOM/2+1
      NF=(NC+1)*NATOM/2
      DO 25 I=1,NC
      J=(I-1)*NATOM
      JZ=I*DZ
25    CALL SHIFT(1,NATOM,0.00,0.00,JZ,J)
      CALL ASSIGN(1,NQ,0)
C  HEXAGONAL LATTICE ENERGY
      CALL ROTATE(-30.00,3,1,NQ)
      READ,JR,NA,NB
```

```
      CALL SHIFT(1,NQ   ,0.00,0.00,0.00,0)
      C60=DCOS(60*PI/180)
      S60=DSIN(60*PI/180)
      LA=(NA-1)/2 +1
      LB=(NB-1)/2   +1
      ECRYST=0.
      DO 29 I=1,NA
      DO 29 J=1,NB
      JX=(I-LA)*JR+(J-LB)*JR*C60
      JY=(J-LB)*JR*S60
      IF(JX.EQ.0.0.AND.JY.EQ.0.)GO TO 30
      CALL SHIFT(1,NATOM,JX,JY,0.00,NQ)
      GO TO 29
   30 ECRYST=ECRYST+ENERGY(NQ   ,1,NATOM,1)
   29 ECRYST=ECRYST+ENERGY(NQ,NI,NF,1)
      PRINT,NQ,JR
      PRINT,'  LATTICE ENERGY=',ECRYST,'KCAL/MOLE'
      STOP
      END
      FUNCTION ENERGY(NQ,L1,L2 ,LX)
      INTEGER CHAR
      COMMON/Q   /X(400 ),Y(400 ),Z(400 )/ELEMT/CHAR(400 )
      ENERGY=0.
      DO 10 I=L1,L2
      DO 10 J=LX,NQ
      R= SQRT((X(I)-X(J))**2+(Y(I)-Y(J))**2+(Z(I)-Z(J))**2)
      M=CHAR(I)
      N=CHAR(J)
      MN=M+N-1
C  SCOTT -SCHERAGA ENERGY PAR(
      GO TO (3,2,1),MN
    1 IF(IABS(I-J).LT.10) GO TO 10
      ENERGY=ENERGY+E(370.,2860000.,R)
      GO TO 10
    2 IF(IABS(I-J).LT.8 ) GO TO 10
      ENERGY=ENERGY+E(129.,225000.,R)
      GO TO 10
    3 IF(IABS(I-J).LT.4 ) GO TO 10
      ENERGY=ENERGY+E(46.7,44.50,R)
   10 CONTINUE
      RETURN
      END
      FUNCTION E(A,B,R)
      E=-A/(R**6)+B/(R**12)
      RETURN
      END
      SUBROUTINE ASSIGN(NI,NF,J)
      DOUBLE PRECISION X,Y,Z
      INTEGER CHAR
      COMMON/ELEMT/CHAR(400 )
      COMMON/CART/X(400),Y(400),Z(400)/D/U(400 ),V(400 ),W(400 )
      DO 1 I=NI,NF
      CHAR(I+J)=CHAR(I)
      X(I+J)=U(I)
      Y(I+J)=V(I)
    1 Z(I+J)=W(I)
      RETURN
      END
      SUBROUTINE CRTSN(I1,I2,I3,I4,CASE,PHIP,PI )
      INTEGER CASE
```

```
      DOUBLE PRECISION X,Y,Z,R,PHI,DCOS,DSIN,DARCOS,DABS,DSQRT,PHIP,
     1AX,AY,AZ,BX,BY,BZ,CX,CY,CZ,RP,BR,F1,F3,F4,TAU,CTAU,THETA,DI,DII,D
     1III,TX,TY,TZ,PI,PI2
      COMMON/CART/X(200 ),Y(200 ),Z(200 )
      T=1.E-5
      PI2=2*PI
      CALL CROSS(I2,I1,I2,I3,BX,BY,BZ)
      BR=DSQRT(BX*BX+BY*BY+BZ*BZ)
      BX=BX/BR
      BY=BY/BR
      BZ=BZ/BR
      CX=(X(I3)-X(I2))/R(I2,I3)
      CY=(Y(I3)-Y(I2))/R(I2,I3)
      CZ=(Z(I3)-Z(I2))/R(I2,I3)
      IF(CASE.EQ.2)GO TO 15
      L=I3
      BX=-BX
      BY=-BY
      BZ=-BZ
      RP=R(I3,I4)
      THETA=PI-(PHI(I2,   I4)*PI2/360
      TAU=(PHIP*PI2)/360
      AX=BY*CZ-BZ*CY
      AY=-BX*CZ+CX*BZ
      AZ=BX*CY-BY*CX
      GO TO 16
   15 F1=PHI(I3,   I4)*PI2/360
      F3=PHI(I1,   I4)*PI2/360
      F4=PHI(I1,   I3)*PI2/360
      RP=R(I2,I4)
      CTAU=(DCOS(F3)-DCOS(F4)*DCOS(F1))/(DSIN(F4)*DSIN(F1))
      TAU =DARCOS(CTAU)
      L=I2
      THETA =PI-F1
      CX=-CX
      CY=-CY
      CZ=-CZ
      AX=BY*CZ-BZ*CY
      AY=-BX*CZ+CX*BZ
      AZ=BX*CY-BY*CX
   16 DI=RP*DCOS(THETA)
      DII=RP*DSIN(TAU)*DSIN(THETA)
      DIII=RP*DCOS(TAU)*DSIN(THETA)
           TX=AX*DIII+BX*DII+CX*DI+X( L)
      X(I4)=TX
           TY=AY*DIII+BY*DII+CY*DI+Y( L)
      Y(I4)=TY
           TZ=AZ*DIII+BZ*DII+CZ*DI+Z( L)
      Z(I4)=TZ
      IF(DABS(TZ).LE.T) Z(I4)=0.00
      IF(DABS(TY).LE.T) Y(I4)=0.00
      IF(DABS(TX).LE.T) X(I4)=0.00
      RETURN
      END
      SUBROUTINE   AXB(AX,AY,AZ,BX,BY,BZ,CX,CY,CZ)
      DOUBLE PRECISION AX,AY,AZ,BX,BY,BZ,CX,CY,CZ
      CX=AY*BZ-BY*AZ
      CY=-AX*BZ+BX*AZ
      CZ=AX*BY-BX*AY
      RETURN
```

```
      END
      SUBROUTINE SHIFT(NI,NF,DX,DY,DZ,DI)
      IMPLICIT DOUBLE PRECISION (A-H,O-Z)
      INTEGER DI
      INTEGER CHAR
      DOUBLE PRECISION X,Y,Z,DX,DY,DZ
      COMMON/C   /J(400 ),Y(400 ),Z(400 )/ELEMT/CHAR(400 )
     1/CART/X(200),Y(200),Z(200)
      DO 10 I=NI,NF
      CHAR(I+DI)=CHAR(I)
      X(I+DI)=X(I)+DX
      Y(I+DI)=Y(I)+DY
   10 Z(I+DI)=Z(I)+DZ
      RETURN
      END
      SUBROUTINE TRSFRM(XI,YI,ZI,XJ,YJ,ZJ,XK,YK,ZK,NI,NF)
      DOUBLE PRECISION X,Y,Z,XI,YI,ZI,XJ,YJ,ZJ,XK,YK,ZK
      COMMON/CART/X(200 ),Y(200 ),Z(200 )
      DO 10 I=NI,NF
      TX=X(I)*XI+Y(I)*YI+Z(I)*ZI
      TY=X(I)*XJ+Y(I)*YJ+Z(I)*ZJ
      TZ=X(I)*XK+Y(I)*YK+Z(I)*ZK
      X(I)=TX
      Y(I)=TY
   10 Z(I)=TZ
      RETURN
      END
      FUNCTION F(I,J)
      DOUBLE PRECISION R,PHI,RE,FE
      COMMON/LENGTH/RE(22)/ANGLE/FE(40)/INDEX/IRE(22),JRE(22),IFE(40),
     1JFE(40),NRE,NFE
      DO 10 K=1,NRE
      KAY=K
      IF (I.EQ.IRE(K).AND.J.EQ.JRE(K) .OR.I.EQ.JRE(K).AND.J.EQ.IRE(K)) G
     1O TO11
   10 CONTINUE
   11 R=RE(KAY)
      GO TO 14
      ENTRY PHI(I,J)
      DO 12 K=1,NFE
      KAY=K
      IF (I.EQ.IFE(K).AND.J.EQ.JFE(K) .OR.I.EQ.JFE(K).AND.J.EQ.IFE(K)) G
     1O TO13
   12 CONTINUE
   13 PHI=FE(KAY)
   14 RETURN
      END
      SUBROUTINE REFLCT(NA1,NA2,NI,NF,Q,DI)
      DOUBLE PRECISION X,Y,Z,Q
      INTEGER P,DI,CHAR
      COMMON/CART/X(200 ),Y(200 ),Z(200 )
      COMMON/ELEMT/CHAR(400 )
      P=NA1+NA2-2
      DO 10 I=NI,NF
      CHAR(I+DI)=CHAR(I)
      GO TO (1,2,3),P
    1 Z(I+DI)=2*Q-Z(I)
      X(I+DI)=X(I)
      Y(I+DI)=Y(I)
      GO TO 10
    2 Y(I+DI)=2*Q-Y(I)
```

```
      X(I+DI)=X(I)
      Z(I+DI)=Z(I)
      GO TO 10
    3 Z(I+DI)=2*Q-Z(I)
      Y(I+DI)=Y(I)
      Z(I+DI)=Z(I)
   10 CONTINUE
      RETURN
      END
      SUBROUTINE ROTATE(PHI,NAXIS,NI,NF)
      DOUBLE PRECISION X,Y,Z,PHI,PI,CPHI,SPHI,DARCOS,DCOS,DSIN
      COMMON/ELEMT/CHAR(400)
      COMMON/CART/X(200),Y(200),Z(200)
      PI=DARCOS(-1.D0)
      CPHI=DCOS(PHI*PI/180)
      SPHI=DSIN(PHI*PI/180)
      DO 10 I=NI,NF
      GO TO (1,2,3),NAXIS
    1 TY=Y(I)*CPHI+Z(I)*SPHI
      TZ=-Y(I)*SPHI+Z(I)*CPHI
      TX=X(I)
      GO TO 4
    2 TX= X(I)*CPHI+Z(I)*SPHI
      TZ=-X(I)*SPHI+Z(I)*CPHI
      TY=Y(I)
      GO TO   4
    3 TX= X(I)*CPHI+Y(I)*SPHI
      TY=-X(I)*SPHI+Y(I)*CPHI
      TZ=Z(I)
    4 X(I)=TX
      Y(I)=TY
      Z(I)=TZ
   10 CONTINUE
      RETURN
      END
      SUBROUTINE TAB(NI,NF)
      INTEGER CHAR
      DOUBLE PRECISION X,Y,Z
      COMMON/CART/X(200),Y(200),Z(200)/ELEMT/CHAR(400)
      WRITE(6,1)
      DO 10 I=NI,NF
   10 WRITE(6,2)I,X(I),Y(I),Z(I),CHAR(I)
    1 FORMAT('0' ,20X,'X',10X,'Y',10X,'Z')
    2 FORMAT(' ',I10,7X,3(F8.5,3X),5X,I2  )
      RETURN
      END
      SUBROUTINE CROSS(N1,N2,M1,M2,AX,AY,AZ)
      DOUBLE PRECISION BX,BY,BZ,AX,AY,AZ,CX,CY,CZ
      CALL UNIT(BX,BY,BZ,N1,N2)
      CALL UNIT(CX,CY,CZ,M1,M2)
      AX=BY*CZ-BZ*CY
      AY=-BX*CZ+BZ*CX
      AZ=BX*CY-BY*CX
      RETURN
      END
      SUBROUTINE UNIT(UX,UY,UZ,N1,N2)
      DOUBLE PRECISION X,Y,Z,A,AX,AY,AZ,DSQRT,UX,UY,UZ
      COMMON/CART/X(200),Y(200),Z(200)
      AX=X(N2)-X(N1)
      AY=Y(N2)-Y(N1)
```

```
      AZ=Z(N2)-Z(N1)
      A=DSQRT(AX*AX+AY*AY+AZ*AZ)
      JX=AX/A
      JY=AY/A
      JZ=AZ/A
      RETURN
      END
***ERROR*** END OF FILE ENCOUNTERED ON UNIT    5 (IBM CODE 140217)
        PROGRAM WAS EXECUTING LINE     3 IN ROUTINE M/PROG WHEN TERMINATION
CORE USAGE      OBJECT CODE=     624 BYTES,ARRAY AREA=      72 BYTES,TOTAL
DIAGNOSTICS     NUMBER OF ERRORS=      1, NUMBER OF WARNINGS=      0, N
COMPILE TIME=     0.19 SEC,EXECUTION TIME=    13.19 SEC,  DATE= JUL 1973
```

APPENDIX B

The heat capacity of PTBD computed at 80°C by the method of generalized frequencies

Monomer formula $(-CH_2-CH_2-CH=CH-)$

N=10, n=10, a=0 $\phi=(3x10-10-4)/10=1.6$

n_i	Type	$\bar{\nu}_i(cm^{-1})$	$C_i(cal.mole.^{-1}deg^{-1})$
6	ν_{C-H}	2914	0.012
1	$\nu_{C=C}$	1664	0.104
3	ν_{C-C}	989	1.783
6ø	δ_{C-H}	1247	3.095
ø	$\delta_{C=C}$	599	1.979
3ø	δ_{C-C}	390	7.760
4	ν(lattice)	41*	7.930

C_p(total)= 22.663 $cal.mole.^{-1}deg^{-1}$

= 0.419 $cal.g.^{-1}deg^{-1}$

* Computed from the Scott-Scheraga function for a form II lattice with σ=4.95 Å

APPENDIX C

Translation Operations for Generating Monoclinic and 'Hexagonal' lattices

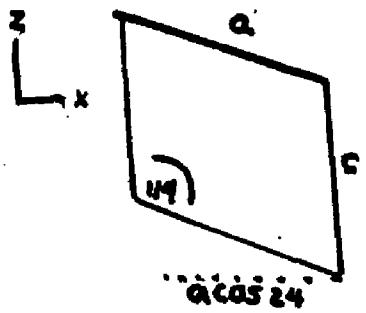

Fig. C1

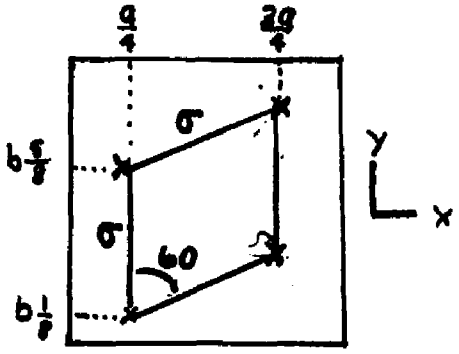

Fig. C2

Figures C1 and C2 depict XZ and XY projections of the unit cells used to generate the monoclinic lattices used in the computer experiments. The crosses in Fig. C2 show the positions of the four PTBD chains. The a and b parameters are related to by

$$a = 2\sigma\frac{\cos(30^\circ)}{\cos(24^\circ)}, \qquad b = 2\sigma$$

c is the fiber period and is equal to the distance between atom 1 and atom n+1 for a monomer unit oriented with its symmetry axis coincident with the z axis. Atom n+1 is an auxiliary atom. n is the number of atoms per monomer unit. The translations applied to the unit cell are given below in terms of simple integers

$$U_x = n_x a\cos(24^\circ)$$
$$U_y = n_y b$$
$$U_z = n_z c - n_x a\sin(24^\circ)$$

Fig. C3 difines the translations needed to generate the'hexagonal'lattice.

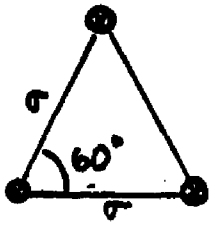

Fig. C3

The translations are applied to a chain of N monomer units whose symmetry axis coincides with the z axis. These translations are given in terms of σ below.

$$U_x = 2n_x\sigma\,COS(60)+n_y\sigma\,SIN(60) = (n_x+\tfrac{1}{2}n_y)\sigma$$

$$U_y = n_y\sigma\,SIN(60)$$

REFERENCES

1. A. Keller, Phil. Mag., 2, 1171(1957)
2. P. H. Geil, Polymer Single Crystals, Interscience, New York(1963)
3. A. W. Adamson, A Textbook of Physical Chemistry, Academic Press, New York(1973)
4. E. B. Wilson Jr., J. C. Decius, and P. C. Cross, Molecular Vibrations, McGraw-Hill Book Company, New York, 1955
5. F. A. Cotton, Chemical Applications of Group Theory, Wiley Interscience, New York, 1971
6. G. Turrell, Infrared and Raman Spectra of Crystals, Academic Press, New York, 1972
7. W. G. Fately, F.R. Dollish, N.T. McDevitt, F.F. Bentley, Infrared and Raman Selection Rules for Molecular and Lattice Vibrations, Wiley Interscience, New York, 1972
8. E.B. Wilson Jr., J. Chem Phys., 7, 1047(1939)
9. Idem, ibid., 9,76(1941)
10. P.W. Higgs, Proc. Roy. Soc. Lond., A220, 472(1953)
11. T. Miyazawa, J. Chem. Phys., 53, 693(1961)
12. C.W. Wilson III, G.E. Pake, J. Chem. Phys., 27, 115(1957)
13. G. Natta, T. Corradini, Nuovo Cimento, 15 Supple. 1, 9 (1960)
14. S. Iwayanagi, I. Sakurai and T. Sakurai, J. Macromol. Sci., Phys., B2(2), 163(1968)
15. S-B. Ng, J.M. Stellman and A.E. Woodward, ibid., B7, 539 (1973)
16. K. Suehiro and M. Takayanagi, ibid., B4(1), 39(1970)
17. J.M. Stellman, A.E. Woodward and S.D. Stellman, Macromolecules, 6, 330(1970)

18. N. Neto and C. di Lauro, Euro. Polym. J., 3, 645(1967)

19. D. Morero, F. Ciampelli and E. Mantica, Advances in Molecular Spectroscopy, Vol. 2, A. Mangini Ed., Pergammon Press, Oxford, 1962, p. 898

20. S.L. Hsu, W.H. Moore, and S. Krimm, J. Appl. Phys., 46, 4185(1975)

21. H. Evans and A.E. Woodward, Macromolecules, 9, 88(1976)

22. J.M. Stellman and A.E.Woodward, J. Polym.Sci., A-2, 9, 59(1971)

23. C. Hendrix, D.A. Whiting and A.E. Woodward, Macromolecules, 4, 571(1971)

24. B. Newman, J.M. Stellman and A.E. Woodward, J. Polym. Sci., Polym. Phys. Ed., 10, 2311(1972)

25. S-B. Ng and A.E. Woodward, J. Macromol. Sci., Phys., 10, 627(1974)

26. S. Takamuku, T.Tatsumi and M. Takayanagi, Reports on Progress in Polymer Physics in Japan, X, 333(1967)

27. F.S. Dainton, D.M. Evans, F.E. Hoare, T.P. Melia, Polymer, 3, 297(1967)

28. S.L. Hsu, S. Krimm, J. Polym. Sci., Polymer Phys. Ed., 47, 521(1976)

29. T. Tatsumi, T. Fukushima, K. Imada and M. Takayanagi, J. Macromol. Sci., Phys., B1, 459(1967)

30. A. Marchetti and E. Martuscelli, J. Polym. Sci., Polym. Phys. Ed., 14, 151(1976)

31. idem., ibid., 14,323(1976)

32. J.M. Stellman and A.E. Woodward, ibid., B7, 755(1969)

33. G. Natta, P. Corradini, L. Porri and D. Morero, Att.

Accad., Naz. Lince. Cl. Sci. Fis., Mat., Natur., Rend., 20, 728(1956)

34. G. Moraglio, G. Polizzotti and F. Danusso, Eur. Polym. J., 1, 183(1965)

35. S.F. Bermudez and J.MA.G. Fatou, ibid., 8, 575(1972)

36. S.W. Cornell and J.L. Koenig,Macromolecules, 2, 240(1972)

37. H. Wilski, Kolloid Z-Z. Polymere, 248, 867(1971)

38. A.E. Woodward, A. Odajima and J.A. Sauer, J. Phys. Chem., 65, 1384(1961)

39. H. Eyring, J. Waller and G. Kimball, Quantum Chemistry, John Wiley & Sons, Inc., New York, 1944

40. M.C. Tobin, Laser Raman Spectroscopy, John Wiley & Sons, New York,1971

41. Ph.D. dissertation of J.M. Stellman

42. I.M. Klotz and R.M. Rosenberg, Chemical Thermodynamics, W.A. Benjamin, Inc., Menlo Park, Calif., 1972

43. G.J. Janz, Thermodynamic Properties of Organic Compounds, Academic Press, New York, 1967

44. M. Born, K. Huang, The Dynamical Theory of Crystal Lattices, Clarendon Press, Oxford, England, 1954

45. O.K. Rice, Statistical Mechanics, Thermodynamics and Kinetics, W.H. Freeman and Co., San Francisco, 1967

46. K. Bennewitz, W. Rossner, Z. Physik Chem., B39, 126 (1938)

47. C.J. Dobratz, Ind. Eng. Chem., 33,759(1941)

48. D.R. Stull, ibid., 35, 1301(1943)

49. idem., ibid., 35, 639(1943)

50. E. Kreysig, Advanced Engineering Mathematics, 2nd Ed., J. Wiley & Sons, New York, 1967

51. R.A. Scott, H.A. Scheraga, J. Chem. Phys., 45, 2091(1966)

52. D.R. Hirshbach, Bibliography for Hindered Internal Rotation and Microwave Spectroscopy, Lawrence Radiation Laboratory, Univ. of Calif. at Berkeley, Berkeley, Calif. 1962

53. A.I. Kitaigorodsky, Tetrahedron, 14, 230(1961)

54. N.A. Ahmed, A.I. Kitaigorodsky, K.V. Mirskaya, Acta Crystallogr. Sect. B,, 27, 867(1971)

55. L.E. Nielsen, Mechanical Properties of Polymers, Reinhold Publ. Corp., New York, 1962

56. J. Brandrup, E.H. Immergut, Polymer Handbook, 2nd Ed., John Wiley and Sons, New York, 1975(pp. III-215)

57. B. Wunderlich and H. Baur, Advances in Polymer Science, 7, 260(1970)

58. W. Cooper, D.E. Evans, G. Vaughan, J. Polymer Sci., 59, 241(1962)

59. E. Blade, G.E. Kimball, J. Cheml Phys., 18, 630(1950)

60. D.R. Gee, T. Melia, Polymer, 10, 239(1969)

61. F.S. Dainton, D.M. Evans, F.E. Hoare, T.P. Melia, ibid., 3, 297(1962)

62. R. Cleland, J. Polymer Sci., 27, 349(1958)

63. E.W. Fischer and G. Schmidt, Angew. Chem., 74, 551(1962)

64. B. Wunderlich, M. Dole, J. Polymer Sci., 24, 201(1957)

65. B. Wunderlich, J. Phys. Chem., 69, 2078(1965)

66. Abu-Isa, M. Dole, J. Chem. Phys., 69, 2668(1965)

67. F.S. Dainton, D.M. Evans, F.E. Hoare, T.P. Melia, Polymer, 3, 263(1962)

68. idem.,ibid., 12,271(1962)

69. A.P. Gray, N.Brenner, Am. Chem. Soc. Div. Polymer Sci., Preprint, 6, 956(1965)

70. K.H. Hellwege, W. Knapp, W. Wetzel, Kolloid Z., 180, 126(1962)

71. L-L. Isaacs, G.W. Garland, J. Phys. Chem. Solids, 23, 311(1962)

72. F.E. Karasz, H.E. Bair, J.M. O'Reilly, J. Phys. Chem., 69, 2657(1965)

73. idem. Polymer, 8, 547(1967)

74. T.P. Melia, A. Tyson, Makromol. Chem., 109, 87(1967)

75. E. Passaglia, H.K. Kevorkian, J. Appl. Phys., 34, .90 (1963)

76. idem. J. Appl. Polym. Sci., 7, 119(1963)

77. W. Reise, J.E. Tucker, J. Chem. Phys., 43, 105(1965)

78. M.J. Richardson, Trans. Faraday Soc., 61, 1876(1965)

79. E. Yu. Koinishvili, N.N. Tavkhilidze, V-B. Akopyan, Vysokomolekul, Soedin, B9, 254(1967)

80. C.W. Smith, M. Dole, J. Polymer Sci., 21, 37(1965)

81. J.E. Tucker, W. Reise, J. Chem. Phys., 46, 1388(1967)

82. R.C. Wilhoit, M. Dole, J. Phys. Chem., 57, 14(1953)

83. H. Wilski, T. Brewer, J. Polym. Sci., C6, 33(1964)

84. J.O. Hirschfelder, C.F. Curtiss, R.B. Bird, Molecular Theory of Gases and Liquids, John Wiley and Sons, New York, 1954

85. J.C. Slater and J.G. Kirkwood, Phys. Rev., 37, 682(1931)

86. J.G. Kirkwood, Physik. Z., 33, 57(1932)

87. A. Bundi, J. Phys. Chem. 68, 441(1964)

88. S. Yoshida, M. Sakiyama, S. Seki, Polymer, J. 1, 573 (1970)

89. R. Hoffman, W. Knappe, Kolloid Z-Z., Polymere, 247, 763(1971)